THERMAL ASPECTS OF GRINDING

WOLFGANG JOACHIM SAUER

DEPARTMENT OF MECHANICAL ENGINEERING

CARNEGIE-MELLON UNIVERSITY

PITTSBURGH, PENNSYLVANIA 15213

MARCH, 1971

Carnegie-Mellon University

CARNEGIE INSTITUTE OF TECHNOLOGY

THESIS

SUBMITTED IN PARTIAL FULFILLMENT OF THE REQUIREMENTS

FOR THE DEGREE OF Doctor of Philosophy

TITLE THERMAL ASPECTS OF GRINDING

PRESENTED BY Wolfgang Joachim Sauer

ACCEPTED BY THE DEPARTMENT OF Mechanical Engineering

Milton C. Shaw — April 28, 1971
MAJOR PROFESSOR — DATE

Milton C. Shaw — April 28, 1971
DEPARTMENT HEAD — DATE

APPROVED BY THE COMMITTEE ON GRADUATE DEGREES

[signature] — 5/3/71
CHAIRMAN — DATE

ACKNOWLEDGEMENTS

The author expresses his sincere appreciation to Professor M. C. Shaw for the encouragement, advice, and suggestions which he gave during the course of this investigation. The author also wishes to express his gratitude for the financial support provided by the Grinding Wheel Institute without which this work could not have been undertaken.

TABLE OF CONTENTS

LIST OF TABLES

LIST OF FIGURES

LIST OF SYMBOLS

A	cross-sectional area of workpiece	in^2
Ac_1	temperature at the beginning of allotropic transformation and carbon solution	^oF
a	radius of indentation of hardness test	in
a_i	constants	
a_P	radius of elastic-plastic boundary	in
B	width of workpiece	in
b_C	width of undeformed grinding chip	in
b_G	width of plane over which single grain heat sources extend	in
b_n	mean value of average chip width	in
C	number of cutting points per unit area	$\frac{1}{in^2}$
C_0	constant	
C_1	constant	
c	specific heat	$\frac{Btu}{lbm\ ^oF}$
c_L	specific heat of water	$\frac{Btu}{lbm\ ^oF}$
c_{ST}	specific heat of steel	$\frac{Btu}{lbm\ ^oF}$
D	wheel diameter	in
D_0	constant	
$D(i)$	constants	
d	depth of cut	in
$\dot{d}$	downfeed rate	ipm
E	sum of squared temperature differences	$(^oF)^2$
E_0	constant	

$E(j)$	constants	
F	load of hardness test	lbf
F_P	tangential component of grinding force	lbf
F_Q	radial component of grinding force	lbf
F'_P	tangential component of single grain force	lbf
F'_Q	radial component of single grain force	lbf
F'_{PO}	average value of F'_P over length of contact	lbf
g	constant	
H	dimensionless cooling coefficient	
H_G	dimensionless cooling coefficient for single grain source	
H_I	dimensionless cooling coefficient for interference zone source	
H_W	bulk hardness of work material	$\frac{lbf}{in^2}$
h	coefficient of Newtonian cooling from the workpiece surface $z = 0$	$\frac{Btu}{in^2\ sec\ ^oF}$
h_O	convection coefficient at $x = 0$	$\frac{Btu}{in^2\ sec\ ^oF}$
h_l	convection coefficient for the long side of the cut-off workpiece	$\frac{Btu}{in^2\ sec\ ^oF}$
I	moment of inertia of drive-wheel system	$\frac{in\ lbf}{sec^2}$
i	index of summation	
j	index of summation	
$K(i)$	constants	
K_O	constant	
K_l	constant	

K_2	constant	
K_3	constant	
k	thermal conductivity	$\frac{\text{Btu}}{\text{in sec } ^\circ\text{F}}$
$\bar{k}$	average value of thermal conductivity over a range of temperatures	$\frac{\text{Btu}}{\text{in sec } ^\circ\text{F}}$
L	dimensionless half-length of heat source	
ℓ	half-length of heat source	in
ℓ_c	length of contact between wheel and workpiece	in
ℓ_e	mean value of undeformed chip length	in
ℓ_G	length of plane over which single grain heat sources extend	in
ℓ_v	table displacement between two cutting points	in
ℓ_{SS}	length of motion until steady state temperature distribution has developed	in
M	number of grains passing over one point of the workpiece while it is in contact with the wheel	
M_C	number of grains in contact with the workpiece at any instance of time	
M_P	number of temperature measurements considered	
$\dot{M}$	metal removal rate	$\frac{\text{in}^3}{\text{sec}}$
m_B	mass of steel base plate	lbm
m_L	mass of water	lbm
m_W	mass of workpiece	lbm
N	spindle speed under load	rpm
N_0	spindle speed without load	rpm
ΔN	drop of spindle speed under load	rpm
n_C	constant	

n_t	constant	
n_u	constant	
p	constant	
Q_F	total grinding energy	Btu
Q_H	total heat energy in the workpiece	Btu
Q'_H	measured heat energy	Btu
Q_P	strength of instantaneous point heat source	Btu
$\dot{Q}_F$	average rate of mechanical energy consumption during grinding	Btu/sec
$\dot{Q}_G$	instantaneous rate of heat energy input per grain	Btu/sec
$\dot{Q}_{GO}$	average rate of heat energy input per grain	Btu/sec
$\dot{Q}_{GS}$	rate of heat energy input of single grain surface heat source	Btu/sec
$\dot{Q}_{GV}$	rate of heat energy input of single grain volume heat source	Btu/sec
$\dot{Q}_I$	instantaneous rate of heat energy input during grinding	Btu/sec
$\dot{Q}_{IO}$	average rate of heat energy input during grinding	Btu/sec
$\dot{Q}_{IS}$	rate of heat energy input of interference zone surface heat source	Btu/sec
$\dot{Q}_{IV}$	rate of heat energy input of interference zone volume heat source	Btu/sec
$\dot{Q}_S$	total rate of heat energy input of surface heat sources	Btu/sec
$\dot{Q}_V$	total rate of heat energy input of volume heat sources	Btu/sec

$\dot{\Delta Q}$	loss of heat energy from calorimeter	Btu/sec
q	strength of heat source	$\frac{\text{Btu}}{\text{in}^2\ \text{sec}}$
q_{GS}	strength of single grain surface heat source	$\frac{\text{Btu}}{\text{in}^2\ \text{sec}}$
q_{GV}	strength of single grain volume heat source	$\frac{\text{Btu}}{\text{in}^2\ \text{sec}}$
q_H	strength of surface cooling	$\frac{\text{Btu}}{\text{in}^2\ \text{sec}}$
q_{IS}	strength of interference zone surface heat source	$\frac{\text{Btu}}{\text{in}^2\ \text{sec}}$
q_{IV}	strength of interference zone volume heat source	$\frac{\text{Btu}}{\text{in}^2\ \text{sec}}$
q_L	strength of line source	$\frac{\text{Btu}}{\text{in sec}}$
q_O	average strength of heat source	$\frac{\text{Btu}}{\text{in}^2\ \text{sec}}$
q_S	strength of surface heat source	$\frac{\text{Btu}}{\text{in}^2\ \text{sec}}$
q_V	strength of volume heat source	$\frac{\text{Btu}}{\text{in}^2\ \text{sec}}$
q_{VO}	strength of volume heat source at the surface $z = 0$	$\frac{\text{Btu}}{\text{in}^2\ \text{sec}}$
R	semi-infinite region representing the workpiece in horizontal spindle surface grinding	
r	ratio of undeformed chip width to undeformed chip thickness	
S	peripheral length of workpiece	in
s	variable	
T	workpiece temperature	^{o}F
T_C	temperature at interface between wheel and workpiece	^{o}F

$T_{C,max}$	maximum interface temperature	^{o}F
T_E	equilibrium temperature of calorimeter	^{o}F
T_F	temperature in plane of finished surface	^{o}F
T_L	initial water temperature	^{o}F
T_P	temperature in semi-infinite solid due to instantaneous point source	^{o}F
T_S	temperature due to surface heat sources	^{o}F
T_{ST}	initial temperature of steel parts	^{o}F
T_V	temperature due to volume heat sources	^{o}F
T_c	calculated temperatures	^{o}F
T_e	experimental temperatures	^{o}F
T_{max}	maximum temperature	^{o}F
T_1	temperature due to constant surface heat source ϕ_1	^{o}F
T_2	temperature due to constant volume heat source ϕ_2	^{o}F
T_3	temperature due to linearly varying surface source ϕ_3	^{o}F
T_4	temperature due to linearly varying volume source ϕ_4	^{o}F
T_5	temperature reduction due to surface cooling for source ϕ_1	^{o}F
T_6	temperature reduction due to surface cooling for source ϕ_2	^{o}F
T_7	temperature reduction due to surface cooling for source ϕ_3	^{o}F
T_8	temperature reduction due to surface cooling for source ϕ_4	^{o}F
ΔT	standard deviation of calculated temperatures from experimental ones	^{o}F

ΔT_{max}	maximum temperature difference between solutions for constant thermal properties and for temperature dependent properties	^{o}F
t	maximum undeformed chip thickness	in
t'	instantaneous undeformed chip thickness	in
t_n	mean value of maximum chip thickness	in
t_0	constant	
t_1	constant	
t_2	constant	
U	dimensionless time	
U_{SS}	dimensionless time at which a steady state temperature distribution is practically obtained	
u	specific grinding energy	$\frac{\text{in lbf}}{\text{in}^3}$
V	velocity of heat source	ips
V_S	wheel speed	ips
V_W	table speed	ips
W	dimensionless width of area heat source	
w	width of area heat source	in
X	dimensionless coordinate of horizontal position	
X'	dimensionless horizontal position of line heat source	
x	coordinate of horizontal position	in
x'	coordinate of horizontal position of point source	in
x_G	horizontal coordinate of system attached to a grain	in
x_L	length of cut-off workpiece	in

x_0	horizontal distance between the thermocouple and the wheel center at the instance at which the step in the reference signal occurs	in
x_1	horizontal distance between the thermocouple and the wheel center as measured from the photograph	in
Y	yield stress, equivalent yield stress	$\frac{lbf}{in^2}$
Z	dimensionless coordinate of depth	
Z'	dimensionless depth of line heat source	in
z	coordinate of depth	in
z'	coordinate of depth of instantaneous point heat source	in
z_G	coordinate of depth of system attached to a grain	in
α	total fraction of grinding energy which is converted into heat energy in the workpiece	
α_1	fraction of grinding energy entering the workpiece through the surface z = 0	
α_2	fraction of grinding energy entering the workpiece due to deformation	
β	decay coefficient of deformation energy with depth	1/in
γ	transformed depth coordinate	
η	dimensionless decay coefficient	
κ	thermal diffusivity	$\frac{in^2}{sec}$
λ_j	eigenvalues	
μ	ratio of tangential to radial component of grinding force	
ξ	transformed horizontal coordinate	
ξ_ℓ	transformed horizontal coordinate for $x \leq 0$	

ξ_r	transformed horizontal coordinate for $x \geq 0$	
ρ	density	$\frac{lbm}{in^3}$
τ	time	sec
τ'	time of action of instantaneous point source	sec
τ_c	time of contact of a point of the workpiece with the wheel	sec
τ_{SS}	time to reach a steady state temperature distribution in the workpiece	sec
τ_0	time of cut	sec
$\Delta\tau$	time difference between the occurrence of the step in the reference signal and the photo flash	sec
ϕ	dimensionless temperature	
ϕ_L	dimensionless temperature due to line source	
ϕ_{max}	maximum dimensionless temperature	
ϕ_1	dimensionless temperature due to a constant surface heat source	
ϕ_2	dimensionless temperature due to a constant volume heat source	
ϕ_3	dimensionless temperature due to a linearly varying surface heat source	
ϕ_4	dimensionless temperature due to a linearly varying volume heat source	
ϕ_5	dimensionless temperature reduction due to surface cooling for source ϕ_1	
ϕ_6	dimensionless temperature reduction due to surface cooling for source ϕ_2	
ϕ_7	dimensionless temperature reduction due to surface cooling for source ϕ_3	

ϕ_8 dimensionless temperature reduction due to surface cooling for source ϕ_4

θ angle of inclination of load in the hardness test model

ABSTRACT

The problem of determining the temperatures encountered in grinding is approached both analytically and experimentally. Thermal models of the workpieces for the abrasive cut-off operation and for horizontal spindle grinding are developed. The workpiece temperatures are measured in grinding tests with thermocouples inserted into the workpiece. The calculated and the experimental temperatures are compared and a small number of parameters is determined in such a way that the best possible fit between both temperatures is obtained. One of the parameters so evaluated is the fraction of the total grinding energy which appears in the workpiece in the form of heat energy. This is an important parameter in studying the chip formation process in grinding. The cooling ability of the grinding fluid used in the tests is another important result which can be evaluated using this procedure.

The model of the workpiece for surface grinding is then used to investigate the effect of the table speed on the workpiece temperatures. In the conventional range of speed the temperatures are found to increase with decreasing table speed. However, if the table speed is reduced by a factor of about 100, the temperature begins to decrease again due to more effective cooling. There exists a range of small table speeds for which the workpiece temperatures are lower than at conventional table speeds.

1 INTRODUCTION

1.1 Statement of the Problem

In recent years the application of the grinding process has been increasing at a rapid rate. Once it was only a toolroom operation used for sharpening cutting tools. Now improvements in abrasive grain compositions, wheel manufacturing techniques, and grinding machine design enable it to compete successfully with other metal removal processes on the bases of production cost or even metal removal rates. Today, grinding is used both as a finishing and as a roughing operation eliminating in some cases the need for milling or turning operations.

This increased use of grinding as a production technique has prompted extensive research of the underlying principles of the grinding process. The material to be ground is removed by the action of many small cutting points of abrasive grains of unidentified geometry which are held together in the grinding wheel by some bond material. Rotating at high speed each cutting point removes a small chip by means of a combined ploughing and shearing action. The exact manner in which chips are formed in grinding has not yet been determined. Originally thought of as a miniature milling process it was assumed that chips are sheared off in grinding as they are by the teeth of a milling cutter [21]. This approach does not yield the answers to many problems encountered in grinding and the need for new models arose. New techniques

based on the theories of elasticity and plasticity are now being applied. Slip-line field solutions [23] are worked out for the onset of chip formation and models based on Hertz's solution of the stress field in a semi-infinite solid due to a distributed load are suggested.

The basic difference between these models and the cutting tool model is that they allow for plastic deformation in the workpiece under a grain. The occurrence of flow under the workpiece surface has been confirmed in microscopic studies. The conversion of mechanical energy into other forms of energy will, therefore, take place not only at the workpiece surface but also in its interior. A large percentage of the energy is transformed into heat energy which causes temperature rises of the workpiece, the wheel, and the chips. By far, the most important of these is the temperature rise in the workpiece because the danger of overheating is great. Three characteristic temperatures with their own separate problem areas can be identified [7].

a) The maximum temperature in the area of contact between the wheel and the workpiece determines the rate of chemical reaction between the grains and the work material.

b) The maximum temperature of the finished workpiece surface is responsible for thermal damage of the workpiece.

c) The average temperature of the bulk of the workpiece is critical for its dimensional accuracy after grinding.

The determination of the first two of these characteristic temperatures is one goal of this thesis. Both temperatures are caused by a single pass of the wheel over the workpiece while the average temperature is the result of many repeated passes and, therefore, is also effected by events such as cooling which take place between grinding passes. The first two temperatures are closely dependent on the physical process of energy conversion in the workpiece. For this reason, it is hoped that a study of the workpiece temperatures will provide a means of evaluating models of chip formation for the grinding process. The results of this investigation can also be used for the selection of grinding conditions and grinding fluids for an improved grinding operation.

1.2 Intended Method of Solution

The problem of determining the temperatures encountered in grinding has been approached both analytically and experimentally by several investigators. Analytical investigations were hampered by the great complexity of the problem and by a lack of accurate information about chip geometry, chip formation, and the amount of heat energy liberated during grinding in the workpiece, the wheel and the chips. Experimental procedures for measuring grinding

temperatures in the wheel-workpiece contact zone are complicated by the very small size of the chips and by the extremely high grinding speed. Both properties of the grinding process cause very steep temperature gradients in the workpiece as well as in the wheel. Temperature measurements which yield an average value over some finite area such as the contact area between thermocouple wire and workpiece or the area of observation in radiation measurements will, therefore, strongly be affected by these gradients and the size of the area in question. The closer to the cutting zone of an individual grain one tries to measure the greater the difficulties encountered. Extrapolating from temperature measurements below the cutting zone is a common technique to determine the temperatures in the cutting zone itself. But because of the steep gradients in that region, widely varying results have been published.

In this thesis a procedure is described which overcomes most of the shortcomings of purely analytical or purely experimental methods. With this method the problem is approached from both sides. The temperatures in the workpiece are measured with a thermocouple at positions which are remote from the point of heat energy input. The local gradients are, therefore, small and accurate measurements can be obtained. Also, the disturbance of the temperature field in the workpiece caused by the thermocouple inserted through a small hole to the desired position is minimized.

Even though these measured temperatures are of no practical importance by themselves, they can provide information which is necessary for calculations of the workpiece temperatures in the areas of practical importance, at the interface between the workpiece and the wheel and in the plane of the final surface which remains after the grinding wheel has completed its pass over or through the workpiece.

The calculations are carried out with the aid of a mathematical model of the process which must allow the accurate prediction of the temperatures at least at the locations where the measurements are performed. The calculated temperatures will, of course, depend on some parameters which, so far, are unknown, such as total heat energy input and cooling rates. If the single goal of the investigation is the determination of these parameters the above stated condition is the only one which the model must satisfy. If in addition the temperatures at other positions are to be calculated, the model must also be accurate at these points of the workpiece.

In the next step the measured temperatures are compared point for point with temperatures which are calculated at the same locations with an assumed set of the unknown parameters. The sum of the squared differences between the measured and the calculated temperatures over all points is a measure of how close the assumed

set of parameters is to the correct set of parameters. If there were no error in the temperature measurements and if the model would describe the workpiece temperatures exactly the root-mean-square error would be zero if the correct set of parameters were used. Due to the inaccuracies of the experiment and the model, only a set which minimizes the root-mean-square error can be found. The methods used for this minimization process depend on the equations describing the model and on the parameters. The resultant set is assumed to be the correct set of parameters and used in further temperature calculations if desired.

Depending on one's point of view this procedure can be summarized in either of two ways:

a) It is an experimental method which measures temperatures a "safe" distance away from the cutting zone and uses an analytical model to extrapolate the temperatures at any point in the workpiece.

b) It is an analytical method which utilizes experimental temperature measurements to determine important parameters such as heat generation rate and cooling coefficient.

The advantages of the analytical method which allows the calculation of temperatures anywhere in the workpiece are combined with the advantages of the experimental method so that the heat generation rate and cooling coefficients need not be known. This procedure

is first applied to the workpiece for the abrasive cut-off operation. A simplified model is developed which only accurately predicts the temperatures some distance away from the cutting zone but already allows accurate predictions of the heat energy input into the work.

After being tested with a simple model, the procedure is applied to horizontal spindle surface grinding. A complex model of the workpiece is developed based on the theory of moving sources of heat by Jaeger [13]. Temperature measurements at points of the workpiece where reliable data can be obtained are used to calculate heat source strength and convection cooling coefficients at the surface. The use of these data in the model allows the calculation of temperatures at any point of the work, and specifically, directly in the grinding zone.

Finally, the above mentioned model is used to explore the effect on temperatures of a much wider range of grinding parameters than would be feasible to investigate in grinding tests. Experiments are conducted at extremely small table speeds and compared to theoretical predictions by the model. An explanation of the effectiveness of grinding fluids is offered based on experiments and model calculations.

2. THERMAL ENERGY IN THE ABRASIVE CUT-OFF OPERATION

2.1 Mechanics of the Process

One of the many forms of the grinding process which was studied extensively during the last years is the abrasive cut-off operation. This process is used to cut workpieces from bar stock which mostly will be finished in subsequent machining or forming operations. Thus, the main objective of the operation is to remove material as fast and as cheaply as possible. Relatively low accuracy and finish can be tolerated in many applications as well as some degree of thermal damage of the produced surfaces.

Only the example of a straight chop-stroke process is considered here. It was found that the most important parameters with respect to wheel wear and metal removal rate and total cost per cut over which the operator has control are the wheel speed, V_s, and the downfeed rate, $\dot{d}$. Figure 2.1 illustrates the dependence of the grinding ratio, G, which is defined as the ratio of the volume of metal removed to the volume of wheel worn on wheel speed [29] and in Figure 2.2 the effect of downfeed rate on the grinding ratio is demonstrated [30]. It is believed that the increasing trend of the grinding ratio with increasing downfeed rate at small values of $\dot{d}$ (left branch) is due to a temperature effect while the decrease of G for further increasing $\dot{d}$ (right branch) is caused by overcrowding of chips in the pores between the cutting grains.

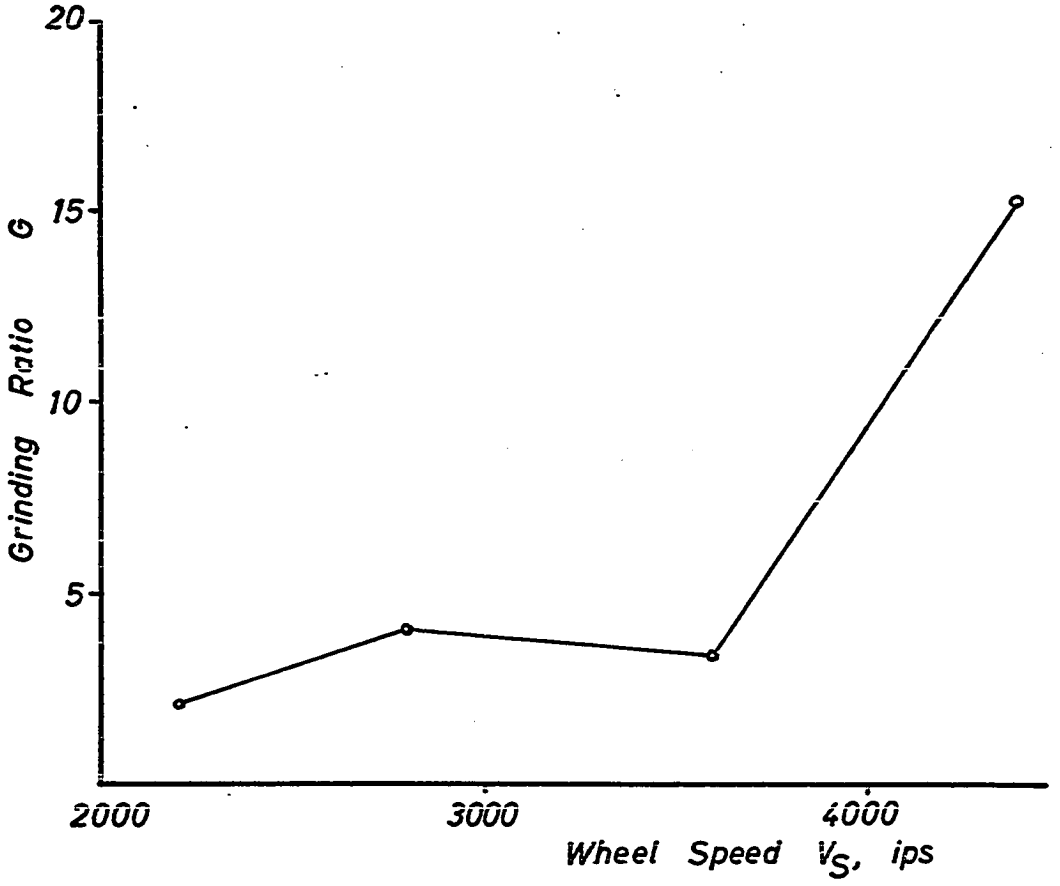

Figure 2.1 Grinding Ratio as a Function of Wheel Speed in Abrasive Cut-Off (From reference [21])

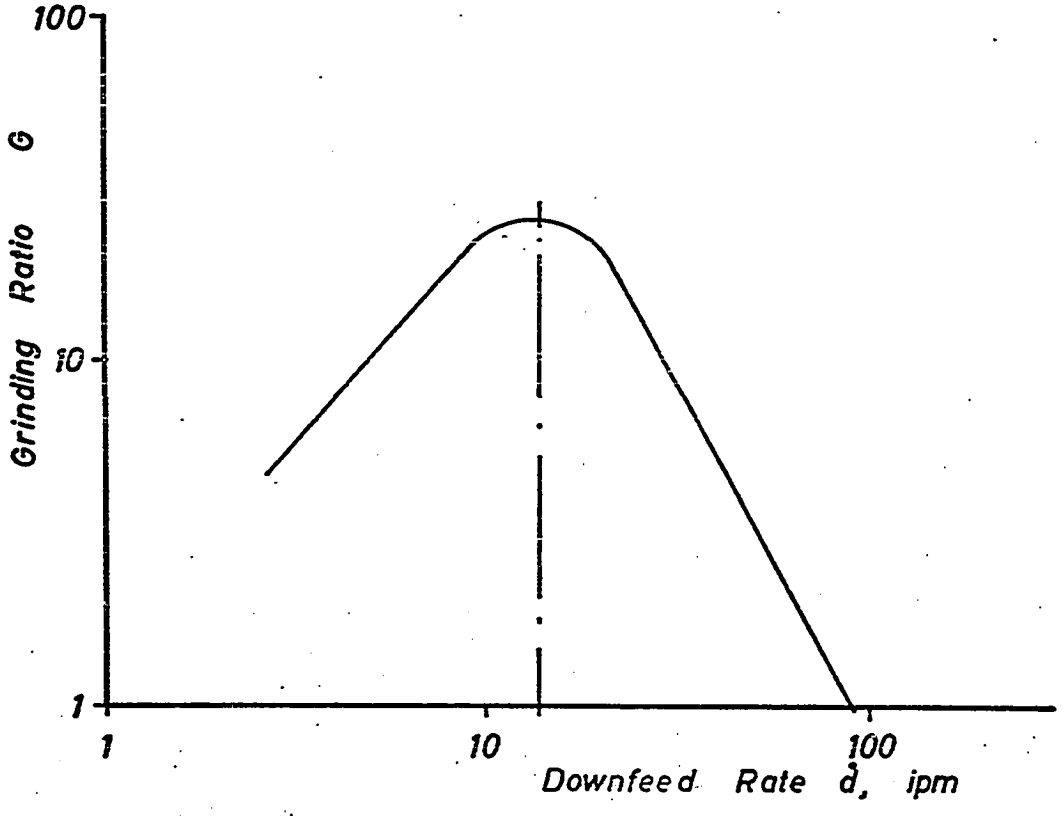

Figure 2.2 Grinding Ratio as a Function of Downfeed Rate

The grinding forces were measured and from these values of specific energy, u, were computed. A value of

$$u = 2 \cdot 10^6 \frac{\text{in lbf}}{\text{in}^3}$$

was found to be a reasonable average value.

Grinding temperatures developed in this process have two main effects concerning

a) the workpiece, and

b) the cut-off wheel.

High workpiece temperatures can cause structural changes, introduce residual stresses, and initiate cracks in cases of extreme overheating. The wheels are resin bonded and lose their strength and ability to retain abrasive grains when heated to about 500°F to 600°F. In reference [29] workpiece temperatures are measured with temperature sensitive paints. From these measurements the temperature at the interface between wheel and workpiece was estimated to lie between 1300°F and 1900°F for the range of conditions investigated. Similar results are obtained with a mathematical model of the wheel-workpiece system [8]. In order to simplify the model so that a solution becomes possible, heat losses sideways into the workpiece were neglected. At the end of the paper it is estimated that between 3% and 25% of the total cutting energy is conducted into parts of the workpiece which will not be removed by subsequent grinding.

2.2 Calorimetric Study

A calorimeter was designed to fit on top of a milling dynamometer. Figure 2.3 shows a schematic view of the instrument. A bowl made from 1/4 in. thick plexiglass is screwed to the dynamometer. The bowl is big enough so that the wheel fits into it to a depth sufficient to cut through a 1 inch high workpiece. Inside the bowl the workpiece is mounted with four screws to a base plate made from steel, which in turn is fixed to the bottom of the bowl.

During the cut a tin cover is inserted which collects all chips so that they are easily removed after the cut. The bowl is then filled with a premeasured quantity of water (m_L = 2400 mℓ ≈ 5.291 lbm) at an initial temperature T_L. The amount of fluid is sufficient to cover the workpiece completely. If there were no heat losses to the surroundings the heat energy input into the workpiece would be given by equation (2.1):

$$Q'_H = m_L c_L (T_E - T_L) + (m_B + m_W) c_{ST} (T_E - T_{ST}) \qquad (2.1)$$

where Q'_H = heat energy to work (assuming no losses from the calorimeter), Btu

m_L = mass of water, lbm

m_B = mass of steel base plate, lbm

m_W = mass of steel workpiece, lbm

c_L = specific heat of water, 1.0 Btu/(lbm ^{o}F)

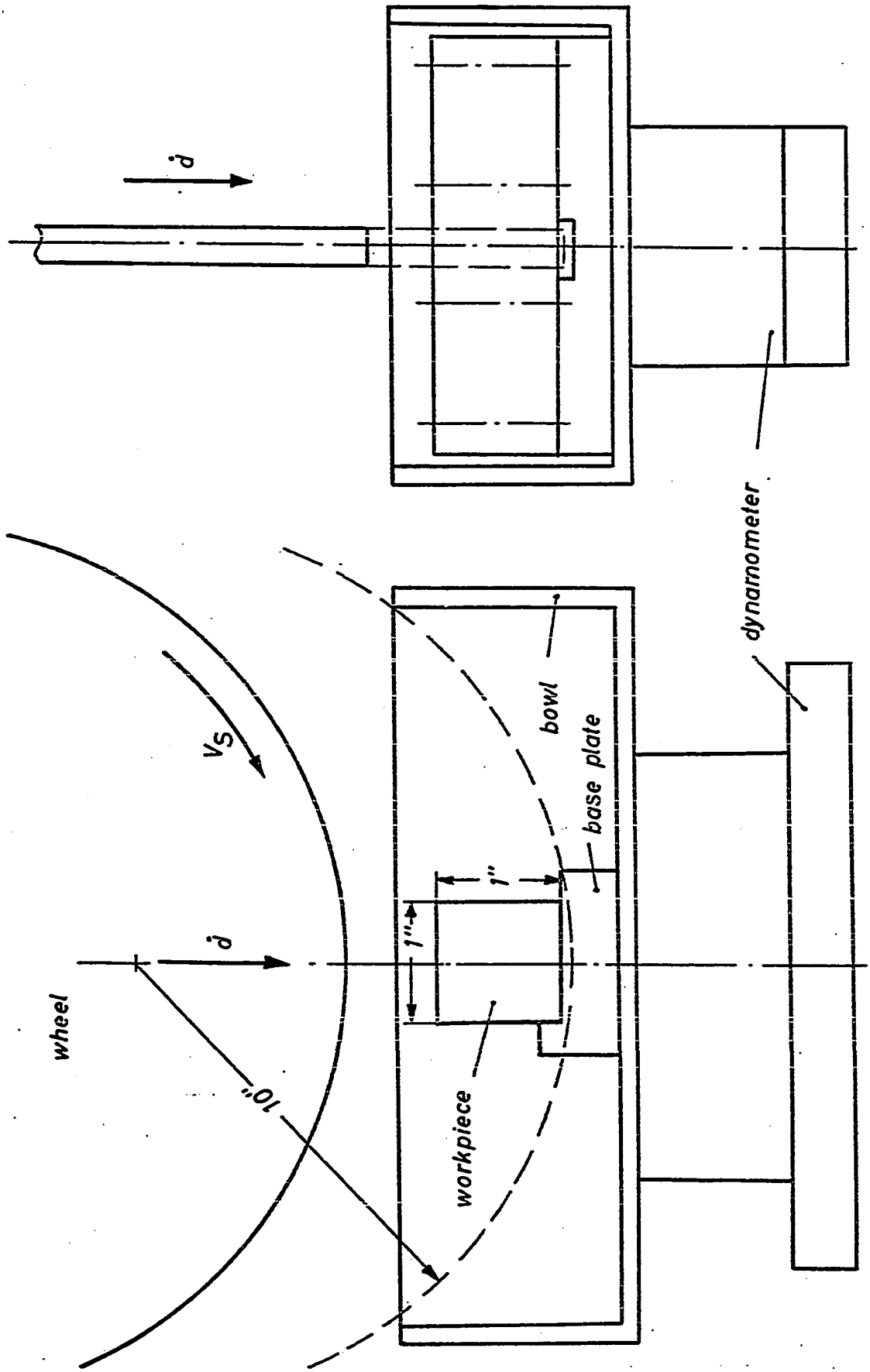

Figure 2.3 Schematic View of Calorimeter for Cut-Off Tests

c_{ST} = specific heat of mild steel, 0.106 Btu/(lbm ^{o}F)

T_E = equilibrium temperature, ^{o}F

T_L = initial water temperature, ^{o}F

T_{ST} = initial temperature of base plate and workpiece, ^{o}F

Initial tests showed that it takes approximately 180 sec. to establish an equilibrium temperature which is about 3^{o}F higher than the initial temperatures. The cooling curve of the calorimeter was determined by pouring water of known quantity and temperature into the calorimeter and measuring its temperature as a function of time. It was found that the cooling rate for the temperature and time ranges in question is

$$\frac{\dot{\Delta Q}}{Q_H} = 0.0002 \frac{1}{\text{sec}} \tag{2.2}$$

or the heat losses are about 0.02% per second. The total amount of heat energy in the workpiece at the moment in which the bowl is filled is then given by:

$$Q_H = (1 + 0.0002\ \tau)Q_H' \tag{2.3}$$

where τ is the time in seconds after the filling of the calorimeter with water at which Q_H' is determined and Q_H is the total thermal energy in the workpiece generated during the grinding.

The total amount of energy consumed in making the cut is determined by measuring the actual grinding forces during the cut with the

milling dynamometer. Equation (2.4) allows the total energy to be calculated from these measurements.

$$Q_F = \frac{F_P}{12} \frac{V_S \tau_0}{778} , \text{ Btu} \qquad (2.4)$$

where Q_F = total cutting energy, Btu

F_P = tangential component of grinding force, lbf

V_S = wheel speed, ips

τ_0 = time to make one cut, sec

Two cut-off tests were performed under the conditions given in Table 2.1.

Table 2.1 Cutting Conditions

Machine:	deSanno Radiac, 25 hp
Wheel:	A243-R6-B (20 x 3/16 x 1)
Wheel Speed:	V_S = 2500 ips
Work:	AISI 1020 hr
	size 1" x 1"

The results of force and calorimeter measurements are summarized in Table 2.2. Both tests give almost the same result and indicate that under cutting conditions as in Table 2.1 on the average 32% of the total cutting energy ends up as heat energy in the workpiece.

Table 2.2 Energy Balance

Test No.	$\dot{d}$, ipm	τ_0, sec	F_P, lbf	Q_F, Btu
1.1	20.0	3.75	59	59.3
1.2	20.0	3.74	65	65.2

a. Force Balance

Test No.	T_L, °F	T_{ST}, °F	m_L, lbm	m_W, lbm	T_E, °F	Q_H, Btu	Q_H/Q_F, %
1.1	70.6	72.1	5.291	1.333	73.8	18.35	31.0
1.2	61.1	63.5	5.291	1.562	65.0	22.20	33.5

b. Calorimeter Measurements

2.3 Thermal Model of the Workpiece

This result of the calorimeter measurements will be used as a reference value for calculations of the energy input into the workpiece using a thermal model and temperature measurements at one point of the piece. A temperature model of a workpiece used in the abrasive cut-off operation which would accurately predict the temperatures in the cutting zone would have to be very complex because it would involve three spatial and one time dimensions. For the purpose of determining the total energy input during cutting, however, a very simple one-dimensional model is sufficient. This is possible because the temperature in the workpiece at a point far removed from the cutting zone is not affected by flux variations in the plane of cut during the time

of cut. To a very good approximation this temperature can be determined from the integral value of the heat flux over the cutting area and the cutting time.

Figure 2.4 shows schematically the experimental set-up for measuring the workpiece temperature at the end of the piece a distance x_L away from the plane of cut.

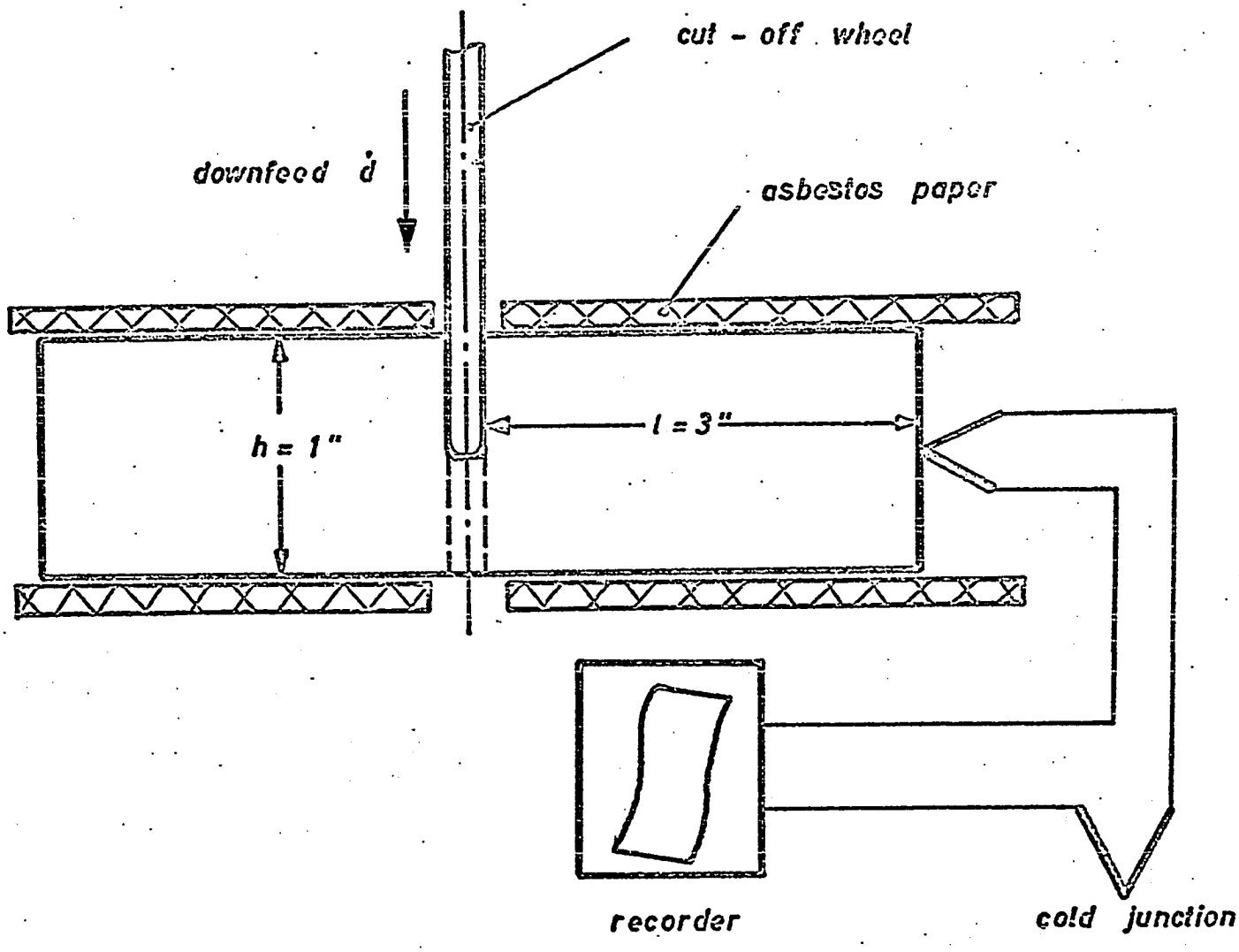

Figure 2.4 Thermocouple Measurements of Workpiece and Temperature

A copper-constantan thermocouple is attached at that end. With a Sanborn Recorder this thermocouple allows a continuous recording of the workpiece end temperature. The workpiece is insulated from the vice by a blanket of asbestos paper so that heat losses from the length of the piece are greatly reduced.

The model of the workpiece is shown in Figure 2.5 (a one-dimensional transient heat conduction model). The model assumes a constant heat source at the end $x = x_L$ for the time of cut, τ_0, and thereafter Newtonian cooling from the face $x = x_L$ with a convection coefficient h_0. There is convection cooling (coefficient h_1) for the long sides of the workpiece, during the entire time.

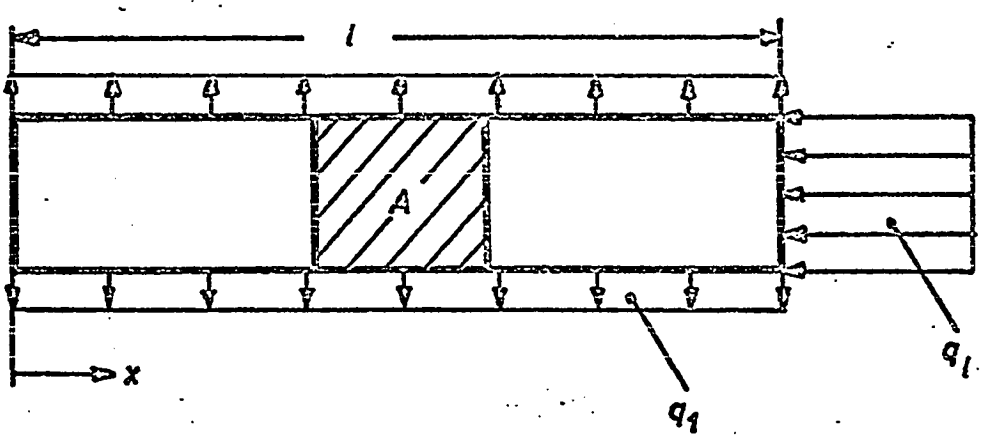

Figure 2.5 One-Dimensional Temperature Model

Mathematically this model is described by equation (2.5) with the boundary conditions of equation (2.6) and the initial conditions of equation (2.7).

$$\frac{\partial^2 T}{\partial x^2} - \frac{S}{A}\frac{h_l}{k} T(x,\tau) = \frac{1}{\kappa}\frac{\partial T}{\partial \tau} \tag{2.5}$$

for $0 \leq \tau \leq \tau_0$

$$\left.\frac{\partial T}{\partial x}\right|_{x=0} = 0$$

$$\left.\frac{\partial T}{\partial x}\right|_{x=x_L} = \frac{q_0}{k} \tag{2.6a}$$

$$T(x,0) = 0 \tag{2.7a}$$

for $\tau_0 \leq \tau < \infty$

$$\left.\frac{\partial T}{\partial x}\right|_{x=0} = 0$$

$$\left.\frac{\partial T}{\partial x}\right|_{x=x_L} = -\frac{h_0}{k} T(0,x_L) \tag{2.6b}$$

$$T(x,\tau_0) = T^*(x) \tag{2.7b}$$

In these equations

$T(x,\tau)$ = temperature rise above ambient temperature in the workpiece, ^oF

x = coordinate of length, in

S = peripheral length of workpiece, in

A = cross-sectional area, in^2

h_0 = convection coefficient at face $x = x_L$, $\frac{Btu}{in^2\ ^oF\ sec}$

h_l = convection coefficient at long sides, $\frac{Btu}{in^2\ ^oF\ sec}$

κ = thermal conductivity of workpiece material, $\frac{\text{Btu}}{\text{in } ^{\circ}\text{F sec}}$

K = thermal diffusivity of workpiece material, $\frac{\text{in}^2}{\text{sec}}$

q_0 = heat flux, $\frac{\text{Btu}}{\text{in}^2 \text{ sec}}$

τ = time, sec

τ_0 = time of cut, sec

These equations can be solved analytically and it is possible to calculate the temperature at any point in the model workpiece for any instant of time.

for $0 \leq \tau \leq \tau_0$; $h_1 = 0$:

$$T(x,\tau) = \frac{q_0 \kappa}{x_L k} \{\tau + 2 \sum_{i=1}^{\infty} \frac{(-1)^i}{K(i)} (1 - e^{-K(i)\tau}) \cos \frac{i\pi x}{x_L}\} \qquad (2.8)$$

$h_1 \neq 0$:

$$T(x,\tau) = \frac{q_0 \kappa}{x_L k} \{\frac{1}{K_0} (1 + e^{-K_0 \tau}) + 2 \sum_{i=1}^{\infty} \frac{(-1)^i}{K(i)} (1 - e^{-K(i)\tau}) \cos \frac{i\pi x}{x_L}\} \qquad (2.9)$$

where:

$$K_0 = \frac{S}{A} \frac{h_1}{k} \kappa$$

$$K(i) = K_0 + \kappa (\frac{i\pi}{x_L})^2$$

for $\tau_0 \leq \tau < \infty$; $h_0 = 0$:

$$T(x,\tau) = D_0 e^{-K_0(\tau-\tau_0)} + \sum_{i=1}^{\infty} (-1)^i D(i) e^{-K(i)(\tau-\tau_0)} \cos \frac{i\pi x}{x_L} \qquad (2.10)$$

$\underline{h_0 \neq 0:}$

$$T(x,\tau) = \sum_{j=1}^{\infty} E(j) e^{-(\kappa\lambda_j^2 + K_0)(\tau - \tau_0)} \cos \lambda_j x \qquad (2.11)$$

where

$$D_0 = \begin{cases} \dfrac{q_0 \kappa \tau_0}{x_L k} & (\text{for } h_1 = 0) \\ \dfrac{q_0 \kappa}{x_L k K_0} (1 - e^{-K_0 \tau_0}) & (\text{for } h_1 \neq 0) \end{cases}$$

$$D(i) = \frac{2q_0 \kappa}{x_L k K(i)} (1 - e^{-K(i)\tau_0})$$

$$(\lambda_j x_L)\mathrm{Tan}(\lambda_j x_L) = \frac{h_0 x_L}{k}$$

$$E(j) = \begin{cases} [D_0 - \sum_{i=1}^{\infty} \dfrac{D(i)}{(\frac{i\pi}{\lambda_j x_L})^2 - 1}] \dfrac{2 \sin \lambda_j x_L}{\pi_j x_L + \frac{1}{2} \sin 2\lambda_j x_L} & (\text{for } \lambda_j x_L \neq n\pi) \\ D(j) & (\text{for } \lambda_j x_L = n\pi) \end{cases}$$

For small values of x this simple model quite accurately indicates the temperatures in the cut-off workpiece. These positions are too far removed from where the heat source is applied to be affected by local variations in the cutting zone. As a test of the validity of this statement the model was modified such that the applied heat source was not constant during the time τ_0 but varied linearly with time:

$$q(\tau) = 2q_0 \frac{\tau}{\tau_0} \tag{2.12}$$

The total energy input of both models is the same and the calculated temperatures at x = 0 agree perfectly to within five significant figures for all instances of time of interest. In order to calculate the actual workpiece temperatures with equations (2.8, 2.9, 2.10, 2.11) it is necessary to determine three parameters which in addition to several material and geometric constants affect the temperatures. They are:

q_0 = input energy flux

h_0 = convection coefficient at face $x = x_L$

h_1 = convection coefficient for the long sides of the workpiece

Since all three parameters have a different effect on the resulting temperature profile in the model it is possible to determine them from actually measured temperature profiles. Figures 2.6 and 2.7 show the temperatures at the end x = 0 of the modeled workpiece

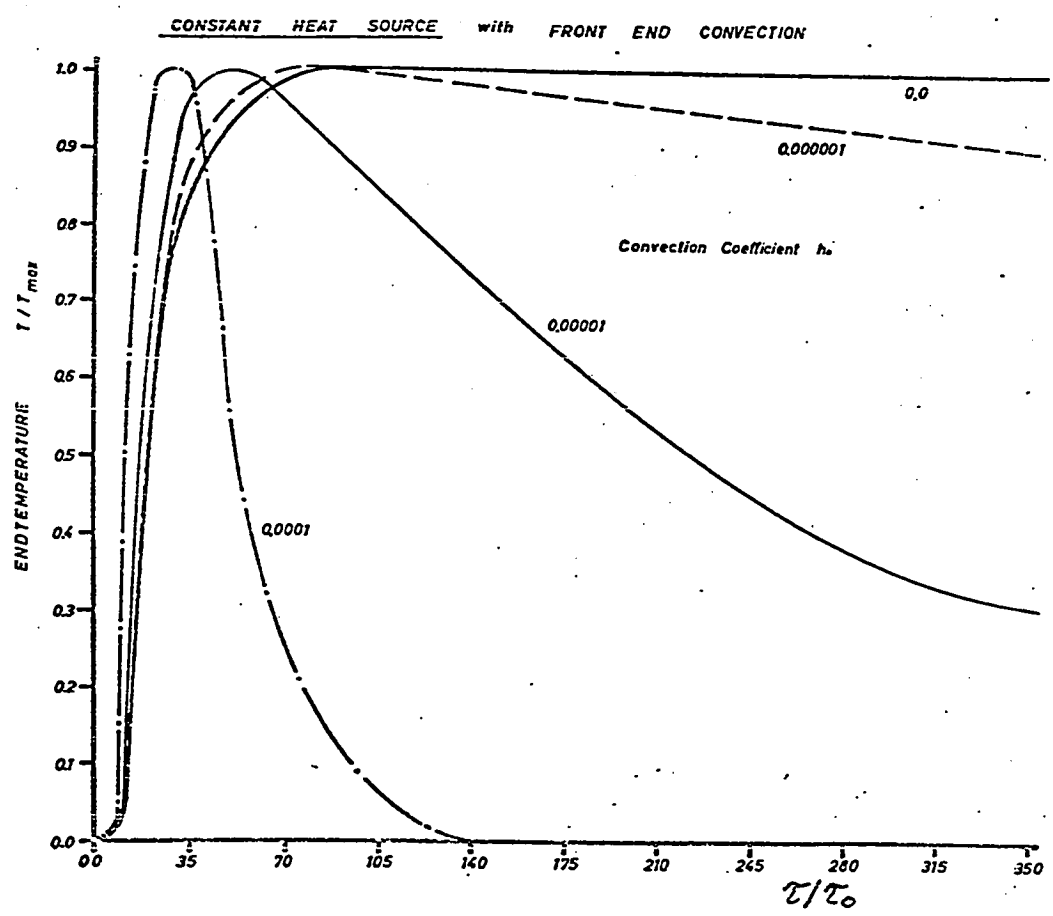

Figure 2.6 Normalized Temperature of the Model as a Function of Time for $h_1 = 0$

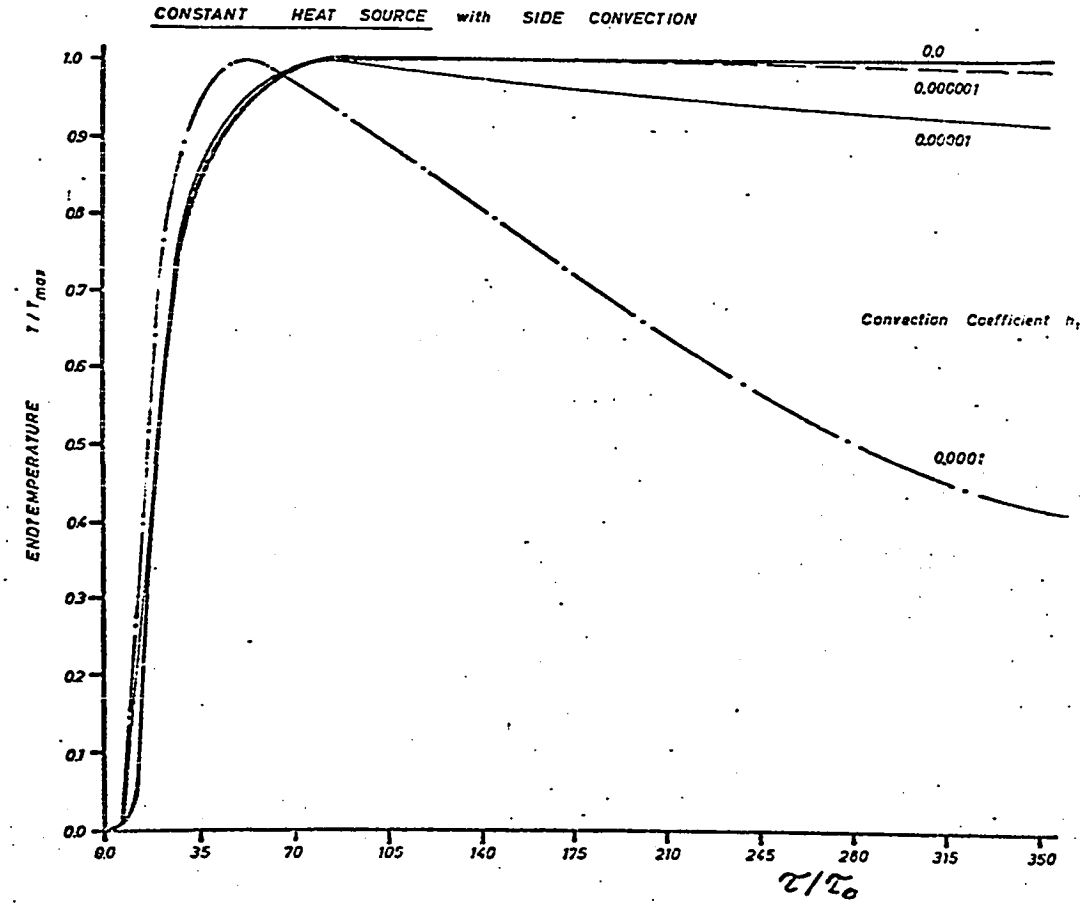

Figure 2.7 Normalized Temperature of the Model as a Function of Time for $h_0 = 0$

normalized with respect to their maximum values as a function of time normalized with respect to the time of cut. These normalized temperatures are independent of q_0 which only has the effect of linearly scaling the end temperatures. The other two parameters vary the shape of the temperature profiles as well as scaling it. Figure 2.6 shows that increasing the value of h_0 shifts the maximum of the temperature profiles to shorter times and greatly reduces the temperatures for large times. In Figure 2.7 convection coefficient h_1 is used as the parameter. Increasing h_1 reduces the temperatures for large times and causes a much smaller shift of the maximum temperature. Figure 2.8 compares the curves with almost identical behavior at small times, one for $h_0 = 0.00001$, $h_1 = 0.0$ and the other one for $h_0 = 0.0$, $h_1 = 0.0001$. It can be seen that there is a distinct difference between the two curves for large times.

The fact that both convection coefficients result in distinctly different temperature profiles makes it possible to determine both values from a measured temperature profile as well as the uniform heat flux q_0 which acts only as a scaling factor. The three parameters are found by means of a least-error-squares fit of the calculated profile to the measured one. Because of the nonlinear dependence of the temperature profile on the parameters a three-dimensional search routine for a general purpose digital computer, is employed to accomplish the parameter optimization.

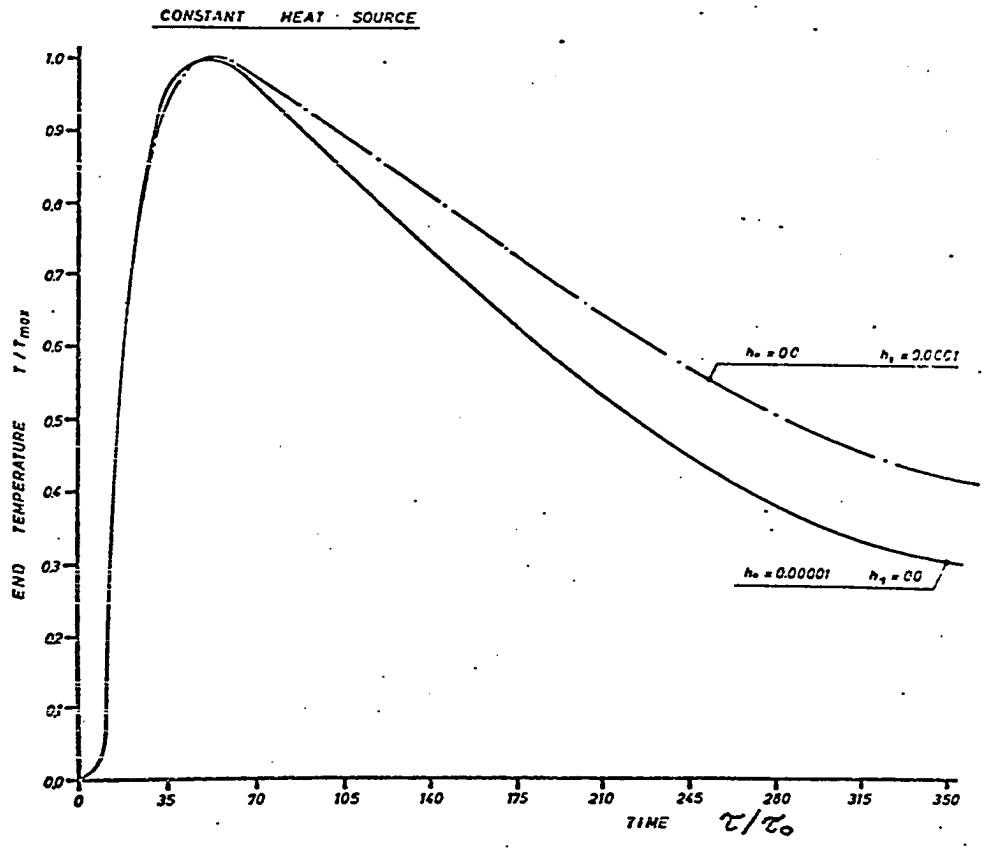

Figure 2.8 Comparison of the Effects of h_0 and h_1 on Shape of the Temperature Profile.

Using arbitrary starting values for the three parameters, the standard deviation (root-mean-square error) between the calculated and the experimental temperatures are calculated and the parameters are varied one after the other in increments so as to minimize the deviation. The increments for each parameter are defined relative to its range of possible values which are

$$0 \leq q_0 \leq \frac{Q_F}{A\tau_0}$$

$$0 \leq h_0 \leq 0.0001$$

$$0 \leq h_1 \leq 0.0001$$

Beginning with large increments their size is reduced if no further improvement is possible with the old step size. The search is stopped when the increments have been reduced below a fixed relative tolerance of $\varepsilon = 0.0001$ such that the resultant values of the parameters are determined to within 0.01% of their respective range.

A cut-off test was run under conditions given in Table 2.1 and the end temperature recorded. From the curve fit the following optimized values for the three parameters were obtained:

$$q_0 = 2.74 \frac{\text{Btu}}{\text{in}^2 \text{ sec}}$$

which corresponds to $Q_H = 18.9$ Btu

$$h_0 = 0.0 \frac{\text{Btu}}{\text{in}^2 \, ^\circ\text{F sec}}$$

$$h_1 = 0.0000097 \frac{\text{Btu}}{\text{in}^2 \, ^\circ\text{F sec}}$$

The ratio of heat energy to total energy is calculated to be $\alpha = Q_H/Q_T = 31.5\%$ which is in perfect agreement with the results obtained in calorimeter measurements (Table 2.2). In Figure 2.9 the measured and the calculated temperatures are plotted as a

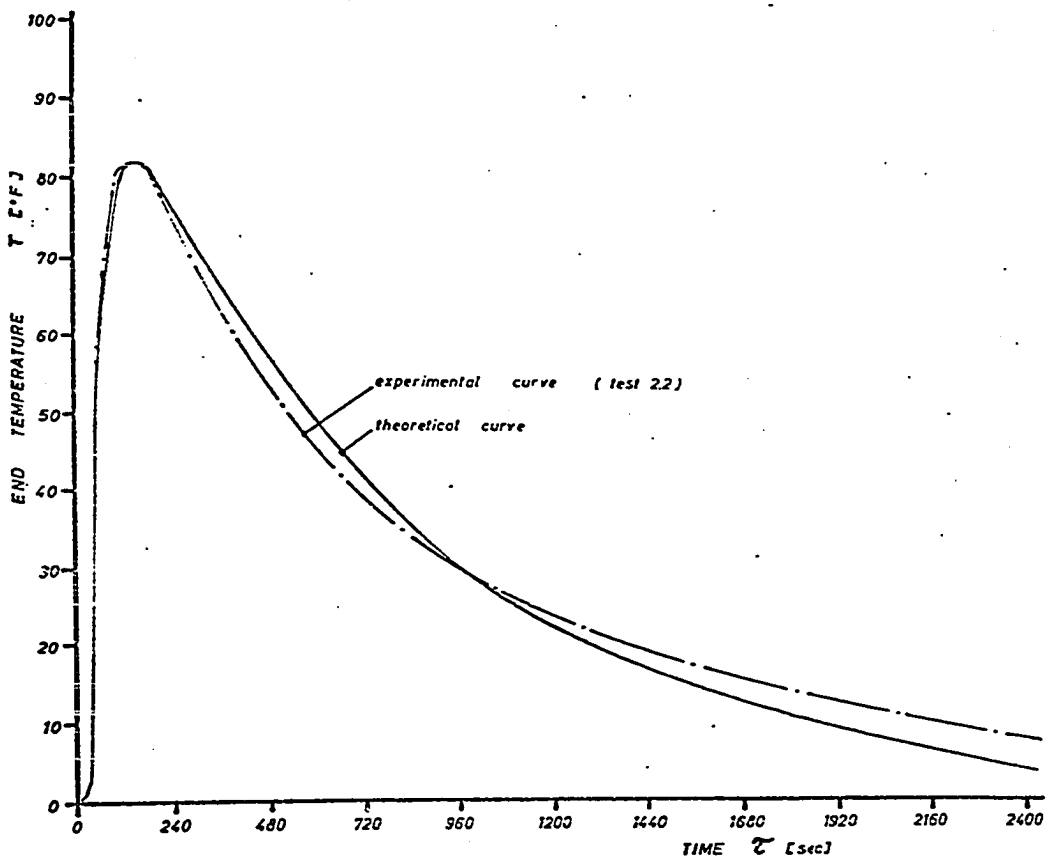

Figure 2.9 Comparison of Experimental Data with Least-Error-Squares Fitted Curve

function of time. These results show that it is possible to determine the heat energy input into the workpiece from very simple temperature measurements with the help of a mathematical model of the workpiece. In this case the model cannot be used to calculate the temperatures of the real workpiece directly in the cutting zone. As was pointed out initially, a much more complex model would be required for this task. For the same reason, it is not possible to determine directly the cooling coefficients

of grinding fluids if used. Its effect could only be inferred from a possible reduction of the heat input if compared with the value for q_0 obtained by grinding under otherwise constant conditions in air. The two convection coefficients in equations (2.8), (2.9), (2.10), (2.11) are introduced only to account for heat losses after the cut is finished. A more elaborate model will be developed in the following chapter for the workpiece in horizontal spindle grinding.

2.4 Abrasive Cut-Off Tests

Using this combined analytical and experimental method the effect of feed rate and wheel speed was studied using two cut-off wheels having different compositions and manufacturers.

Three test series were run and the conditions and results of the calculations are summarized in Table 2.3. All tests were run using the deSanno Cut-Off Machine. The workpieces of size 1 inch by 1 inch were cut dry. Both tangential and radial components of the grinding force, the downfeed rate, and the temperature in the free end of the workpiece were measured and recorded continuously on two two-channel Sanborn recorders.

The variation of the tangential component of the grinding force, F_p, with downfeed rate is shown in Figure 2.10 and the variation of total cutting energy, Q_F, is plotted in Figure 2.11. In

Test No.	Wheel	V_s ips	$\dot{d}$ ipm	F_P lbf	μ	Q_F Btu	u 10^6 psi	Q_H Btu	α
2.1	A (A243-R6-B)	2500	12.0	50.5	0.63	69.0	3.37	20.6	0.298
2.2		2500	20.0	67.0	0.73	65.5	2.68	19.7	0.301
2.3		2500	35.5	97.0	0.81	59.8	2.18	13.8	0.231
3.1	B (A24SG)	2500	15.5	36.0	0.57	37.4	1.92	6.1	0.163
3.2		2500	24.5	53.5	0.48	35.1	1.75	4.5	0.129
3.3		2500	44.0	76.5	0.54	33.8	1.39	3.6	0.106
4.1	B (A24SG)	3200	13.0	27.5	0.45	39.6	1.69	7.4	0.188
4.2		3200	25.0	40.0	0.56	35.4	1.28	4.6	0.129
4.3		3200	46.0	61.0	0.53	32.4	1.06	3.1	0.096

Table 2.3 Workpiece Thermal Energy in Abrasive Cut-Off

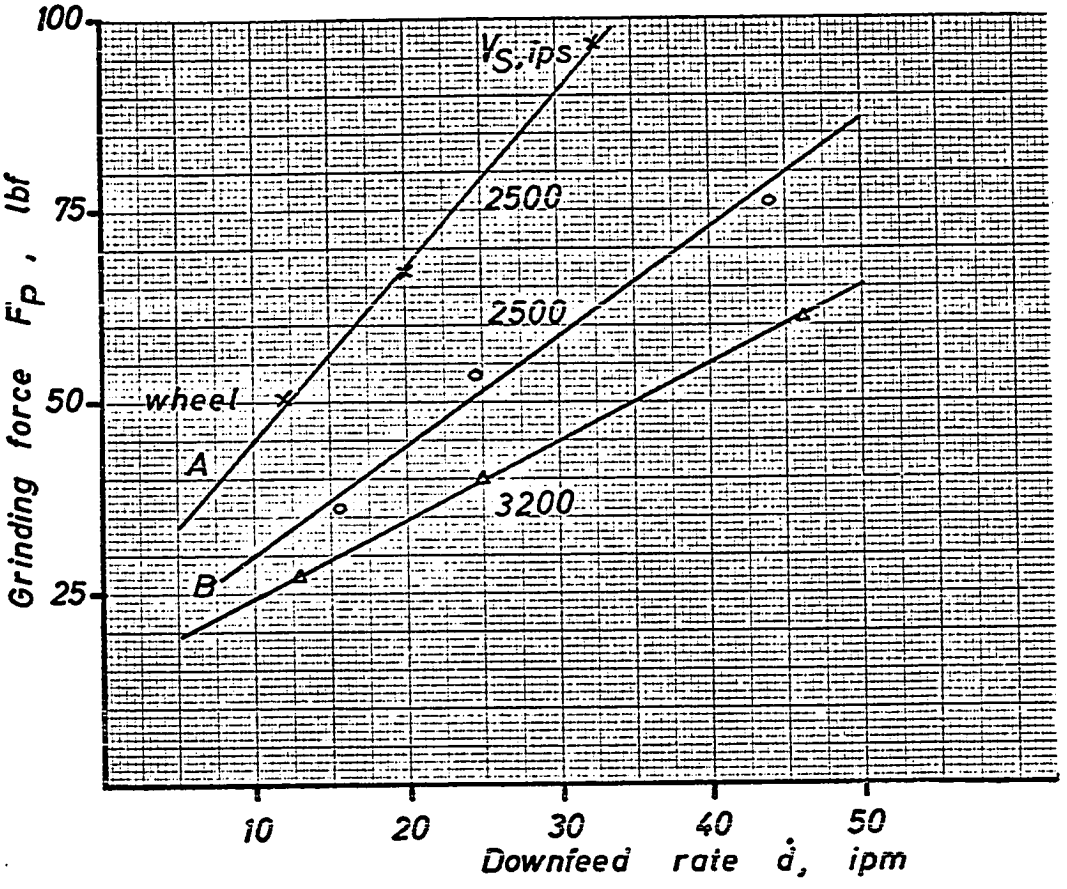

Figure 2.10 Horizontal Grinding Force as a Function of Downfeed Rate

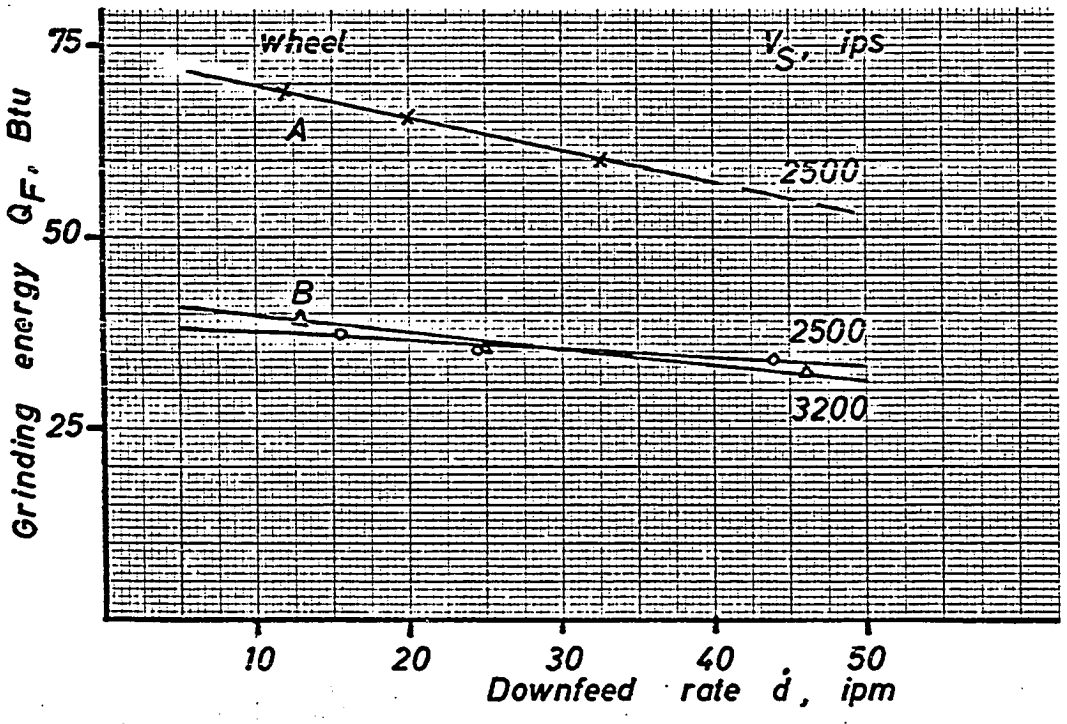

Figure 2.11 Grinding Energy as a Function of Downfeed Rate

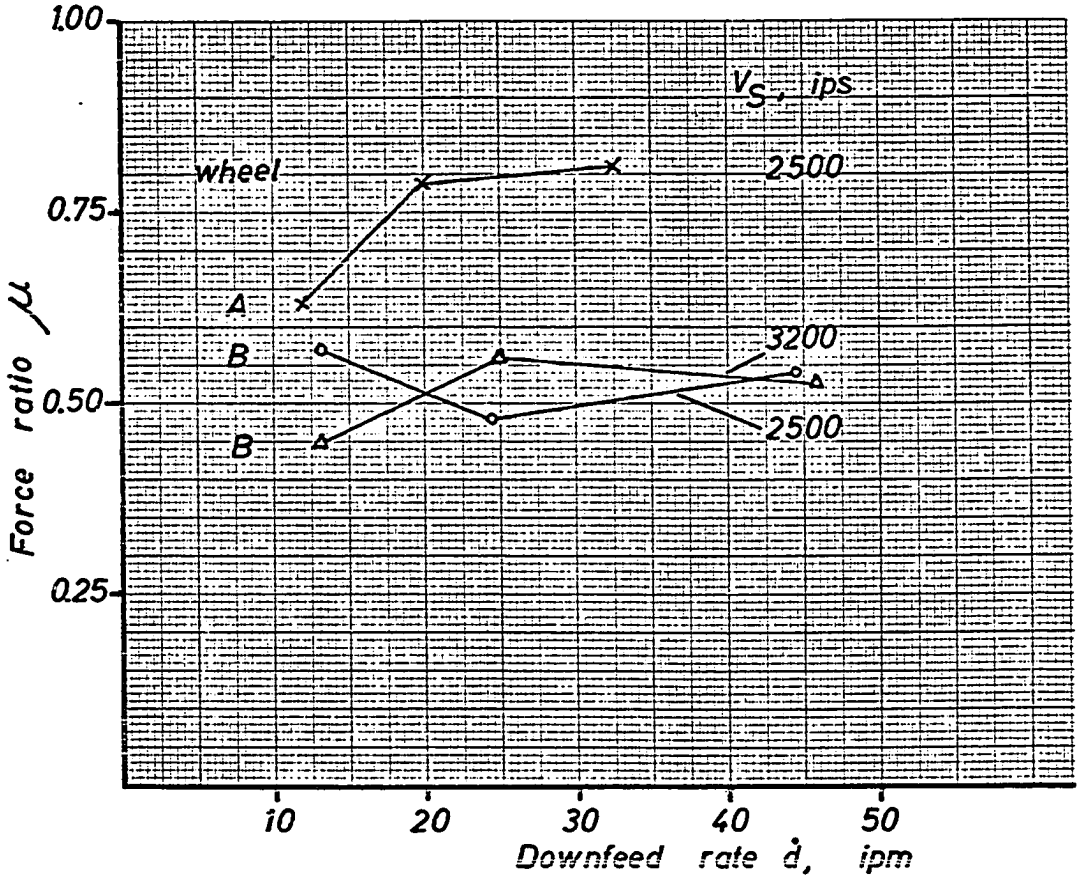

Figure 2.12 Ratio of Horizontal to Vertical Grinding Force as a Function of Downfeed Rate

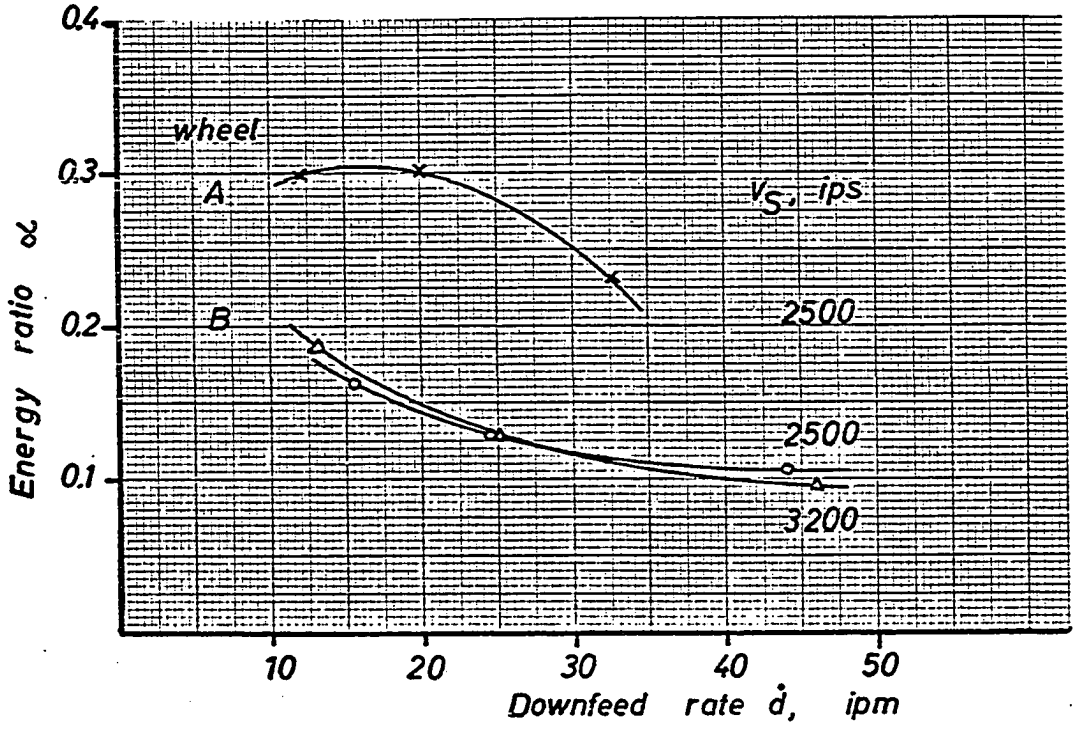

Figure 2.13 Ratio of Heat Energy Generated in the Workpiece to Mechanical Energy Consumed in Abrasive Cut-Off

Figure 2.12 and 2.13 the ratio, μ, of tangential to radial component of the grinding force and the ratio, α, of heat energy to total energy are plotted, respectively.

It can be seen that wheel A requires almost twice as much energy for the same cut as wheel B. In addition, about twice as much of the energy consumed remains in the work as heat energy which totals four times the value of wheel B when the cut is made with wheel A (Figure 2.14). The reason for this large difference in performance is believed to be the fact that wheel A was untreated while wheel B contains effective fillers (lubricants). Furthermore, measurements of wheel wear indicate that wheel B was of softer grade than wheel A. This means the wheel is effectively sharper since dull grains are lost earlier than with harder grade wheels and there will be less rubbing of bond material against the workpiece. The effect of feed rate on α is that α decreases with increasing downfeed rate. This result is in agreement with statements made in references [8, 30] that with reduced feed rates the heat front travels faster than the wheel through the workpiece, thus raising the workpiece temperature under the wheel and because of the longer cutting time allowing more heat energy to be conducted sideways into the workpiece.

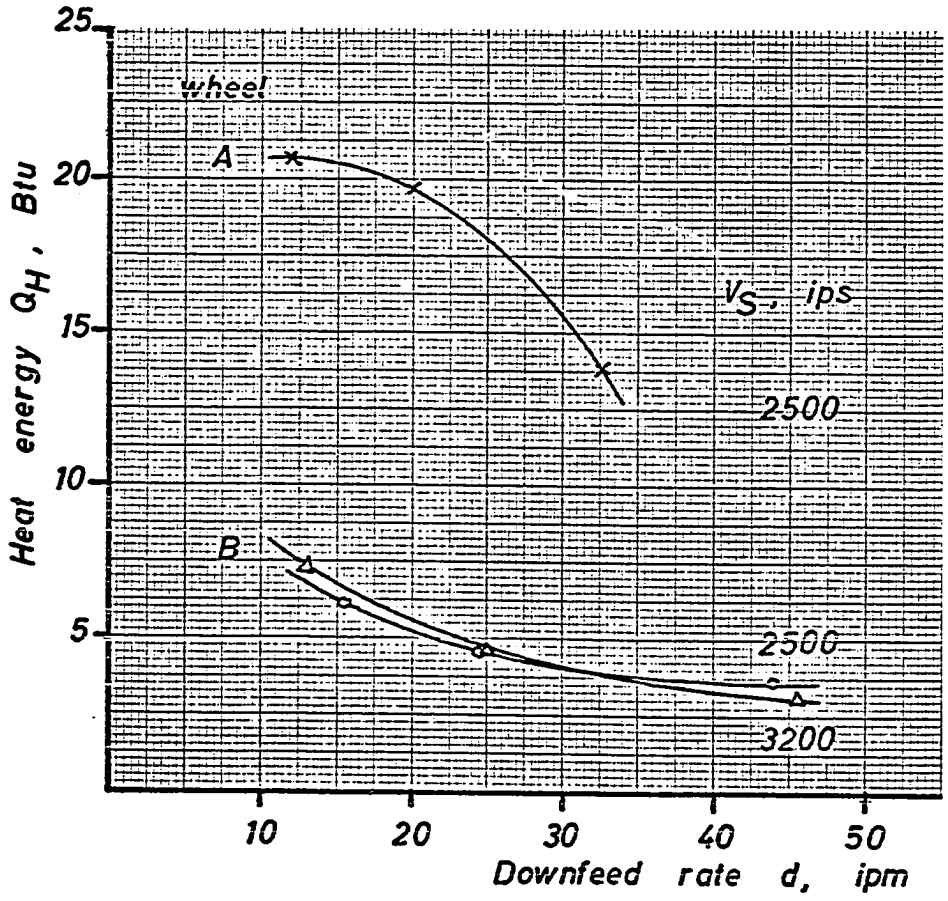

Figure 2.14 Heat Energy Generated in the Workpiece as a Function of Downfeed Rate

The dependence of feed rate is more pronounced for a high wheel speed than it is for a lower wheel speed. Other than that raising the wheel speed from V_S = 2500 ips to V_S = 3200 ips does not greatly effect the ratio α and also the absolute values of energy consumed in making the cuts remain approximately constant.

While it is not possible to predict the temperature in the contact zone using this model some conclusions can be drawn by comparing the results obtained under various grinding conditions. The amount of energy going into the workpiece increases with increasing average temperature in the contact zone and increasing time of duration of the cut if identical workpieces, wheels of constant width, and the same coolants are used. Also, it is assumed that all the energy conversion takes place in the contact zone.

These conditions were approximately satisfied in the three test series whose results are given in Table 2.3. In Figure 2.14 the total heat energy in the workpiece is plotted versus the downfeed rate. Keeping the time of cut at a constant value by making the comparison between the three series at the same downfeed rates, shows that the contact zone temperatures in the first series (Wheel A, V_s = 2500 ips) must have been very much higher than the temperatures in the other two series (Wheel B, V_s = 2500 ips and V_s = 3200 ips). In fact this difference was so great that the surfaces cut with Wheel A show signs of severe damage, while cuts with Wheel B at both speeds produced surfaces free of burn marks. A comparison of the two series run with Wheel B shows that the wheel cuts cooler at the lower speeds when low feed rates are used and when cutting is done at high feed rates the higher wheel speed gives the cooler cuts.

3 THERMAL ENERGY AND WORKPIECE TEMPERATURES IN HORIZONTAL SPINDLE SURFACE GRINDING

In the previous chapter it was shown how a relatively simple mathematical model of a complex process can be used to obtain numerical values of parameters. The limitations of the model are such that it is not possible to calculate the temperatures in the grinding zone. In the following, a more complete model of the horizontal spindle surface grinding operation is developed from which the temperatures at any point in the workpiece can be calculated. Using a similar optimization procedure heat energy input and surface convection coefficients will be determined from thermocouple temperature measurements in the workpiece.

3.1 Models of Chip Formation

The temperature rise in the workpiece is the result of the grinding action of a large number of abrasive grains in the matrix of a grinding wheel. In order to satisfactorily predict the workpiece temperatures first a model of the chip generating process must be developed which approximates all the important characteristics with sufficient accuracy and eliminates the less important details of the process.

Such a model of fine grinding operations has been developed by M. C. Shaw and several coauthors in a series of papers, [1, 19, 21, 22]. In those the authors derive equations for the average size and shape of a chip which are repeated here for ease of reference in the form applicable to horizontal spindle surface grinding.

Simplifying it is assumed that all active grains have the same radial position in the wheel and are uniformly distributed over the peripheral area of the wheel such that they produce chips of equal size and shape as shown in the Figure 3.1. The length, ℓ_c, the average width, b_c, and the maximum thickness, t, of this average chip can be computed from the operating parameters as follows:

$$\ell_c = \sqrt{Dd} \tag{3.1}$$

$$b_c = \frac{1}{2} rt = \sqrt{\frac{V_w r}{V_s C}} \sqrt{\frac{d}{D}} \tag{3.2}$$

$$t = \sqrt{\frac{4V_w}{V_s C r}} \sqrt{\frac{d}{D}}$$

In these equations:

D = wheel diameter, in.

d = depth of cut, in.

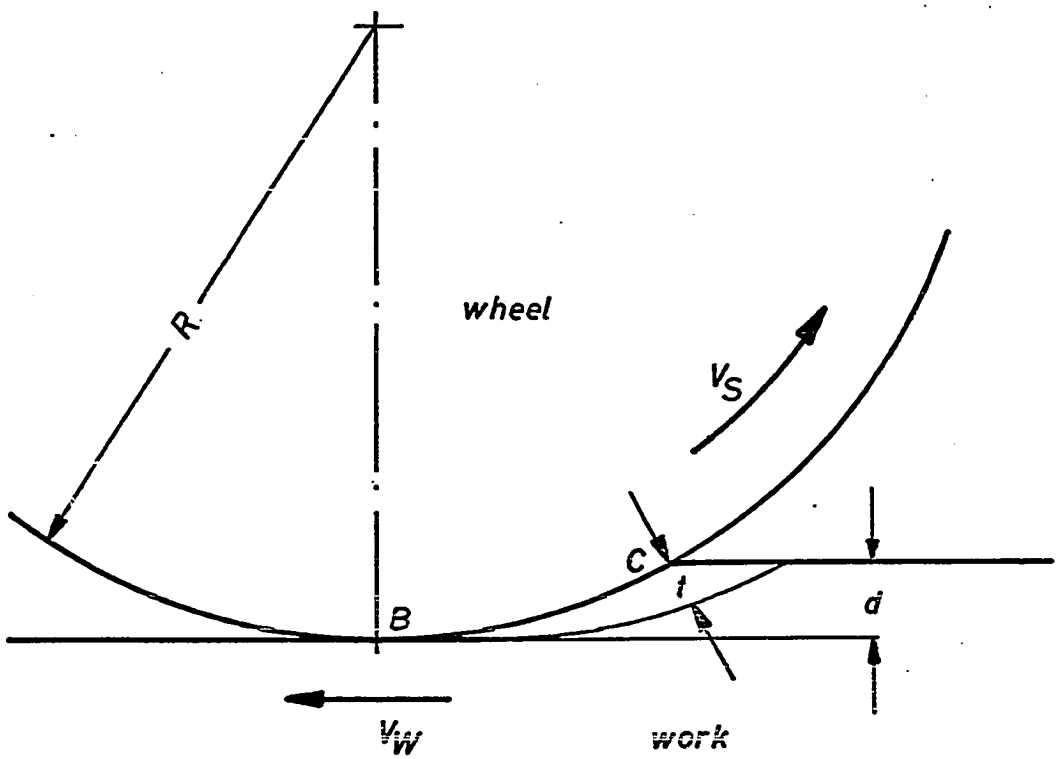

a) Interference Zone

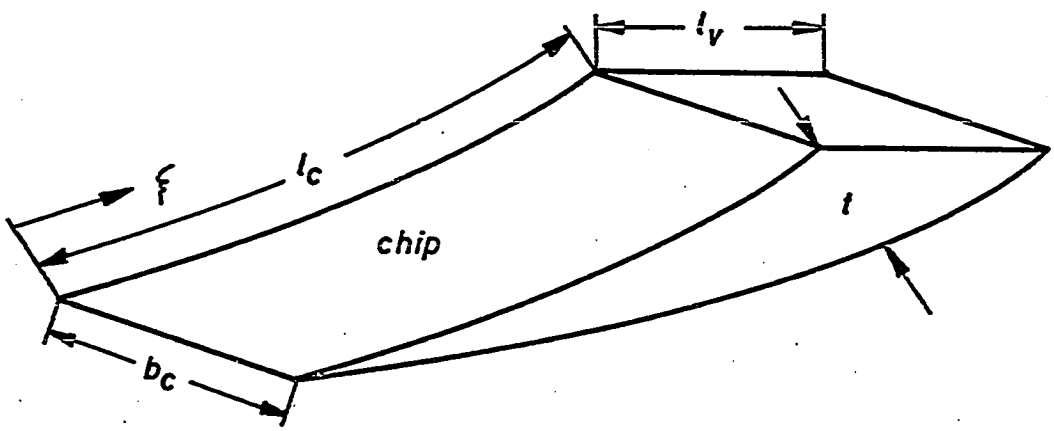

b) Ficticious Chip Shape

Figure 3.1 Interference Zone and Chip

r = ratio of chip width to chip thickness

V_W = table speed, ips

V_S = wheel speed, ips

C = number of active cutting points per unit area, $1/in^2$

In deriving equation (3.3) it was assumed that the wheel speed is much larger than the table speed. If this is not so, for instance if $V_W/V_S \geq 0.1$, it is possible for the chip thickness, t, to be larger than the depth of cut, d. This result is mathematically correct but physically it is not. It is caused by the assumption that $\ell_v/\ell_c \ll 1$ which is not true for large V_W/V_S. If ℓ_v, the amount by which the workpiece advances between two successive grains, is considered and equation (3.3) is rederived it takes the form:

$$t = \frac{V_W/V_S}{Cr\sqrt{Dd}} \left\{ \sqrt{1 + 4 \frac{Crd}{V_W/V_S} \sqrt{Dd}} - 1 \right\} \qquad (3.3a)$$

which reduces to equation (3.3) if

$$\sqrt{4 \frac{Crd}{V_W/V_S} \sqrt{Dd}} \gg 1 \quad .$$

These equations are obtained by considering the undeformed geometries of the wheel and the workpiece. Both will deform under the influence of the grinding forces and the contact geometry will change. Using

an approximate equation given by Lindsay [16] the length of contact due to flattening of the wheel for zero depth of cut was found to be negligibly small for the range of grinding conditions to be considered in the experimental part of this chapter. Since the actual values of depth of cut are measured in all tests no corrections for contact deflections will be made.

In equations (3.2) and (3.3) two variables (C and r) appear which characterize the condition of the cutting surface of the wheel. While C is a measure of the number of active cutting points per unit area, r is defined as the mean value of the ratio chip width to chip thickness. Considerable research effort has been devoted to finding numerical values for both parameters under various grinding conditions. The number of active cutting points per unit area was found to depend strongly on the undeformed chip thickness and the mean grain diameter, g, [20] and on the hardness of the wheel and the dressing conditions [18]. The ratio, r, is considered a function mainly of one variable, the mean grain diameter [4].

A different approach to the problem of determining the average geometry of grinding chips is taken by G. Kassen in his doctoral thesis [15]. He does not assume that all active cutting points have the same height in the wheel, rather he uses statistical methods to determine the average properties of the chips. The resulting equations are similar to the ones obtained assuming that equally sized and shaped chips are produced. The equations

are repeated here for easier reference in the form applicable to surface grinding:

$$\ell_e = 0.715 \sqrt{Dd} \tag{3.4}$$

$$b_n = 1.16\, r \frac{t_n}{2} \tag{3.5}$$

$$t_n = 0.71 \sqrt[3]{\frac{4V_w}{V_s C_l r} \sqrt{\frac{d}{D}}} \tag{3.6}$$

In these equations:

ℓ_e = mean value of undeformed chip length, in.

b_n = mean value of average chip width, in.

t_n = mean value of maximal chip thickness, in.

C_l = slope of the straight line N_{stat} versus z where N_{stat} is the number of cutting points per unit area in the surface layer of thickness, z, of the wheel surface. It is a constant for every wheel.

The forms of equations (3.4, 3.5, 3.6) equal the forms of equations (3.1, 3.2, 3.3) with the following approximation. Nakayama and Shaw expressed the variation of the number of active cutting points with chip thickness as:

$$C = C_0(t - t_0) \tag{3.7}$$

where C_0 and t_0 are constants for a given wheel. If t_0 is assumed to be small compared to t, equation (3.7) can be written as

$$C = C_0 t \tag{3.8}$$

Combining equations (3.3) and (3.8) yields:

$$t = \sqrt[3]{\frac{4V_w}{V_s C_0 r}} \sqrt{\frac{d}{D}} \tag{3.9}$$

which is built similar to equation (3.6). It is thus clear that two approaches give essentially the same results, the differences being only in the numerical values of constants.

It should be noted at this point that the chip shape shown in Figure 3.1b is not the shape of an actual chip. That shape was chosen only on the basis of volume continuity, i.e., it can easily be visualized how a uniform layer of material of thickness, d, is composed of many equally sized chips of the shape shown. At present there is no chip model which shows the correct shape of an actual undeformed chip. Not only is it very difficult to account for the interaction of neighboring grains but also the material to the sides of a groove produced by one grain rises above the original surface as is illustrated in Figure 3.2 which makes it practically impossible to determine the actual chip shape.

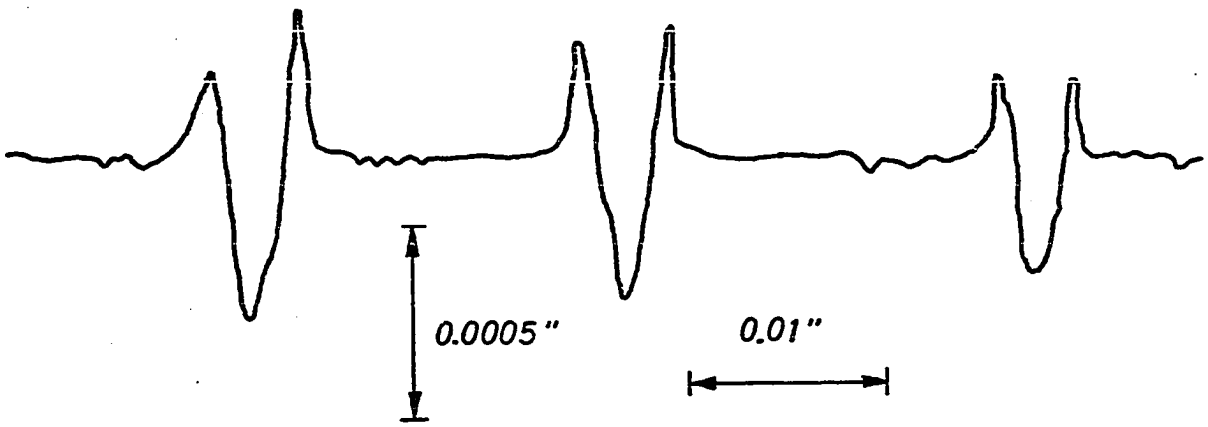

Figure 3.2 Talysurf Trace of Groove Cut by a Single Grain in Overcut Fly Milling Tests. (From Reference [28])

In both derivations of average chip properties the grains are assumed to be of conical shape. Backer and Merchant point out in reference [2] that this assumption may not always be correct and show that spherical or cubic shapes may be possible alternatives as a grain wears. Brueckner [4] finds from measurements of the grooves produced by the grinding wheel that the ratio r of scratch width to scratch depth is approximately constant for smaller grain sizes but finds increasing deviations for larger grain sizes; i.e., the shapes of the cross sectional areas of the grooves change from triangular for small grain sizes to circular for large grain sizes.

In view of the fact that in surfaces grinding grain sizes are used which can be considered small by the above property no attempt will be made in this thesis to rederive equations (3.1) through (3.6) for grains of circular cross sections. Equations (3.1, 3.2, 3.3) will be used since the number of active cutting points per unit area appears explicitly in equation (3.3) which is the fundamental quantity measured by all tracing or imprinting methods. Also, using equations (3.1, 3.2) and (3.3) guarantees that the combined volume of all chips removed during some time interval is equal to the total volume of material removed during the same time.

These geometric simplifications are certainly effecting the calculated temperatures in the workpiece. In view of the aforementioned complexities in the chip forming process it can be said, though, that this simple approach will give results as good as models assuming more complex shapes would.

For the calculations of workpiece temperatures it is also important to characterize the kinematic interaction between a grain and the workpiece and the chip. Previous investigators [21, 18, and 7] have used the model of a single point cutting tool as a model of a single grain forming a chip (Figure 3.3a). In the light of recent studies of the chip formation process this model does appear to be not sufficient. For instance, the amount of heat energy introduced into the workpiece due to the grinding action was found to be greater than 70%. According to the above model one would expect

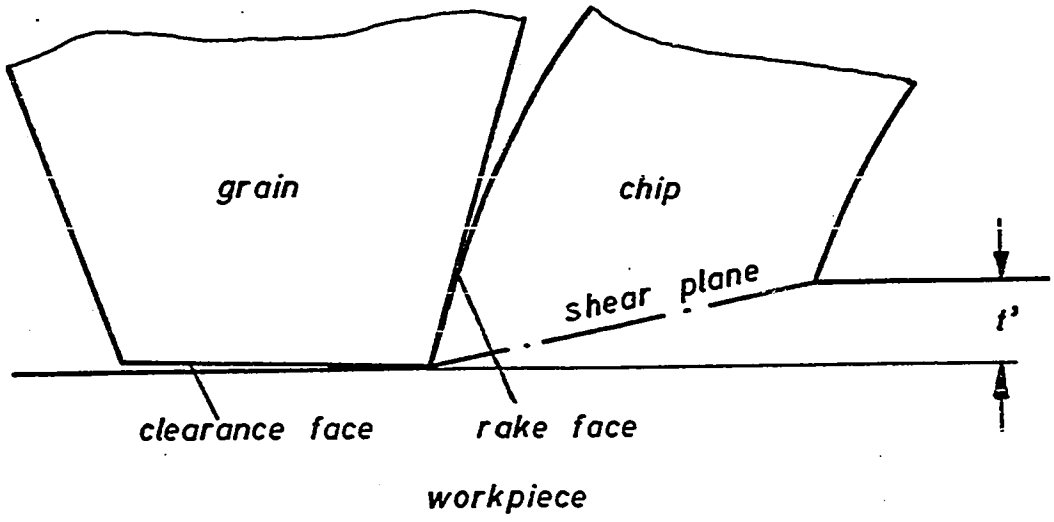

a) Model: Single Point Cutting Tool

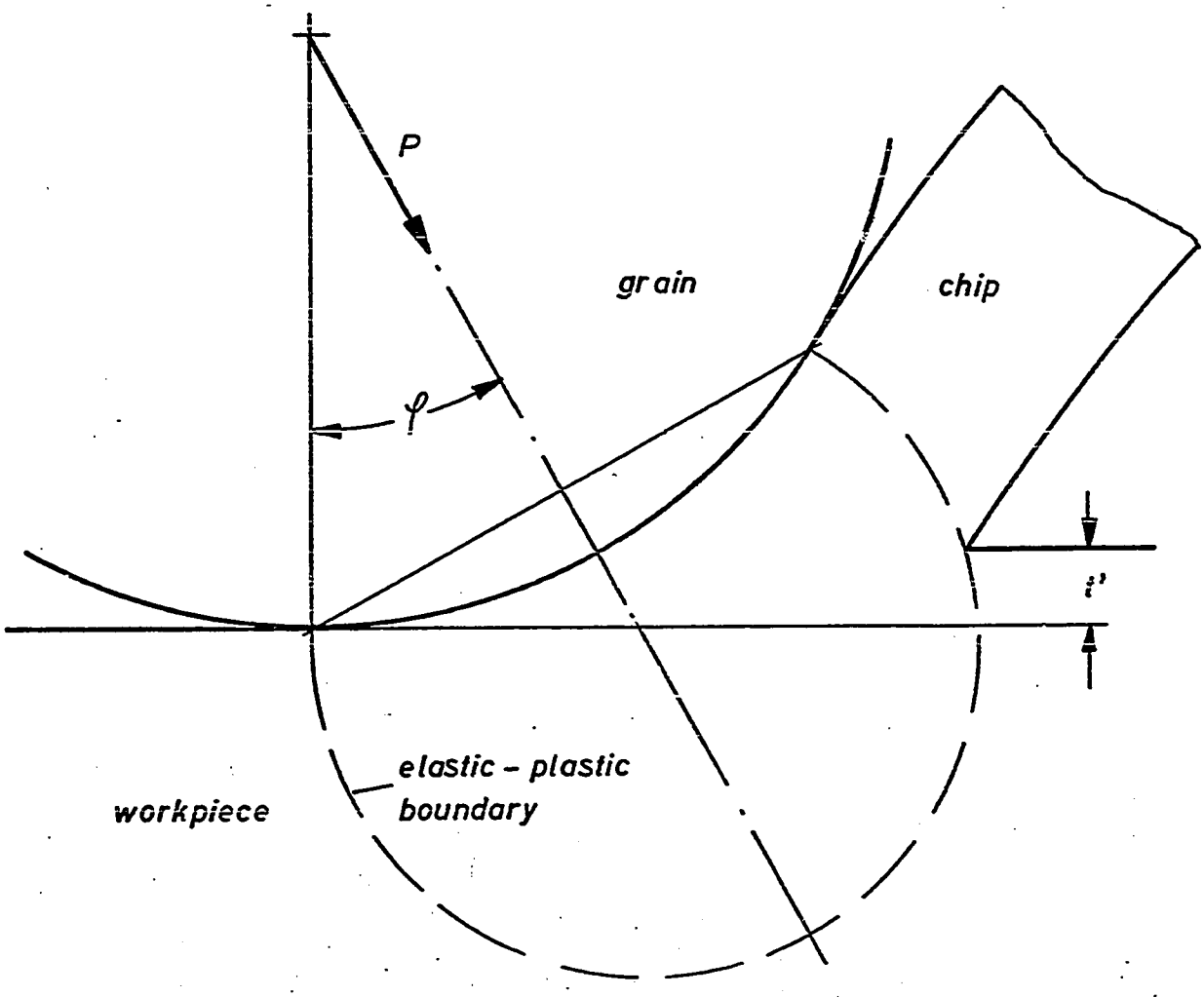

b) Model: Hardness Test (From Shaw [27])

Figure 3.3 Chip Formation in Grinding

this percentage to be much less than 10% which is the value found in cutting with single point tools on a lathe at speeds of 100 fpm since the amount of heat energy was found to decrease with increasing cutting speed and in grinding wheel speeds of 6000 fpm and higher are used. Also, the ratio, μ, of power to pressure force components has a value of about $\mu = 0.5$ in grinding while its value is $\mu = 2.0$ in turning. Here it was found that μ decreases with decreasing rake angle. This suggests that large negative rake angles are present at the tips of the grains in grinding which conclusion is in good agreement with observations of the shapes of the grains.

Hahn discusses in reference [10] the mechanism of metal removal in grinding using a blunt indenter inclined at an angle $\tan \theta = \mu$ as a model of the grain. He shows, that the workpiece material deforms plastically under the grain to a depth larger than the undeformed chip thickness. Similar conclusions were arrived at by Shaw [27] who used an inclined Brinell Hardness indenter as a model of the grain (Figure 3.3b). His model and a newly developed theory for elastic-plastic hardness indentations [26] are shown to be very efficient in describing many phenomena associated with the chip formation process in grinding.

Especially important for studies of grinding temperatures is the fact that a large amount of heat energy is produced deep in the workpiece itself due to the deformation of the workpiece material. Therefore, only a small fraction of the generated heat energy can

be carried away with the chips. At this time it is not known how the energy is distributed over the deformed zone. Nevertheless, a substantial contribution to the temperature rise in the workpiece is expected from the energy necessary to cause deformations beneath the grain of which most is converted into heat energy due to internal friction. In the following this heat source will be called volume heat source. For the purpose of this thesis it is assumed that its strength, q_V, is an exponential function of the depth, z

$$q_V = q_{VO}\, e^{-\beta z} \quad , \qquad \frac{Btu}{sec\ in^2} \tag{3.10}$$

where

q_{VO} = strength of volume heat source at the surface z = 0

β = decay coefficient of deformation energy with depth z

The exponential dependence on z was determined experimentally in modified Brinell Hardness tests during which the test piece was moved relative to the indentor. The value of the decay coefficient was determined as

$$\beta = 27.73\ i/in$$

A description of these tests can be found in the Appendix.

In addition to this volume source there will be heat sources acting at the surface of the workpiece at the interface between the grain and the workpiece and at the interface between the chip and the workpiece. Both will here be treated combined into one single surface heat source of strength q_S. The plane over which both heat sources extend is indicated in Figure 3.4 by line $\overline{B'C'}$. Its width b_G equals the width of the chip:

$$b_G = b_c \tag{3.11}$$

The length of this plane $\overline{B'C'}$ is l_G. It is determined by the region of plastic flow under the grain which depends on the instantaneous chip thickness and on the grain geometry in addition to the material properties and lubrication of the interface. The effects of grain size and shape, sharpness of the grain, and friction between the grain and the work material are discussed qualitatively in reference [27]. Some quantitative results are obtained from the following analysis which compares the chip formation in grinding to a hardness test. For the latter the extent of the zone of plastic deformation can be approximated by a sphere of radius

$$a_p = 1.21\ a \tag{3.12}$$

where a is the radius of the indentation. The load F to produce this indentation is given by

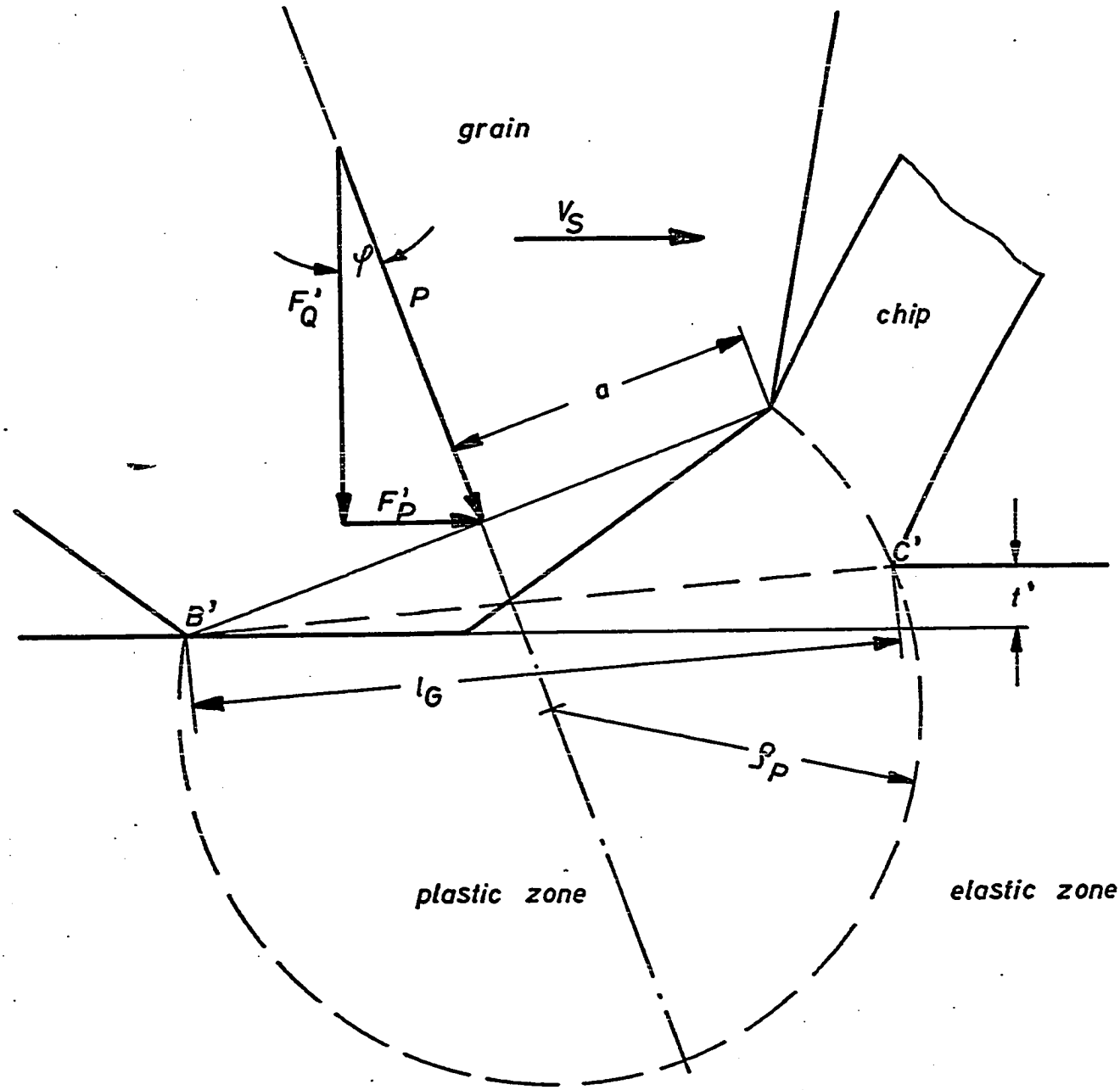

Figure 3.4 Model of Chip Formation Process in Grinding

$$F = \pi a^2 H_W \tag{3.13}$$

with H_W = bulk hardness of the material.

In the chip formation process, a, can be taken as the mean radius of the area of contact between the grain and the workpiece, F is the force exerted by the grain normal to the area of contact and H_W is the hardness of the material at elevated temperature. From Figure 3.4:

$$F = \sqrt{F_P'^2 + F_Q'^2} = \sqrt{\mu^{-2} + 1}\ F_P' \tag{3.14}$$

with

$$\mu = \frac{F_P'}{F_Q'}$$

When equations (3.12), (3.13), (3.14) are combined an equation relating F_P' and a_P results.

$$a_P = 1.21 \left[\sqrt{\mu^{-2} + 1}\ \frac{F_P'}{\pi H_W} \right]^{1/2} \tag{3.15}$$

The horizontal grinding force per grain, F_P', is proportional to the instantaneous chip thickness, t'.

$$F_P' = E_0 t' \tag{3.16}$$

The factor of proportionality, E_0, is obtained by considering all M_C grains in contact with the workpiece at any instance of time:

$$M_C = B \ell_c C \tag{3.17}$$

The total force, F_P, which is measured with a dynamometer is the sum of the contributions of all M_C grains. The average force per grain is, therefore:

$$F'_{P0} = F_P / M_C \tag{3.18}$$

Also

$$F'_{P0} = \frac{1}{t} \int_0^t F'_P \, dt' = \frac{E_0 t}{2}$$

From which equations follows

$$E_0 = 2 \frac{F_P}{M_C t}$$

and

$$F'_P = 2 \frac{F_P}{M_C} \frac{t'}{t} \tag{3.19}$$

Equations (3.15) and (3.19) are combined to yield an expression relating the size of the plastic zone to the instantaneous chip thickness:

$$a_p = 1.21 \left[2\sqrt{\mu^{-2} + 1}\ \frac{F_p}{M_c \pi H_w} \frac{t'}{t} \right]^{1/2} \tag{3.20}$$

Knowing the size of the zone of plastic flow the distance $\overline{B'C'}$ is found to be approximately:

$$\ell_G \doteq 2 \left[2\sqrt{\mu^{-2} + 1}\ \frac{F_p}{M_c \pi H_w} \frac{t'}{t} \left\{ 1.455 - \left(\frac{0.674}{\sqrt{\mu^{-2} + 1}} - \frac{1/\mu}{\sqrt{\mu^{-2} + 1}} \right)^2 \right\} \right]^{1/2}$$

For fine grinding μ has a value of about 0.5. Thus:

$$\ell_G \doteq 3.38 \sqrt{\frac{F_p}{M_c \pi H_w} \frac{t'}{t}} \tag{3.21}$$

The two equations (3.11) and (3.21) describe the geometry of the model of chip formation together with equation (3.10) which describes the depth effect of the interaction between grains and workpiece. Equations (3.1), (3.2), (3.3) relate mean chip dimensions to machining and wheel parameters. In the following section this simplified physical model will be used as the basis for an abstract mathematical model for the calculations of the temperature field in the workpiece due to the grinding action.

3.2 Mathematical Model for Temperature Calculations in Plunge Grinding

3.2.1 Development of Wheel - Workpiece Models

The temperature in the workpiece is the result of the grinding action of all grains. Each of them contributes a small temperature rise to the total temperature as it passes through the contact area. The temperature rise caused by a single grain can be calculated by considering the grain to be a moving source of heat and applying the equations Jaeger derived in reference [13] from the theory of moving sources of heat. However, due to practical limitations in computer size and time it is not possible to simulate the temperature in the workpiece by superimposing many solutions for individual grains. In his thesis [7] DesRuisseaux describes a more elegant way which gives a very good approximation with much less effort.

Noting that even though there is only a small number of grains in contact with the workpiece at any instant of time ($M_C \doteq 0.25 \times 0.1 \times 1000 = 25$) they are moving much faster than the workpiece does. During the time a point of the workpiece enters the contact area until it leaves again ($\tau_C = \frac{\ell_C}{V_W} \doteq \frac{0.1}{10} = 0.01$ sec) a large number of grains has contacted it ($M = CBV_S\tau_C \doteq 1000 \times 0.25 \times 800 \times 0.01 = 2000$).

It is then possible to combine the action of all M grains and to consider the wheel as one single heat source moving with velocity V_W over the workpiece. In doing so instantaneous temperature peaks under the grains are neglected and only the bulk interference zone

temperatures are calculated. The maximum temperature peaks are then introduced by superimposing over the bulk temperature the maximum temperature rise due to a single grain as it moves through the contact area. It is thus possible to obtain an approximate solution by combining the temperature rises due to only two sources:

a.) the interference zone heat source and

b.) the single grain heat source.

For the purpose of this thesis it will be assumed that the workpiece can be represented by a semi-infinite region, R, shown in Figure 3.5:

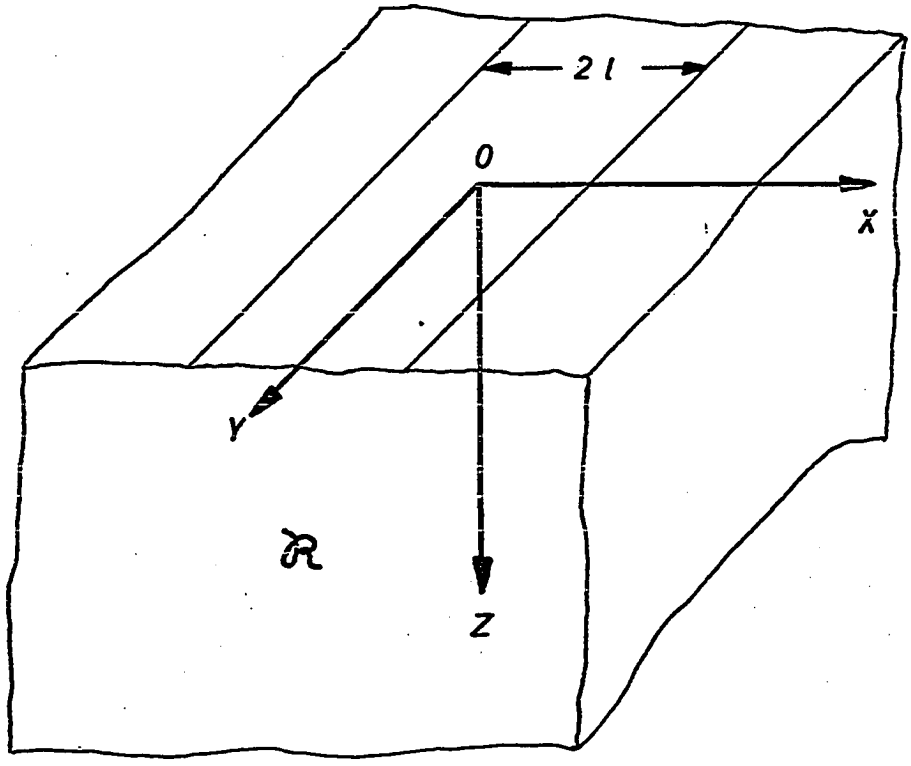

Figure 3.5 Mathematical Model of the Workpiece in Surface Grinding

$$R = \left\{ \begin{array}{l} -\infty < x < \infty \\ -\infty < y < \infty \\ 0 \leq z < \infty \end{array} \right\} \qquad (3.22)$$

The area of contact between the wheel and the workpiece extends from $x = -\ell$ to $x = \ell$ and infinitely far in the y-direction, so that there are no temperature variations in y when the workpiece moves with constant velocity, V_W, relative to the stationary wheel in the negative x-direction. The coordinate system is fixed to the wheel. This description fits well for workpieces in plunge grinding where the wheel width is equal to or greater than the width of the workpiece whose sides are insulated (Figure 3.6) and which is long in the direction of table motion. Crisp [6] showed that the temperature in a four inch long workpiece approaches the temperature in an infinitely long piece after cutting a distance of less than one half of an inch when grinding with a table speed of two inches per second. At higher table speeds the steady state temperature distribution is approached after an even shorter cutting distance. Since the depth of cut, d, is much smaller than the length of contact, ℓ_c, plane $z = 0$ of the model can represent the surface ABOCD of the workpiece (Figure 3.6).

The grinding wheel itself will not be modelled, only its interaction with the workpiece. This interaction takes the form of a heat source of strength

$$\dot{Q}_{IO} = \alpha \dot{Q}_F \ , \qquad \frac{Btu}{sec} \qquad (3.23)$$

distributed over the area of contact between the wheel and the workpiece. In equation (3.23) α is the fraction of total grinding power, $\dot{Q}_F$, which enters the work.

$$\dot{Q}_F = \frac{F_P V_S}{12\ 778}\ , \qquad \frac{Btu}{sec} \tag{3.24}$$

where:

F_P = tangential component of the grinding force, lbf

V_S = wheel speed, ips

The ratio, α, is assumed to be constant over the contact area. This total heat input by the grinding wheel is the sum of contributions of all grains in contact with the workpiece at any instant of time. Total number of active grains, M_C, is given by equation (3.17). Upon combining equations (3.17) and (3.23) the power, $\dot{Q}_{GO}$, per grain is given by:

$$\dot{Q}_{GO} = \frac{\alpha \dot{Q}_F}{\ell_c BC}\ , \qquad \frac{Btu}{sec} \tag{3.25}$$

This is an average value over the length of contact between wheel and workpiece. The instantaneous value of the rate of energy generation depends on the instantaneous chip thickness. This relationship is linear since the force exerted by a grain will be proportional to the cross sectional area of the chip which is a linear function of the chip thickness in the chip model discussed in the previous section (Figure 3.1b). Using the coordinate system

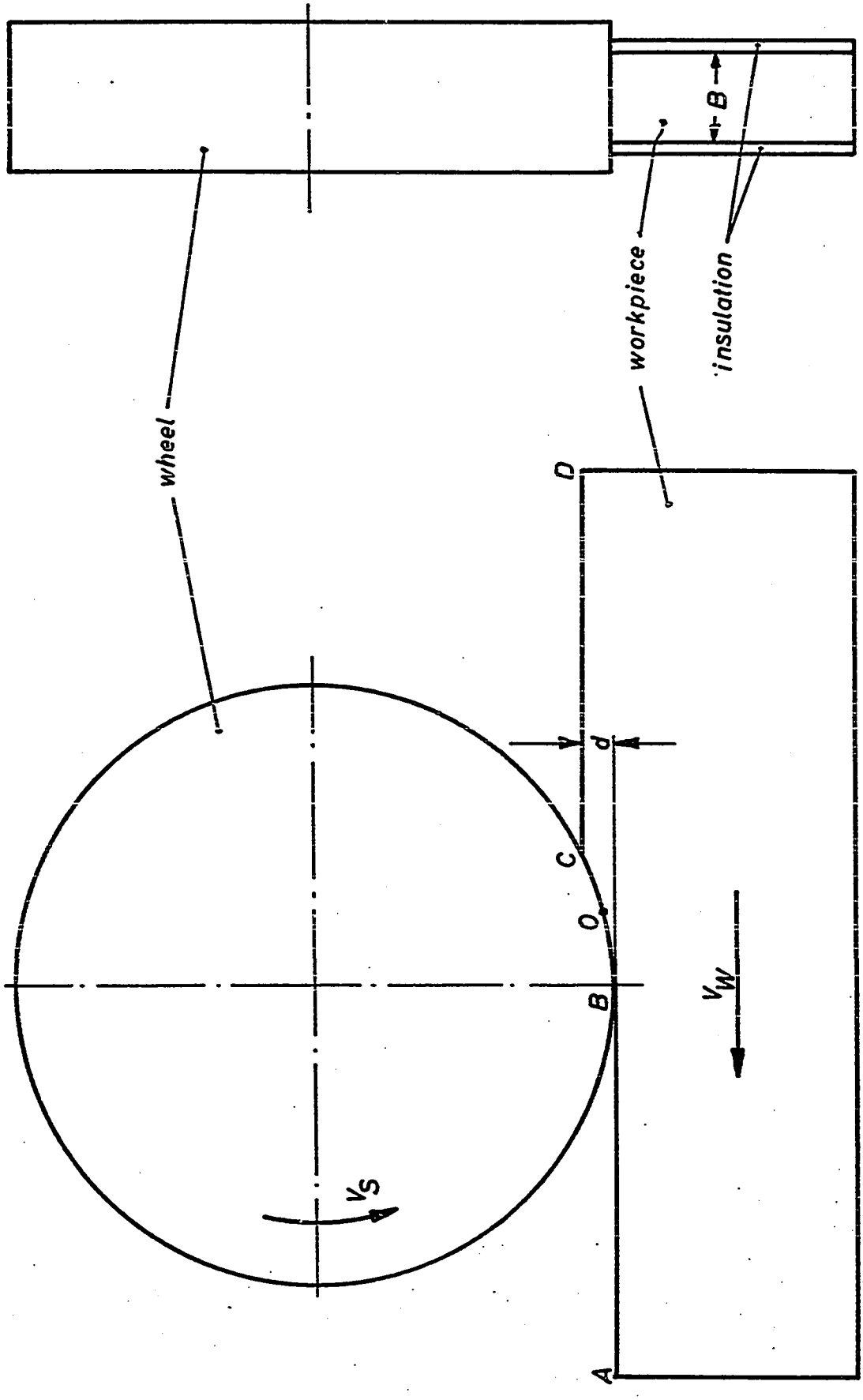

Figure 3.6 Plunge Surface Grinding

defined in Figure 3.5 and attaching it to the wheel at point 0 (Figure 3.6) allows the instantaneous work done by a grain to be calculated as a function of its position, x:

$$\dot{Q}_G = \frac{\alpha}{12\ 778} \frac{F_P V_S}{\ell_c BC} \left(1 + \frac{2x}{\ell_c}\right) , \qquad \frac{Btu}{sec} \tag{3.26}$$

Accordingly, the power converted into heat in the contact zone is a function of location x:

$$\dot{Q}_I = \dot{Q}_{IO} \left(1 + \frac{2x}{\ell_c}\right) , \qquad \frac{Btu}{sec} \tag{3.27}$$

Applying this method of calculating temperatures in the workpiece to the physical model of the process of chip formation derived in section 3.1 results in four sources of heat whose associated temperature rises are superimposed to give the total temperature rise in the workpiece due to one pass of the grinding wheel over the workpiece which initially is assumed to be at uniform bulk temperature, T_B. The equations for the strength of the four sources are:

a) surface heat source

aa) interference zone heat source

$$\dot{Q}_{IS} = \alpha_1 \dot{Q}_F , \qquad \frac{Btu}{sec}$$

$$q_{IS} = \frac{\alpha_1}{12\ 778} \frac{F_P V_S}{\ell_c B} \left(1 + \frac{2x}{\ell_c}\right) , \qquad \frac{Btu}{in^2\ sec} \tag{3.28}$$

ab) single grain heat source

$$\dot{Q}_{GS} = \alpha_1 \frac{\dot{Q}_F}{M_C} , \qquad \frac{Btu}{sec}$$

$$q_{GS} = \frac{\alpha_1}{12\ 778} \frac{F_P V_S}{(\ell_c BC)(\ell_G b_G)} \left(1 + \frac{2x}{\ell_c}\right) , \qquad \frac{Btu}{in^2\ sec} \tag{3.29}$$

b) volume heat source

ba) interference zone heat source

$$\dot{Q}_{IV} = \alpha_2 \dot{Q}_F , \qquad \frac{Btu}{sec}$$

$$q_{IV} = \frac{\alpha_2}{12\ 778} \frac{\beta F_P V_S}{\ell_c B} \left(1 + \frac{2x}{\ell_c}\right) , \qquad \frac{Btu}{in^2\ sec} \tag{3.30}$$

bb) single grain heat source

$$\dot{Q}_{GV} = \alpha_2 \frac{\dot{Q}_F}{M_C} , \qquad \frac{Btu}{sec}$$

$$q_{GV} = \frac{\alpha_2}{12\ 778} \frac{\beta F_P V_S}{(\ell_c BC)(\ell_G bG)} \left(1 + \frac{2x}{\ell_c}\right) , \qquad \frac{Btu}{in^2\ sec} \tag{3.31}$$

In these equations:

α_1 = fraction of total grinding energy entering the workpiece through the surface z = 0

α_2 = fraction of total grinding energy entering the workpiece due to deformation of the material.

such that

$$\alpha_1 + \alpha_2 = \alpha$$

As was mentioned before this model of a semi-infinite body can be used to simulate a finite body if this finite body is large enough so that end effects can be neglected in the center portion of the body and the actual temperature distribution can be approximated by the steady state temperature distribution in the semi-infinite model. In reference [13] Jaeger shows that the temperatures at the center of a rectangular or circular heat source approach the temperature distribution under a surface heat source of the same intensity which extends infinitely far in the direction perpendicular to the direction of motion (band heat source) if its nondimensional width is not too small. It is also shown that large variations of the shape of the heat source area have only a small effect on the resultant temperatures. The non-dimensional width, W, is defined as:

$$W = \frac{V}{2\kappa} w$$

where:

V = velocity of the heat source

κ = thermal diffusivity of the material

w = width of the heat source

From this equation it is clear that large nondimensional widths can be achieved by either large w and/or large V. Taking the example of a grain in the grinding wheel which acts as a heat source for the workpiece as it moves through the contact area the width of this heat source is very small:

$$w = b_G = \frac{1}{2} r t \doteq 0.0001 \text{ in}$$

The contact velocity on the other hand is very large:

$$V = V_S \doteq 800 \text{ ips}$$

Using for κ the value of the thermal diffusivity of mild steel at 1000°F:

$$\kappa = 0.0106 \text{ in}^2/\text{sec}$$

the value of the nondimensional width is found to be:

$$W \doteq 800/(2\ 0.0106)\ 0.0001 = 3.77$$

This value is large enough to justify the treatment of the single grain heat sources as band heat sources. Therefore, the same

mathematical model can be used for both the interference zone heat sources and the single grain heat sources.

In his paper Jaeger also gives an estimate of the time required to reach the peak temperature in the region due to a surface heat source of constant strength. This analysis is extended to include all heat sources necessary to describe the grinding process and the time required to reach the maximum temperature due to each heat source at any point in the region, τ_{SS}, is determined. Theoretically, these times would be infinite. For this reason the times to reach 99.99% of the maximum values are obtained. By curve fitting, the following expression for τ_{SS} is found to hold for all heat sources considered:

$$\tau_{SS} = \frac{2\ell - x + 0.5z + 20\kappa/V}{V} \qquad (3.32)$$

where the coordinate system is defined as in Figure 3.5. It is assumed that a steady temperature field is established in the region when the temperatures at all points have reached 99.99% of their maximum temperatures. The region in which the highest temperature rises are expected is given by:

$$-2 \leq \frac{x}{\ell} \leq 1$$

$$0 \leq \frac{z}{\ell} \leq 2$$

In order to establish here a steady temperature field the heat source must be moving for the time

$$\tau_{SS} = \frac{5\ell + 20\kappa/V}{V} \tag{3.33}$$

through the distance

$$\ell_{SS} = V\tau_{SS} = 5\ell + 20\,\frac{\kappa}{V} \tag{3.34}$$

The use of equations (3.33) and (3.34) will be illustrated by an example. A grain is moving over the workpiece surface with V = 800 ips. The maximum length of contact is approximately ℓ_G = 0.0005 in ($\ell = \ell_G/2$). The value of the thermal diffusivity is as in the previous example κ = 0.0106 in^2/sec. The time for a steady temperature field to build up is thus

$$\tau_{SS} = 15.62\ \mu sec$$

and the distance through which the grain moves during this time is

$$\ell_{SS} = 0.012\ in$$

which is approximately one-eighth of the total length of travel of the grain over the workpiece, ℓ_c. The travel length appears to be sufficiently larger than ℓ_{SS} so that the assumption of a steady temperature field is justified for single grain heat sources although their size and strength vary with position.

One more property of the surface grinding process is needed for a useful description. Most grinding takes place with a heavy stream of coolant running over the surface of the workpiece. There are two reasons for this practice:

a) cooling of the workpiece and the wheel, i.e., removing the heat energy once it has been generated, and
b) lubrication of the interface between wheel and workpiece which reduces the amount of heat energy generated.

While the second property of the coolants can be accounted for in the model by a reduction in the strength of the total heat source and, may be, by different energy ratios, α, it is necessary to introduce a specific boundary condition at the surface $z = 0$ of the model to account for the cooling effect of the grinding fluids. It will be assumed that there is Newtonian cooling at a uniform rate h, Btu/(in^2 sec °F) from the surface $z = 0$ when calculating the bulk temperature rise. This assumes the same rate of convection from the area under the wheel as for the rest of the workpiece surface. Even though this is not quite true, this assumption makes analytical solutions possible. When calculating the maximum temperature rise due to a single grain no cooling from the surface will be assumed. This assumption is very good, as will be shown later, due to the high speed with which the grain moves over the workpiece.

Having thus defined the region and the type and strength of heat sources acting upon it the equations of the temperature fields due to these heat sources in the region will be derived in the following paragraphs. It is postulated that the temperatures so calculated are a good approximation of the temperatures encountered in surface grinding under plunge grinding conditions.

3.2.2 Temperature Field in a Semi-Infinite Solid Due to Moving Sources of Heat

The temperature field T (x, z, τ) in a moving semi-infinite body as shown in Figure 3.7 with stationary surface and volume heat sources is defined by the differential equation:

$$\nabla^2 T = \frac{1}{\kappa}\left(\frac{\partial T}{\partial \tau} - V\frac{\partial T}{\partial x} + \frac{qV}{\rho C}\right) \tag{3.35}$$

where

$$q_V = \begin{cases} 0 & \text{for } |x| > \ell \\ q_V(x,z) & \text{for } |x| \leq \ell \end{cases}$$

and the boundary condition:

$$k\frac{\partial T}{\partial z}(x,0,\tau) = q_H - q_S \tag{3.36}$$

where

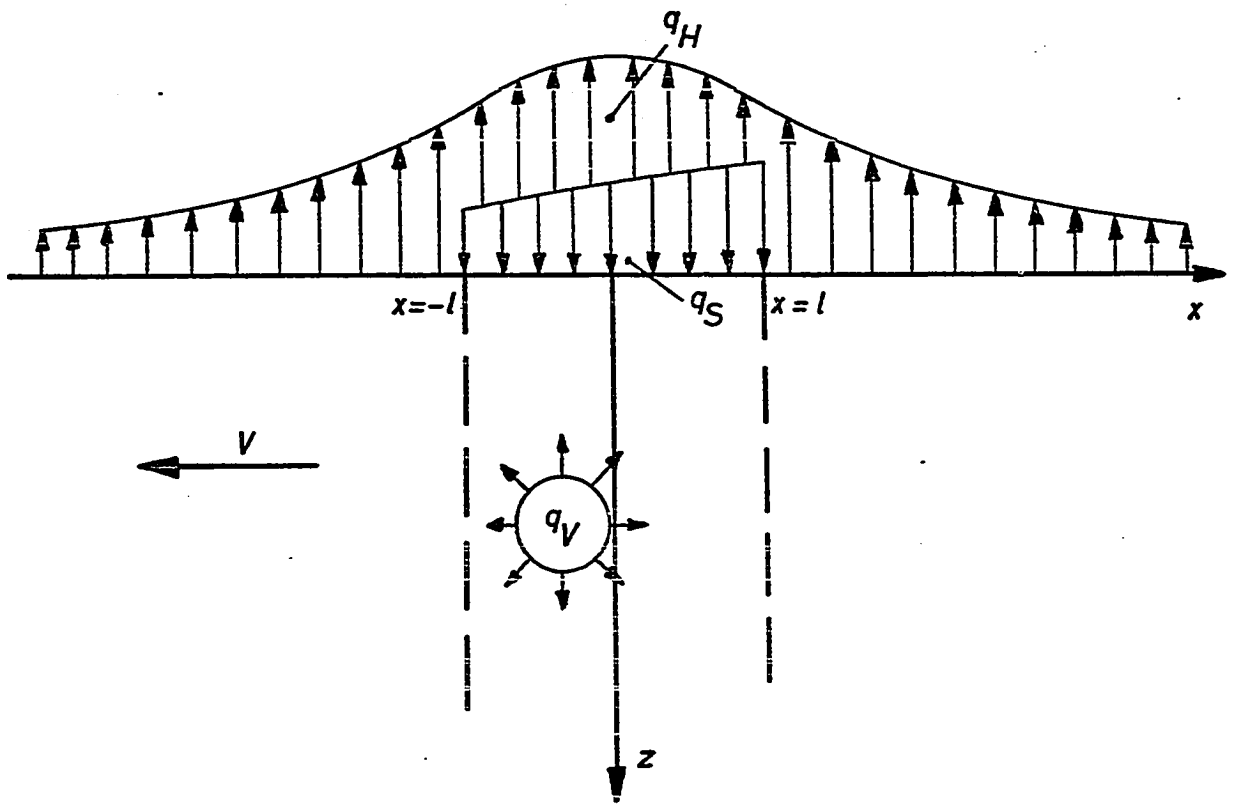

Figure 3.7 Heat Source Model for Semi-Infinite Solid

$$q_H = hT(x,0,\tau)$$

$$q_S = \begin{cases} 0 & \text{for } |x| > \ell \\ q_S(x) & \text{for } |x| \leq \ell \end{cases}$$

and the initial condition:

$$T(x,z,0) = 0 \qquad (3.37)$$

In making this definition it was assumed that the thermodynamic properties of the material of the semi-infinite region remain constant as the temperature varies. For real materials this assumption is not a very good one but it makes analytic solutions possible. In the next section a comparison between analytical solutions and solutions obtained by a numerical method for which the above assumption is not necessary will be described which makes it possible to evaluate for special cases the effect which varying properties have on the resulting temperatures.

The analytical solution to equations (3.35), (3.36) and (3.37) will be obtained by superposition of solutions of the temperature field in a stationary semi-infinite solid due to an instantaneous point heat source which is given in reference [5]:

$$T_P(x,y,z,\tau) = \frac{Q_P}{\rho c} \exp\{-\frac{(x - x')^2 + (y - y')^2}{4\kappa(\tau - \tau')}\}[\frac{e^{-\frac{(z - z')^2}{4\kappa(\tau - \tau')}} + e^{-\frac{(z + z')^2}{4\kappa(\tau - \tau')}}}{8\{\pi\kappa(\tau - \tau')\}^{3/2}}$$

$$- \frac{h/k}{4\pi\kappa(\tau - \tau')} \operatorname{erfc}\{\frac{z + z' + \frac{h}{k} 2\kappa(\tau - \tau')}{2\sqrt{\kappa(\tau - \tau')}}\}$$

$$\cdot \exp\{(z + z')\frac{h}{k} + \kappa(\frac{h}{k})^2 (\tau - \tau')\}] \qquad (3.38)$$

where x', y', z' are the coordinates of the point source of strength Q_P acting at time τ'.

This method has been used by Jaeger [13] and DesRuisseaux [7] to find solutions of the steady state temperature field in a moving solid due to a surface heat source of constant strength. In this section analytical solutions for eight different heat source models shown in Table 3.1 are developed.

Table 3.1 Summary of Heat Source Models

		Surface Heat Source	Volume Heat Source
Without Convection	constant strength in x-direction	$\emptyset_1$	$\emptyset_2$
	linearly variable strength in x-direction	$\emptyset_3$	$\emptyset_4$
Convection Part	constant strength in x-direction	$\emptyset_5$	$\emptyset_6$
	linearly variable strength in x-direction	$\emptyset_7$	$\emptyset_8$

All of them are two-dimensional models, i.e., there is no variation of the temperature field in the y-direction. They are obtained by integrating the solution for the steady temperature field in a moving solid due to a continuously acting line source (equation 3.39) which itself is obtained by integrating equation (3.38) in time and in the y-direction and observing that

$$Q_P = q_L \, dy' \, d\tau'$$

$$T_L(x,z,\tau) = \left[\frac{q_L}{\rho c}\int_0^{\infty} \exp\left\{-\frac{[x - x' + V\tau]^2}{4\kappa\tau}\right\}\right.$$

$$\left. \cdot \frac{e^{-\frac{(z - z')^2}{4\kappa\tau}} + e^{-\frac{(z + z')^2}{4\kappa\tau}}}{4\pi\kappa\tau} \, d\tau\right]$$

$$- \left[\frac{q_L}{2\rho c}\int_0^{\infty} \frac{h/k}{\sqrt{\pi\kappa\tau}} \operatorname{erfc}\left\{\frac{z + z' + 2\frac{h}{k}\kappa\tau}{2\sqrt{\kappa\tau}}\right\}\right.$$

$$\left. \cdot \exp\left\{(z + z')\frac{h}{k} + \kappa\left(\frac{h}{k}\right)^2\tau - \frac{(x - x' + V)^2}{4\kappa\tau}\right\} d\tau\right] \quad (3.39)$$

Equation (3.39) can be split in two parts of which the first one constitutes the temperature rise due to the heat source without convective heat losses from the surface. This part is, therefore, used to develop the first four solutions $\emptyset_1$, $\emptyset_2$, $\emptyset_3$, and $\emptyset_4$ in Table 3.1. The second part of equation (3.39) gives the temperature reduction due to surface cooling. Solutions $\emptyset_5$, $\emptyset_6$, $\emptyset_7$, and $\emptyset_8$ are based on it.

Equation (3.39) can be simplified by introducing the following dimensionless quantities:

$$X = \frac{V}{2\kappa} x$$

$$Z = \frac{V}{2\kappa} z$$

$$U = \frac{V^2}{2\kappa} \tau \qquad (3.40)$$

$$H = \frac{h}{k} \frac{2\kappa}{V}$$

$$\phi = \frac{\pi k V}{2 q_0 \kappa} T$$

It takes the form:

$$\phi_L = \frac{q_L}{q_0} \frac{V}{8\kappa} \int_0^\infty e^{-\frac{(X - X' + U)^2}{2U}} \left\{ e^{-\frac{(Z - Z')^2}{2U}} \right\} \frac{dU}{U}$$

$$- \frac{q_L}{q_0} \frac{VH}{4\kappa} \sqrt{\frac{\pi}{2}} \int_0^\infty \operatorname{erfc}\left(\frac{Z + Z' + HU}{\sqrt{2U}}\right) e^{-\frac{(X - X' + U)^2}{2U}}$$

$$\cdot \exp\left[H(Z + Z') + \frac{H^2 U}{2}\right] \frac{dU}{\sqrt{U}} \qquad (3.41)$$

Surface Heat Source of Constant Strength

The strength of this heat source is uniform over its length. Equation (3.42) relates the strength of the line heat source, q_L, to the strength of this surface area heat source, q_0:

$$q_L = q_0 \, dx' \qquad \text{for } -\ell \leq x' \leq \ell, \; z' = 0 \tag{3.42}$$

If there is no cooling from the surface z = 0 then only the first part of equation (3.41) is integrated over the extent of the heat source to yield the temperature distribution in the solid:

$$\phi_1 = \int_{-L}^{L} \frac{V}{4\kappa} 2 \int_0^{\infty} \exp\{-\frac{(X - X' + U)^2 + Z^2}{2U}\} \frac{dU}{U} \frac{2\kappa}{V} dX'$$

After reversing the order of integration and integrating over X' one obtains:

$$\phi_1 = \frac{1}{2}\sqrt{\frac{\pi}{2}} \int_0^{\infty} \frac{e^{-\frac{Z^2}{2U}}}{\sqrt{U}} \{\operatorname{erfc}(\frac{X - L + U}{\sqrt{2U}}) - \operatorname{erfc}(\frac{X + L + U}{\sqrt{2U}})\} \, dU \tag{3.43}$$

This is the equation of the steady state temperature distribution in a semi-infinite solid without convection cooling due to a uniform surface heat source in band form.

The function under the integral is well behaved and can easily be integrated numerically. Similar integrations will arise in the numerical evaluation of the temperature fields under the other heat sources so that their treatment is referred to the end of this section.

The temperature reduction due to surface cooling of uniform rate, h, is obtained by integration of the second part of equation (3.41)

$$\phi_5 = \int_{-L}^{L} \frac{VH}{4\kappa} \sqrt{\frac{\pi}{2}} \int_0^{\infty} \operatorname{erfc}\left(\frac{Z + HU}{\sqrt{2U}}\right) \exp\left\{HZ + \frac{H^2U}{2} - \frac{(X - X' + U)^2}{2U}\right\}$$

$$\cdot \frac{dU}{\sqrt{U}} \frac{2\kappa}{V} dX$$

from which follows after integration over X':

$$\phi_5 = \frac{\pi}{4} H \int_0^{\infty} \exp\left(HZ + \frac{H^2U}{2}\right) \operatorname{erfc}\left(\frac{Z + UH}{\sqrt{2U}}\right)$$

$$\cdot \left\{\operatorname{erfc}\left(\frac{X - L + U}{\sqrt{2U}}\right) - \operatorname{erfc}\left(\frac{X + L + U}{\sqrt{2U}}\right)\right\} dU \qquad (3.44)$$

The temperature field in the solid with convection is then given by:

$$\phi = \phi_1 - \phi_5$$

Surface Heat Source of Linearly Varying Strength

The strength of this heat source varies linearly from $q_S = 0$ at $x' = -\ell$ to $q_S = 2q_0$ at $x' = \ell$ so that its average strength is q_0. Consequently, the strength of the line source q_L in equation (3.41) is a function of x':

$$q_L = q_0\left(1 + \frac{x'}{\ell}\right) dx' \qquad \text{for } -\ell \leq x' \leq \ell, \; z' = 0 \tag{3.45}$$

The temperature field in the solid is obtained following the same steps as before. Temperature rise due to the heat source:

$$\phi_3 = \int_{-L}^{L} \frac{V}{4\kappa}\left(1 + \frac{X'}{L}\right) \int_0^{\infty} \exp\{-\frac{(X - X' + U)^2 + Z^2}{2U}\} \frac{dU}{U} \frac{2\kappa}{V} dX'$$

$$\phi_3 = \frac{1}{2L} \int_0^{\infty} e^{-\frac{Z^2}{2U}} \left[\sqrt{\frac{\pi}{2U}}(X + L + U)\{\operatorname{erfc}\left(\frac{X - L + U}{\sqrt{2U}}\right)\right.$$

$$\left. - \operatorname{erfc}\left(\frac{X + L + U}{\sqrt{2U}}\right)\} + \{e^{\frac{(X + L + U)^2}{2U}} - e^{\frac{(X - L + U)^2}{2U}}\}\right] dU \tag{3.46}$$

Temperature reduction due to surface cooling:

$$\phi_7 = \int_{-L}^{L} \frac{V}{4\kappa}\sqrt{\frac{\pi}{2}}\left(1 + \frac{X'}{L}\right) H\, e^{HZ} \int_0^{\infty} \operatorname{erfc}\left(\frac{Z + HU}{\sqrt{2U}}\right) \exp\left(\frac{H^2U}{2} - \right.$$

$$\left. \frac{(X - X' + U)^2}{2U}\right) \frac{dU}{\sqrt{U}} \frac{2\kappa}{V} dX'$$

$$\phi_7 = \frac{\pi H}{4L} \int_0^{\infty} \exp\left(HZ + \frac{H^2U}{2}\right) \operatorname{erfc}\left(\frac{Z + HU}{\sqrt{2U}}\right)$$

$$\cdot \left[(X + L + U)\left\{\operatorname{erfc}\left(\frac{X - L + U}{\sqrt{2U}}\right) - \operatorname{erfc}\left(\frac{X + L + U}{\sqrt{2U}}\right)\right\}\right.$$

$$\left. + \sqrt{\frac{2U}{\pi}} \left\{e^{-\frac{(X + L + U)^2}{2U}} - e^{-\frac{(X - L + U)^2}{2U}}\right\}\right] dU \qquad (3.47)$$

The temperature in the moving solid due to heat source and convection is given by:

$$\phi = \phi_3 - \phi_7$$

Volume Heat Source of Constant Strength

The heat source has uniform strength over its length and varies according to equation (3.10) with the depth below the surface.

$$q_V = q_{VO}\, e^{-\beta z'} \qquad (3.10)$$

The strength at the surface, q_{VO}, is determined by the total energy input of the source,

$$\dot{Q}_V = B \int_{-\ell}^{\ell} \int_0^{\infty} q_{VO}\, e^{-\beta z'}\, dz'\, dx'$$

$$\dot{Q}_V = 2\ell B \frac{q_{V0}}{\beta} \quad , \qquad \frac{Btu}{sec} \tag{3.48}$$

such that $\dot{Q}_V$ equals the total energy input of the surface heat sources which is

$$\dot{Q}_S = 2\ell B q_0 \tag{3.49}$$

The strength of the line source, q_L, in equation (3.41) is a function of the depth z':

$$q_L = q_0 \beta \, e^{-\beta z'} \, dz' \, dx' \qquad \text{for } -\ell \leq x' \leq \ell, \quad 0 \leq z' < \infty \tag{3.50}$$

The temperature rise in the solid caused by this heat source is given by:

$$\phi_2 = \int_{-L}^{L} \int_{0}^{\infty} \left(\frac{V}{2\kappa}\right)^2 \frac{\eta}{4} e^{-\eta Z'} \int_{0}^{\infty} \exp\{-\frac{(X - X' + U)^2}{2U}\}\{\exp(-\frac{(Z - Z')^2}{2U})$$

$$+ \exp(-\frac{(Z + Z')^2}{2U})\} \frac{dU}{U} \left(\frac{2\kappa}{V}\right)^2 dZ' \, dX'$$

where

$$\eta = \frac{2\kappa}{V} \beta$$

After interchanging the order of integration the integrals over X' and Z' can be separated:

$$\phi_2 = \frac{\eta}{4} \int_0^{\infty} \left[\int_{-L}^{L} \exp\{- \frac{(X - X' + U)^2}{2U}\} dX' \right.$$

$$\left. \cdot \int_0^{\infty} e^{-\eta Z'} \{\exp(- \frac{(Z - Z')^2}{2U}) + \exp(- \frac{(Z + Z')^2}{2U})\} \, dZ \right] \frac{dU}{U}$$

from which follows:

$$\phi_2 = \frac{\pi}{8} \eta \int_0^{\infty} \{\operatorname{erfc}(\frac{X - L + U}{\sqrt{2U}}) - \operatorname{erfc}(\frac{X + L + U}{\sqrt{2U}})\} \, e^{\eta^2 \frac{U}{2}}$$

$$\cdot \{e^{\eta Z} \operatorname{erfc}(\frac{\eta U + Z}{\sqrt{2U}}) + e^{-\eta Z} \operatorname{erfc}(\frac{\eta U - Z}{\sqrt{2U}})\} \, dU \qquad (3.51)$$

The temperature drop due to surface cooling is given by:

$$\phi_6 = \int_{-L}^{L} \int_0^{\infty} (\frac{V}{2\kappa})^2 \frac{H\eta}{2} \sqrt{\frac{\pi}{2}} \, e^{-\eta Z'} \int_0^{\infty} \operatorname{erfc}(\frac{Z + Z' + HU}{\sqrt{2U}})$$

$$\cdot \exp\{H(Z + Z') + \frac{H^2 U}{2}\} \exp\{- \frac{(X - X' + U)^2}{2U}\} \frac{dU}{\sqrt{U}} (\frac{2\kappa}{V})^2 \, dZ' \, dX'$$

which results in

$$\phi_6 = \frac{\pi}{4}\eta H \int_0^\infty \left[\operatorname{erfc}\left(\frac{X - L + U}{\sqrt{2U}}\right) - \operatorname{erfc}\left(\frac{X + L + U}{\sqrt{2U}}\right)\right]$$

$$\cdot \left[\frac{e^{\left(HZ + \frac{H^2U}{2}\right)}}{\eta - H} \operatorname{erfc}\left(\frac{Z + HU}{\sqrt{2U}}\right) + \frac{e^{\left(\eta Z + \frac{\eta^2 U}{2}\right)}}{H - \eta} \operatorname{erfc}\left(\frac{Z + \eta U}{\sqrt{2U}}\right)\right] dU \qquad (3.52)$$

The complete temperature field due to a volume heat source of constant strength and with convection is given by:

$$\phi = \phi_2 - \phi_6$$

Volume Heat Sources of Linearly Varying Strength

The strength of this heat source varies linearly from $q_{V0} = 0$ at $x' = -\ell$ to $q_{V0} = 2\,q_0$ at $x' = \ell$ and exponentially with the depth below the surface:

$$q_V = \beta q_0 \left(1 + \frac{x'}{\ell}\right) e^{-\beta z'}$$

from which the strength q_L of the line source in equation (3.41) is derived.

$$q_L = \beta q_0 \left(1 + \frac{x'}{\ell}\right) e^{-\beta z'}\, dx'\, dz' \qquad (3.53)$$

$$\text{for } -\ell \leq x' \leq \ell$$
$$0 \leq z' < \infty$$

The temperature rise in the solid is given by:

$$\phi_4 = \int_{-L}^{L} \int_{0}^{\infty} \left(\frac{V}{2\kappa}\right)^2 \frac{\eta}{4} \left(1 + \frac{X'}{L}\right) e^{-\eta Z'} \int_{0}^{\infty} \exp\left\{-\frac{(X - X' + U)^2}{2U}\right\}$$

$$\cdot \left\{e^{-\frac{(Z - Z')^2}{2U}} + e^{-\frac{(Z + Z')^2}{2U}}\right\} \frac{dU}{U} \left(\frac{2\kappa}{V}\right)^2 dZ'\, dX'$$

Executing the same steps as above results in:

$$\phi_4 = \frac{\pi}{8L} \eta \int_{0}^{\infty} e^{\frac{\eta^2 U}{2}} \left[e^{\eta Z} \operatorname{erfc}\left(\frac{\eta U + Z}{\sqrt{2U}}\right) + e^{-\eta Z} \operatorname{erfc}\left(\frac{\eta U - Z}{\sqrt{2U}}\right)\right]$$

$$\cdot \left[(X + L + U)\left\{\operatorname{erfc}\left(\frac{X - L + U}{\sqrt{2U}}\right) - \operatorname{erfc}\left(\frac{X + L + U}{\sqrt{2U}}\right)\right\}\right.$$

$$\left. + \sqrt{\frac{2U}{\pi}} \left\{\exp\left(-\frac{(X + L + U)^2}{2U}\right) - \exp\left(-\frac{(X - L + U)^2}{2U}\right)\right\}\right] dU$$

(3.54)

The temperature reduction due to surface cooling follows from:

$$\phi_8 = \int_{-L}^{L} \int_{0}^{\infty} \left(\frac{V}{2\kappa}\right)^2 \frac{H\eta}{2} \sqrt{\frac{\pi}{2}} \left(1 + \frac{X'}{L}\right) e^{-\eta Z'} \int_{0}^{\infty} \exp\left\{-\frac{(X - X' + U)^2}{2U}\right\}$$

$$\cdot \operatorname{erfc}\left(\frac{Z + Z' + HU}{\sqrt{2U}}\right) \exp\left\{H(Z + Z') + \frac{H^2U}{2}\right\} \frac{dU}{\sqrt{U}} \left(\frac{2\kappa}{V}\right)^2 dZ'\, dX'$$

which can be integrated to yield:

$$\phi_8 = \frac{\pi}{4L} \eta H \int_{0}^{\infty} \left[(X + L + U)\left\{\operatorname{erfc}\left(\frac{X - L + U}{\sqrt{2U}}\right) - \operatorname{erfc}\left(\frac{X + L + U}{\sqrt{2U}}\right)\right\}\right.$$

$$+ \sqrt{\frac{2U}{\pi}} \left\{\exp\left(-\frac{(X + L + U)^2}{2U}\right) - \exp\left(-\frac{(X - L + U)^2}{2U}\right)\right\} \left\{\frac{e^{\left(HZ + \frac{H^2U}{2}\right)}}{\eta - H}\right.$$

$$\left.\left. \cdot \operatorname{erfc}\left(\frac{Z + HU}{\sqrt{2U}}\right) + \frac{e^{\left(\eta Z + \frac{\eta^2 U}{2}\right)}}{H - \eta} \operatorname{erfc}\left(\frac{Z + \eta U}{\sqrt{2U}}\right)\right\}\right] dU \qquad (3.55)$$

The temperature field in the moving solid due to the nonuniform volume heat source and surface cooling is given by

$$\phi = \phi_4 - \phi_8 \ .$$

A check of the validity of equations can be obtained by considering limiting values of the parameters. For instance, it can be observed that equation (3.50) reduces to equation (3.42) for $z' \neq 0$ and for

β increasing beyond limit. This means the volume heat sources become surface heat sources as $\beta \to \infty$. Consequently, the equations describing the temperature fields of volume heat sources should reduce to the equations for surface heat sources. This they do, i.e.:

$$\lim_{\eta \to \infty} \phi_2 = \phi_1$$

$$\lim_{\eta \to \infty} \phi_4 = \phi_3$$

$$\lim_{\eta \to \infty} \phi_6 = \phi_5$$

$$\lim_{\eta \to \infty} \phi_8 = \phi_7$$

A second check is provided by considering the effect of increasing values of the convection coefficient. The temperatures in the solid can never be negative. In the limit as $H \to \infty$ all the energy generated by surface heat sources is carried away by convection and the workpiece temperatures should be zero. This is the case since

$$\lim_{H \to \infty} \phi_5 = \phi_1$$

$$\lim_{H \to \infty} \phi_7 = \phi_3$$

For volume heat sources the same cannot be said. It can only be established that

$$\lim_{H \to \infty} \phi_6 < \phi_2$$

$$\lim_{H \to \infty} \phi_8 < \phi_4$$

Numerical Integration

The equations describing the steady state temperature distribution in the moving semi-infinite solid cannot be integrated analytically. In order to obtain numerical answers to specific problems programs for a general purpose digital computer were written which use a standard routine to carry out the integrations numerically. Two problems arise from this procedure. First, the computer is limited in the size and the numbers which it can handle. Several of the equations contain terms of the form

$$e^{(s^2 - g^2)} \operatorname{erfc}(s) \tag{3.56}$$

For large values of s the exponential part very soon increases beyond the limit of the computer while the value of the complete term remains finite for all positive values of s and

$$\lim_{s\to\infty}\{e^{(s^2 - g^2)} \operatorname{erfc}(s)\} = 0$$

The values of the complementary error function are calculated by a routine based on an approximation formula given in reference [12]:

$$\operatorname{erfc}(s) \doteq e^{-s^2} \sum_{i=1}^{5} \frac{a_i}{(1 + ps)^i} \tag{3.57}$$

for $0 \leq s$

where a_i and p are constants given in the reference book.

Expression (3.56) can be made fit for computations of all finite positive values of s by defining a new function, the exponential error function:

$$\exp \operatorname{erf}(s) = e^{s^2} \operatorname{erfc}(s) \doteq \sum_{i=1}^{5} \frac{a_i}{(1 + ps)^i} \qquad (3.58)$$

for $0 \leq s$

from which follows:

$$e^{(s^2-g^2)} \operatorname{erfc}(s) = e^{-g^2} \exp \operatorname{erf}(s) \qquad (3.59)$$

For negative values of s this new function is not defined. This is not necessary since here s and g are related such that

$$s^2 < g^2 \quad \text{for } s < 0$$

and, hence, both parts of expression (3.56) remain finite for all finite negative values of s.

The second computation problem is to define a finite upper limit for the integration. This problem is equivalent to defining a finite time at which a point of the coordinate system has reached its maximum temperature. As mentioned before the time, U_{SS}, to reach 99.99% of the maximum temperature is chosen. U_{SS} is calculated by repeatedly integrating over a small time increment until the temperature increases are smaller than the desired limit. A single

equation is found to adequately fit the resultant values of time for all eight models.

$$U_{SS} = 2L - X + 0.5Z + 10 \qquad (3.60)$$

This equation is the dimensionless form of equation (3.32). If the values of U_{SS} from equation (3.60) are used as the upper limit of integration the steady state temperature field is calculated. If smaller values of U are used as the upper limit transient temperature fields are obtained.

In Figures 3.8 through 3.15 the modified equations of the eight temperature fields are shown together with the corresponding Fortran programs and plots of temperature versus horizontal position.

$$\phi_1(X,Z) = \int_0^{\infty} \sqrt{\frac{\pi}{8U}}\, e^{-\frac{Z}{2U}} \left\{ \operatorname{erfc}\left(\frac{X - L + U}{\sqrt{2U}}\right) - \operatorname{erfc}\left(\frac{X + L + U}{\sqrt{2U}}\right) \right\} dU$$

```
      FUNCTION FI01 (U)
C
C     CALCULATES THE INTEGRAND OF EQUATION (22) IN THE PAPER OF
C     J.C. JAEGER, - MOVING SOURCES OF HEAT AND THE TEMPERATURE AT
C     SLIDING CONTACTS -.
C
      COMMON/MOHES0/ PI,X,E,Z,ETA,CONV
C
      V=SQRT(0.5/U)
      FI01=0.5*V*SQRT(PI)*(ERFC(V*(X-E+U))-ERFC(V*(X+E+U)))
     1 *EXP(-Z*Z*V*V)
      RETURN
      END
```

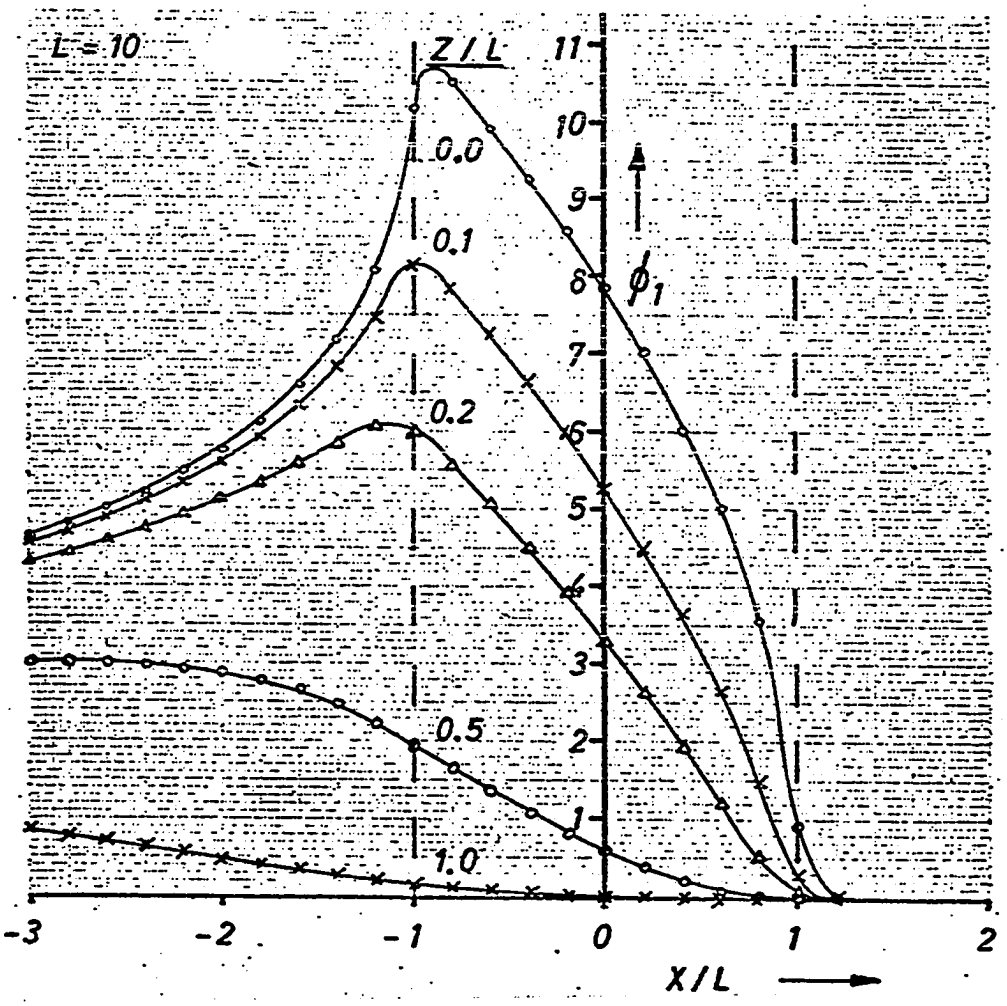

Figure 3.8 Constant Surface Heat Source Without Convection

$$\phi_5(X,Z) = \int_0^{\infty} \frac{\pi}{4} H\, e^{-\frac{Z^2}{2U}} \exp \operatorname{erf}\left(\frac{HU + Z}{\sqrt{2U}}\right)\left\{\operatorname{erfc}\left(\frac{X - L + U}{\sqrt{2U}}\right) - \operatorname{erfc}\left(\frac{X + L + U}{\sqrt{2U}}\right)\right\} dU$$

```
      FUNCTION FIO5 (U)
C
C     CALCULATES THE INTEGRAND OF THE CONVECTION EQUATION FOR A CONSTANT
C     SURFACE HEAT SOURCE.
C
      COMMON/MOHESO/ PI,X,E,Z,ETA,CONV
C
      V=SQRT(0.5/U)
      A=(X+E+U)*V
      B=(X-E+U)*V
      C=(CONV*U+Z)*V
      FIO5=0.25*PI*CONV*EXP(-Z*V*Z*V)*EXPERF(C)*(ERFC(B)-ERFC(A))
      RETURN
      END
```

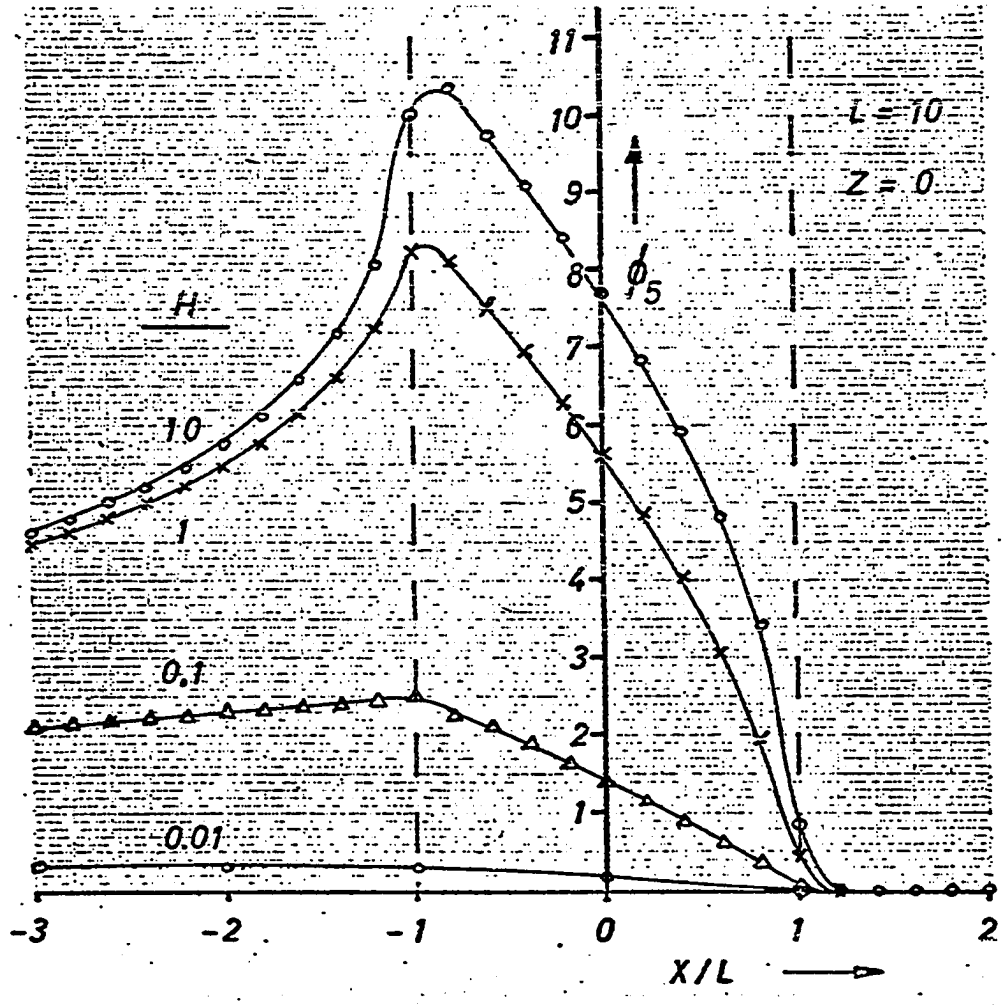

Figure 3.9 Convection Cooling for a Constant Surface Heat Source

$$\phi_3(X,Z) = \int_0^{\infty} \frac{e^{-\frac{Z}{2U}}}{2L} \left[\sqrt{\frac{\pi}{2U}}\,(X + L + U)\left\{\operatorname{erfc}\left(\frac{X - L + U}{\sqrt{2U}}\right) - \operatorname{erfc}\left(\frac{X + L + U}{\sqrt{2U}}\right)\right\}\right.$$

$$\left. + \left\{e^{-\frac{(X + L + U)^2}{2U}} - e^{-\frac{(X - L + U)^2}{2U}}\right\}\right] dU$$

```
      FUNCTION FI03 (U)
C-----------------------------------------------------------------------
C     CALCULATES THE INTEGRAND OF THE TEMPERATURE EQUATION FOR A
C     AREA HEAT SOURCE WITH LINEAR VARIATION IN THE X-DIRECTION.
C
      COMMON/MOHESO/ PI,X,E,Z,ETA,CONV
C
      V=SQRT(0.5/U)
      A=X+E+U
      B=A*V
      C=(X-E+U)*V
      FI03=0.5*EXP(-Z*Z*V*V)*(V*SQRT(PI)*A*(ERFC(C)-ERFC(B))+
     1 (EXP(-B*B)-EXP(-C*C)))/E
      RETURN
      END
```

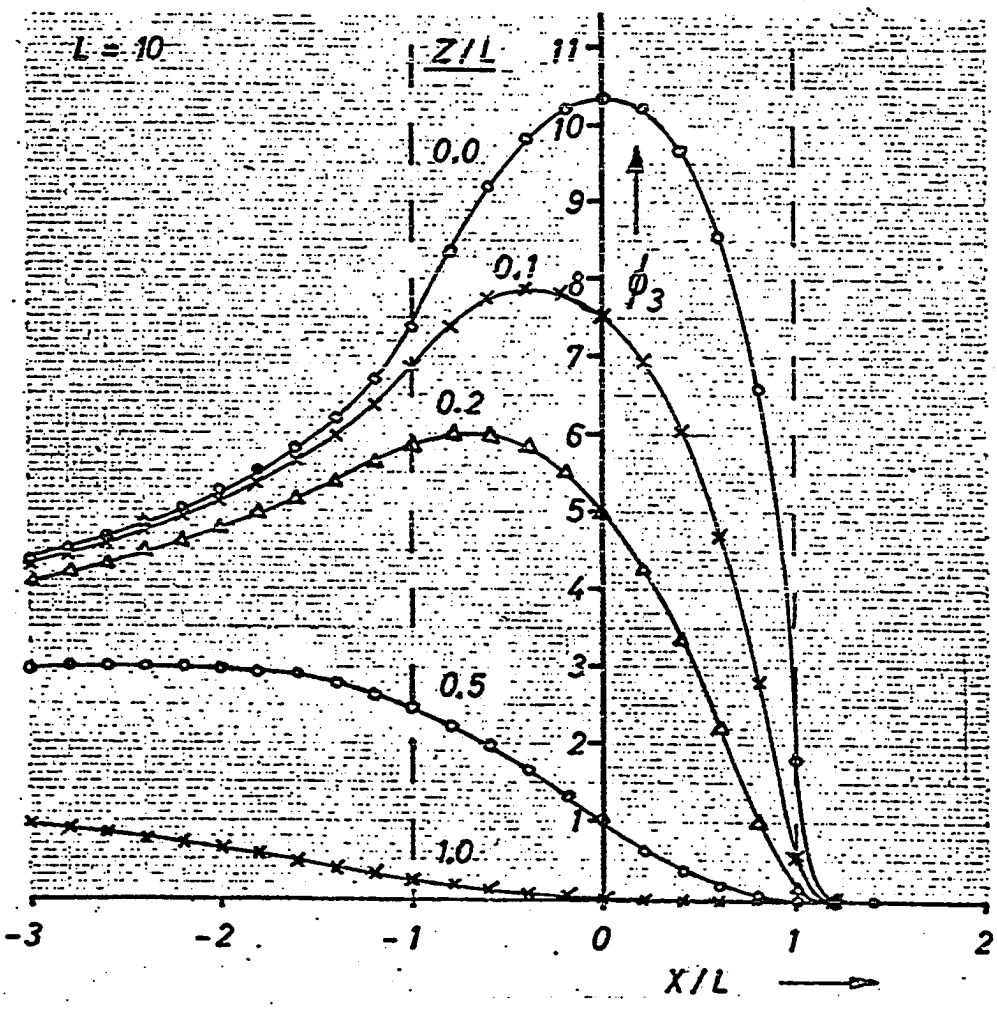

Figure 3.10 Linearly Varying Surface Heat Source Without Convection Cooling

$$\phi_7(X,Z) = \int_0^{\infty} \frac{\pi}{4L} H\, e^{-\frac{Z^2}{2U}} \exp \operatorname{erf}\left(\frac{HU + Z}{\sqrt{2U}}\right)\left[(X + L + U)\left\{\operatorname{erfc}\left(\frac{X - L + U}{\sqrt{2U}}\right)\right.\right.$$

$$\left.\left. - \operatorname{erfc}\left(\frac{X + L + U}{\sqrt{2U}}\right) + \sqrt{\frac{2U}{\pi}}\left\{e^{-\frac{(X + L + U)^2}{2U}} - e^{-\frac{(X - L + U)^2}{2U}}\right\}\right]\right] dU$$

```
      FUNCTION FI07 (U)
C
C     CALCULATES THE INTEGRAND OF THE CONVECTION EQUATION FOR A
C     AREA HEAT SOURCE WITH LINEAR VARIATION IN THE X-DIRECTION.
C
      COMMON/MOHESO/ PI,X,E,Z,ETA,CONV
C
      V=SQRT(0.5/U)
      A=X+E+U
      B=A*V
      C=(X-E+U)*V
      D=(CONV*U+Z)*V
      AA=0.25*PI*CONV/E*EXP(-Z*V*2.*V)*EXPERF(D)
      FI07=AA*(A*(ERFC(C)-ERFC(B))+SQRT(2.*U/PI)*(EXP(-B*B)-EXP(-C*C)))
      RETURN
      END
```

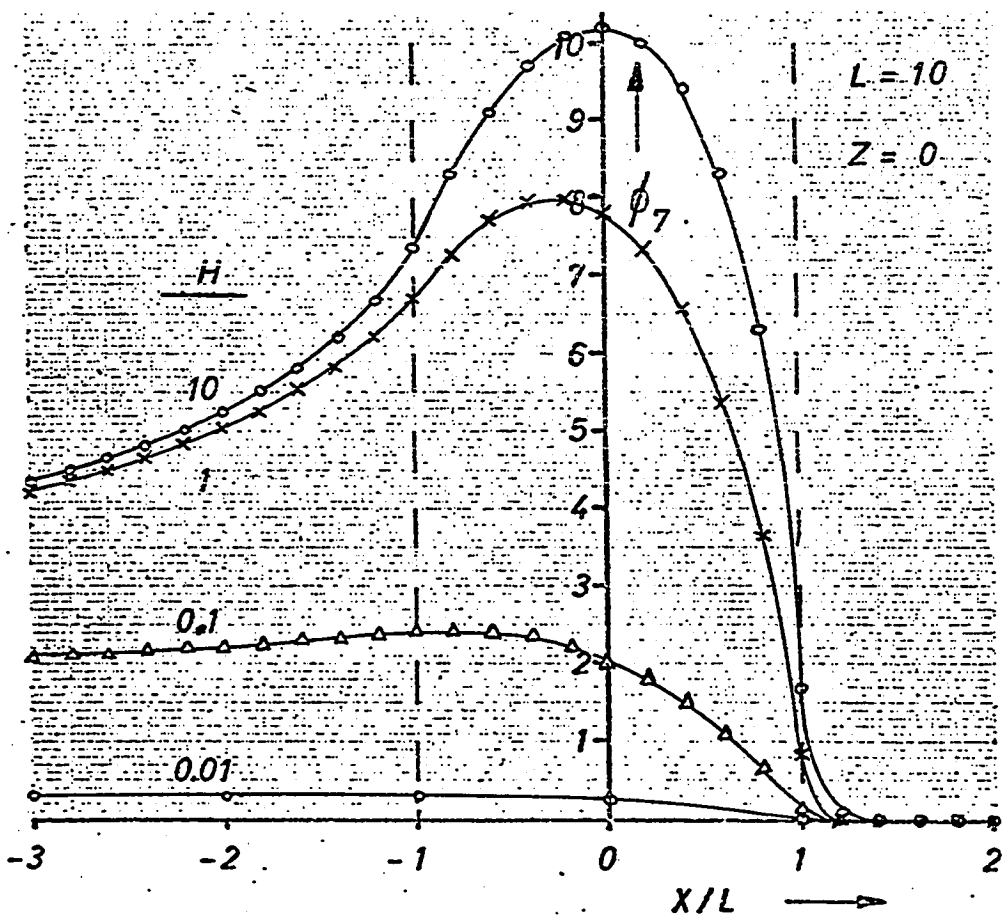

Figure 3.11 Convection Cooling for a Linearly Varying Surface Heat Source

$$\phi_2(X,Z) = \int_0^{\infty} \frac{\pi}{8}\eta\{\operatorname{erfc}(\frac{X - L + U}{\sqrt{2U}}) - \operatorname{erfc}(\frac{X + L + U}{\sqrt{2U}})\}\{\exp \operatorname{erf}(\frac{\eta U + Z}{\sqrt{2U}}) + \exp \operatorname{erf}(\frac{\eta U - Z}{\sqrt{2U}})\}\, e^{-\frac{Z^2}{2U}}\, dU$$

```
      FUNCTION FI02 (U)
C
C     CALCULATES THE INTEGRAND OF THE TEMPERATURE EQUATION FOR A CONSTANT
C     VOLUME HEAT SOURCE WITH EXPONENTIAL DECAY IN THE Z-DIRECTION.
C
      COMMON/MOHES0/ PI,X,E,Z,ETA,CONV
C
      V=SQRT(0.5/U)
      A=(X-E+U)*V
      B=(X+E+U)*V
      C=(ETA*U+Z)*V
      D=(ETA*U-Z)*V
      IF (D .LT. -5.0) GOTO 1
      AA=(EXPERF(C)+EXPERF(D))*EXP(-Z*V*Z*V)
      GOTO 2
    1 CONTINUE
      AA=EXPERF(C)*EXP(-Z*V*Z*V)+ERFC(D)*EXP(D*D-Z*V*Z*V)
    2 CONTINUE
      FI02=AA*0.125*PI*ETA*(ERFC(A)-ERFC(B))
      RETURN
      END
```

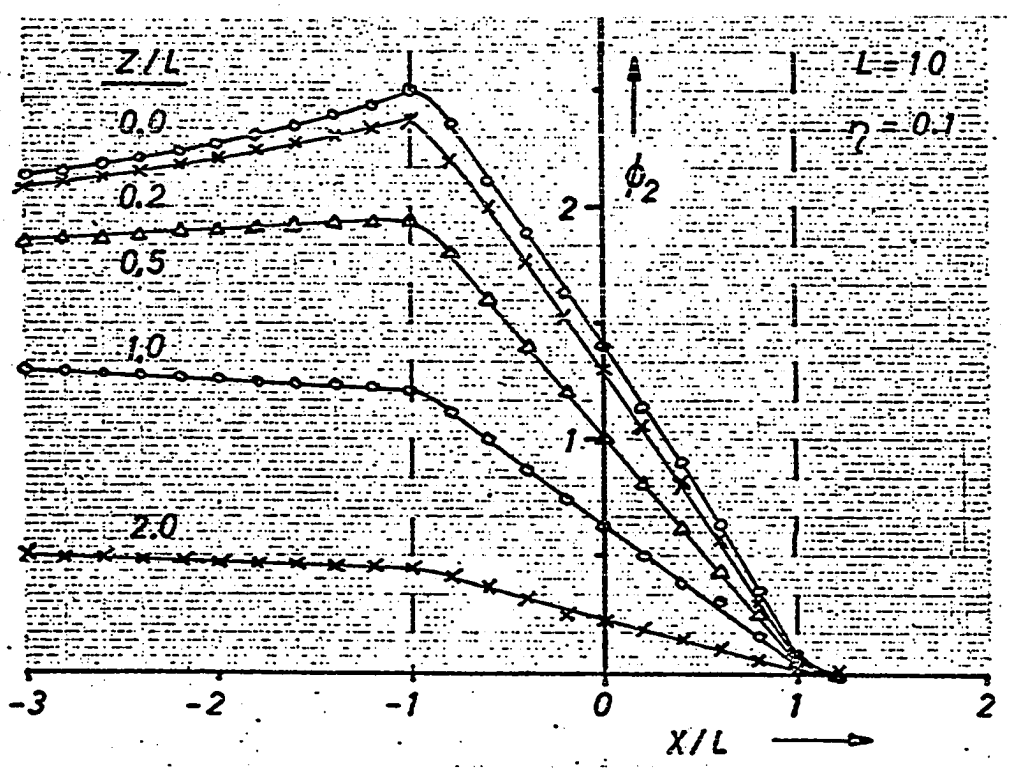

Figure 3.12 Constant Volume Heat Source Without Convection Cooling

$$\phi_6(X,Z) = \int_0^{\infty} \frac{\pi}{4} \frac{\eta H}{\eta - H} \{\operatorname{erfc}(\frac{X - L + U}{\sqrt{2U}}) - \operatorname{erfc}(\frac{X + L + U}{\sqrt{2U}})\}\{\exp \operatorname{erf}(\frac{HU + Z}{\sqrt{2U}})$$

$$- \exp \operatorname{erf}(\frac{\eta U + Z}{\sqrt{2U}})\} e^{-\frac{Z^2}{2U}} dU$$

```
      FUNCTION FI06 (U)
C
C     CALCULATES THE INTEGRAND OF THE CONVECTION EQUATION FOR A CONSTAN
C     VOLUME HEAT SOURCE WITH EXPONENTIAL DECAY IN THE Z-DIRECTION.
C
      COMMON/MOHESO/ PI,X,E,Z,ETA,CONV
C
      V=SQRT(0.5/U)
      A=(X+E+U)*V
      B=(X-E+U)*V
      C=(CONV*U+Z)*V
      D=(ETA*U+Z)*V
      IF (ABS(ETA-CONV) .LT. 1.0E-6*ETA) GOTO 1
      AA=(EXPERF(C)-EXPERF(D))/(ETA-CONV)
      GOTO 2
    1 CONTINUE
      AA=(SQRT(1.0/PI)-C*EXPERF(C))/V
    2 CONTINUE
      AA=0.25*PI*ETA*CONV*EXP(-Z*V*Z*V)*AA
      FI06=AA*(ERFC(B)-ERFC(A))
      RETURN
      END
```

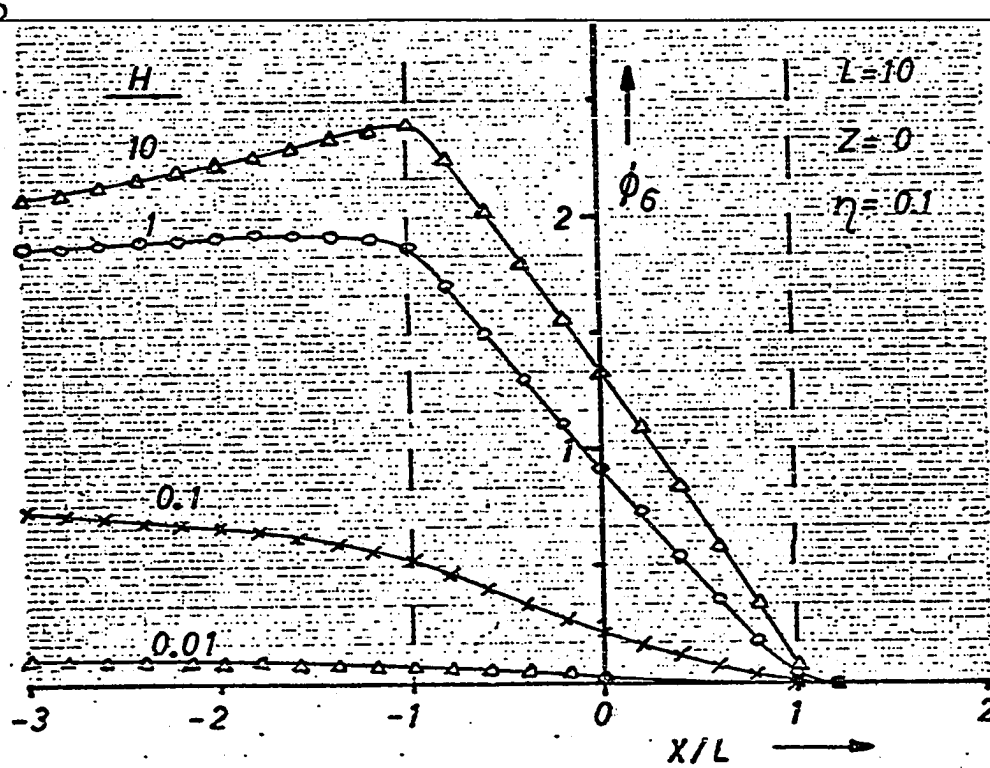

Figure 3.13 Convection Cooling for a Constant Volume Heat Source

$$\phi_4(X,Z) = \int_0^\infty \frac{\pi}{8L}\,\eta\Big[(X+L+U)\Big\{\operatorname{erfc}\Big(\frac{X-L+U}{\sqrt{2U}}\Big) - \operatorname{erfc}\Big(\frac{X+L+U}{\sqrt{2U}}\Big)\Big\}$$

$$+\sqrt{\frac{2U}{\pi}}\Big\{e^{-\frac{(X+L+U)^2}{2U}} - e^{-\frac{(X-L+U)^2}{2U}}\Big\}\Big]\Big\{\exp\operatorname{erf}\Big(\frac{\eta U+Z}{\sqrt{2U}}\Big)$$

$$+\exp\operatorname{erf}\Big(\frac{\eta U-Z}{\sqrt{2U}}\Big)\Big\}\,e^{-\frac{Z^2}{2U}}\,dU$$

```
      FUNCTION FI04 (U)
C
C     CALCULATES THE INTEGRAND OF THE TEMPERATURE EQUATION FOR A
C     VOLUME HEAT SOURCE WITH EXPONENTIAL DECAY IN THE Z-DIRECTION AND
C     LINEAR VARIATION IN THE X-DIRECTION.
C
      COMMON/MOHESO/ PI,X,E,Z,ETA,CONV
C
      V=SQRT(0.5/U)
      A=X+E*U
      B=A*V
      C=(X-E+U)*V
      S=(ETA*U+Z)*V
      T=(ETA*U-Z)*V
      IF (T .LT. -5.0) GOTO 1
      AA=(EXPERF(S)+EXPERF(T))*EXP(-Z*V*Z*V)
      GOTO 2
    1 CONTINUE
      AA=EXPERF(S)*EXP(-Z*V*Z*V)+ERFC(T)*EXP(T*T-Z*V*Z*V)
    2 CONTINUE
      FI04=AA*0.125*PI/E*ETA*(A*(ERFC(C)-ERFC(B))+SQRT(2.0*U/PI)*
     1 (EXP(-B*B)-EXP(-C*C)))
      RETURN
      END
```

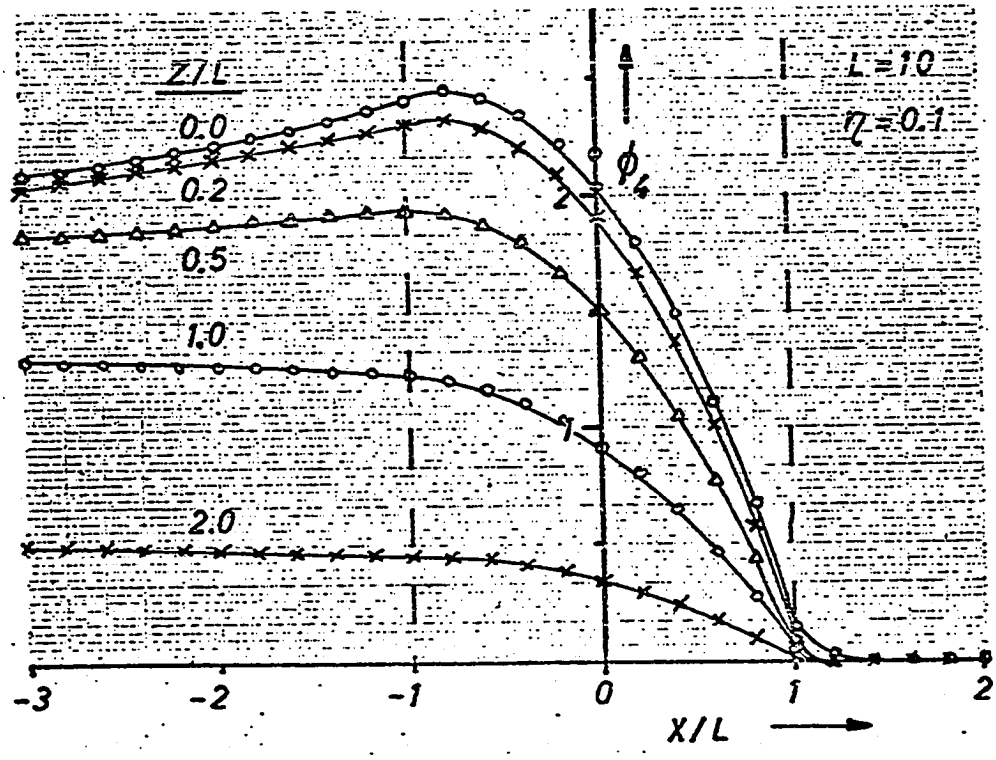

Figure 3.14 Linearly Varying Volume Heat Source Without Convection Cooling

$$\phi_8(X,Z) = \int_0^\infty \frac{\pi}{4L}\frac{\eta H}{\eta - H}\left[(X + L + U)\left\{\operatorname{erfc}\left(\frac{X - L + U}{\sqrt{2U}}\right) - \operatorname{erfc}\left(\frac{X + L + U}{\sqrt{2U}}\right)\right\}\right.$$

$$\left. + \sqrt{\frac{2U}{\pi}}\left\{e^{-\frac{(X + L + U)^2}{2U}} - e^{-\frac{(X - L + U)^2}{2U}}\right\}\right] e^{-\frac{Z^2}{2U}}\left\{\exp\operatorname{erf}\left(\frac{HU + Z}{\sqrt{2U}}\right)\right.$$

$$\left. - \exp\operatorname{erf}\left(\frac{\eta U + Z}{\sqrt{2U}}\right)\right\} dU$$

```
      FUNCTION FI08 (U)
C
C     CALCULATES THE INTEGRAND OF THE CONVECTION EQUATION FOR A
C     VOLUME-HEAT-SOURCE-WITH-EXPONENTIAL-DECAY-IN-THE-Z-DIRECTION
C     WHICH IS LINEARLY VARYING IN THE X-DIRECTION.
C
      COMMON/MOHESO/ PI,X,E,Z,ETA,CONV
C
      V=SQRT(0.5/U)
      A=X+E+U
      B=A*V
      C=(X-E+U)*V
      S=(ETA*U+Z)*V
      T=(CONV*U+Z)*V
      IF (ABS(ETA-CONV) .LT. 1.0E-6*ETA) GOTO 1
      AA=(EXPERF(T)-EXPERF(S))/(ETA-CONV)
      GOTO 2
    1 CONTINUE
      AA=(SQRT(1.0/PI)-S*EXPERF(S))/V
    2 CONTINUE
      AA=0.25*PI*ETA*CONV*EXP(-Z*V*Z*V)*AA/E
      FI08=AA*(A*(ERFC(C)-ERFC(B))+SQRT(2.0*U/PI)*(EXP(-B*B)-EXP(-C*C)))
      RETURN
      END
```

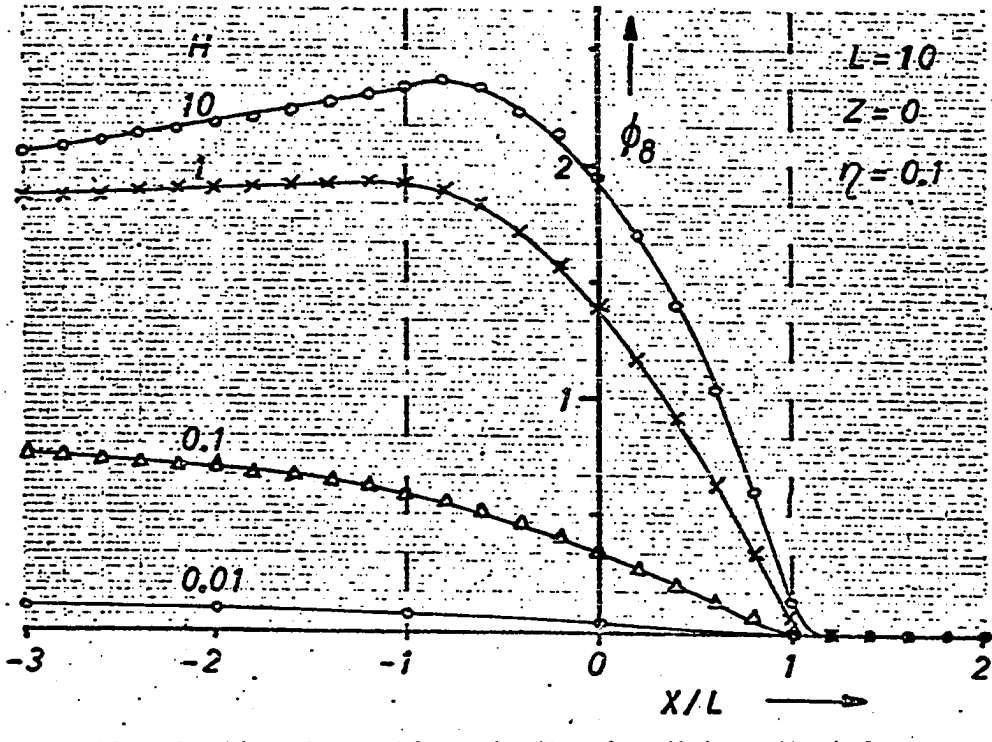

Figure 3.15 Convection Cooling for a Linearly Varying Volume Heat Source

3.2.3 Comparison of the Analytical Model with a Finite Difference Model

The above developed equations can be used to calculate the temperature fields in a semi-infinite solid due to surface and volume heat sources with convection cooling from its surface. These models will be used to calculate the temperatures in the workpiece due to surface grinding. Four types of heat sources were distinguished in an analysis of the process. Each of them has an equivalent mathematical model as indicated in Table 3.2.

Table 3.2 Grinding Heat Sources and Their Models

Temperature Field in the Workpiece Due to	Mathematical Model	Characteristic Parameters		
		V	2ℓ	q_0
interference zone surface heat source	$(\phi_3 - \phi_7)$	V_w	ℓ_c	$\frac{\alpha_1 \dot{Q}_F}{\ell_c B}$
interference zone volume heat source	$(\phi_4 - \phi_8)$	V_w	ℓ_c	$\frac{\alpha_2 \dot{Q}_F}{\ell_c B}$
single grain surface heat source	ϕ_1	V_s	ℓ_G	$\frac{\alpha_1 \dot{Q}_F}{\ell_G b_G M_C}\left(1 + \frac{x}{\ell}\right)$
single grain volume heat source	ϕ_2	V_s	ℓ_G	$\frac{\alpha_2 \dot{Q}_F}{\ell_G b_G M_C}\left(1 + \frac{x}{\ell}\right)$

The maximum temperature at any point in the workpiece is obtained by superposition of the contributions of the individual models.

$$T(x,z) = \{T_3(x,z) - T_7(x,z)\} + \{T_4(x,z) - T_8(x,z)\}$$

$$+ \max\{T_1\} + \max\{T_2\} \qquad (3.61)$$

where the coordinate system is defined in Figure 3.5. The contributions of the single grain heat sources are evaluated as follows. Only one grain is considered. Its contribution will be largest when it is positioned directly above the point (x,z) at which the temperature is to be calculated. The position x determines the area of contact and the strengths of the single grain heat sources. Attached to the grain is a second coordinate system (x_G,z_G) which is the frame of reference for the appropriate heat source models. In this system the maximum temperature rise at the depth of the point of interest $z_G = zV_S/V_W$ is determined and added as $\max(T_1)$ or $\max(T_2)$ respectively in equation (3.61) to the total temperature at point (x,y).

The temperatures so calculated are for an ideal workpiece whose thermodynamic properties do not depend on temperature. The properties of a real material vary with temperature as shown in Figures 3.16, 3.17, and 3.18 for mild steel AISI 1018. For the case of a temperature field in a stationary solid Carslaw and Jaeger [5] show that one can obtain exact solutions of certain problems involving variable properties by defining an average value of the thermal conductivity over the temperature range from T_A to T_B as

$$k = \frac{1}{T_B - T_A} \int_{T_A}^{T_B} k_{(T)}\, dT \qquad (3.62)$$

In the problem at hand this definition does not provide exact solutions but it is believed to be a good definition for average properties. Therefore, the average thermal diffusivity is defined by:

$$\kappa = \frac{1}{T_B - T_A} \int_{T_A}^{T_B} \kappa_{(T)}\, dT \qquad (3.63)$$

Average values of the thermodynamic properties as given by equations (3.62) and (3.63) are used in the computation for the analytical model.

As a check of the effect of variable properties on the temperature field a second analysis of the workpiece is performed which does not include this approximation. The differential equation which describes the steady state temperature distribution in the semi-infinite region shown in Figure 3.8 for non-constant properties reads:

$$0 = V\rho(T \frac{dc}{dT} + c) \frac{\partial T}{\partial x} + \frac{q_V}{k}$$

$$+ \{(\frac{\partial T}{\partial x})^2 + (\frac{\partial T}{\partial z})^2\} \frac{dk}{dT} + k\nabla^2 T \qquad (3.64)$$

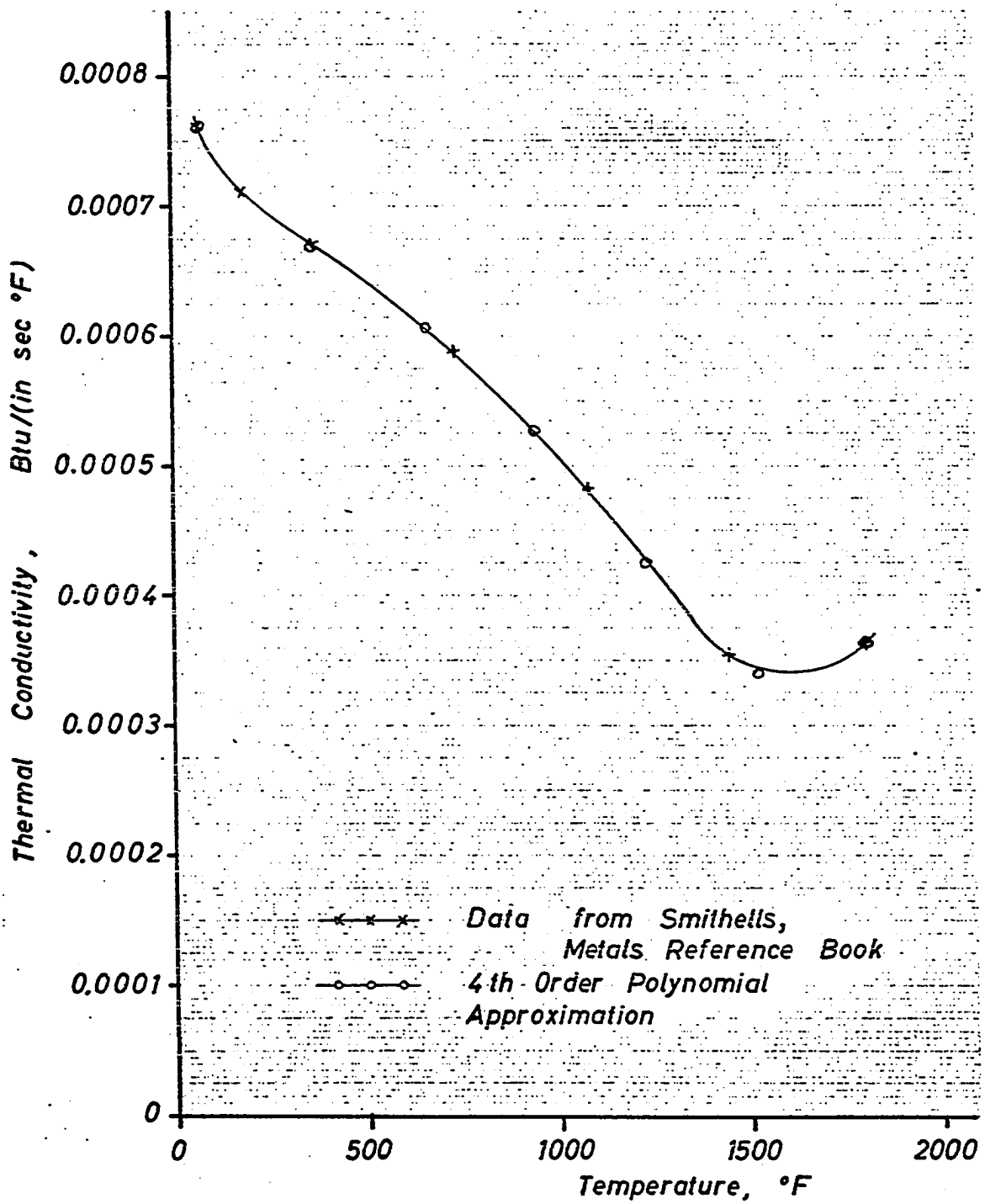

Figure 3.16 Thermal Conductivity as a Function of Temperature for Steel AISI 1018 (From Reference [31])

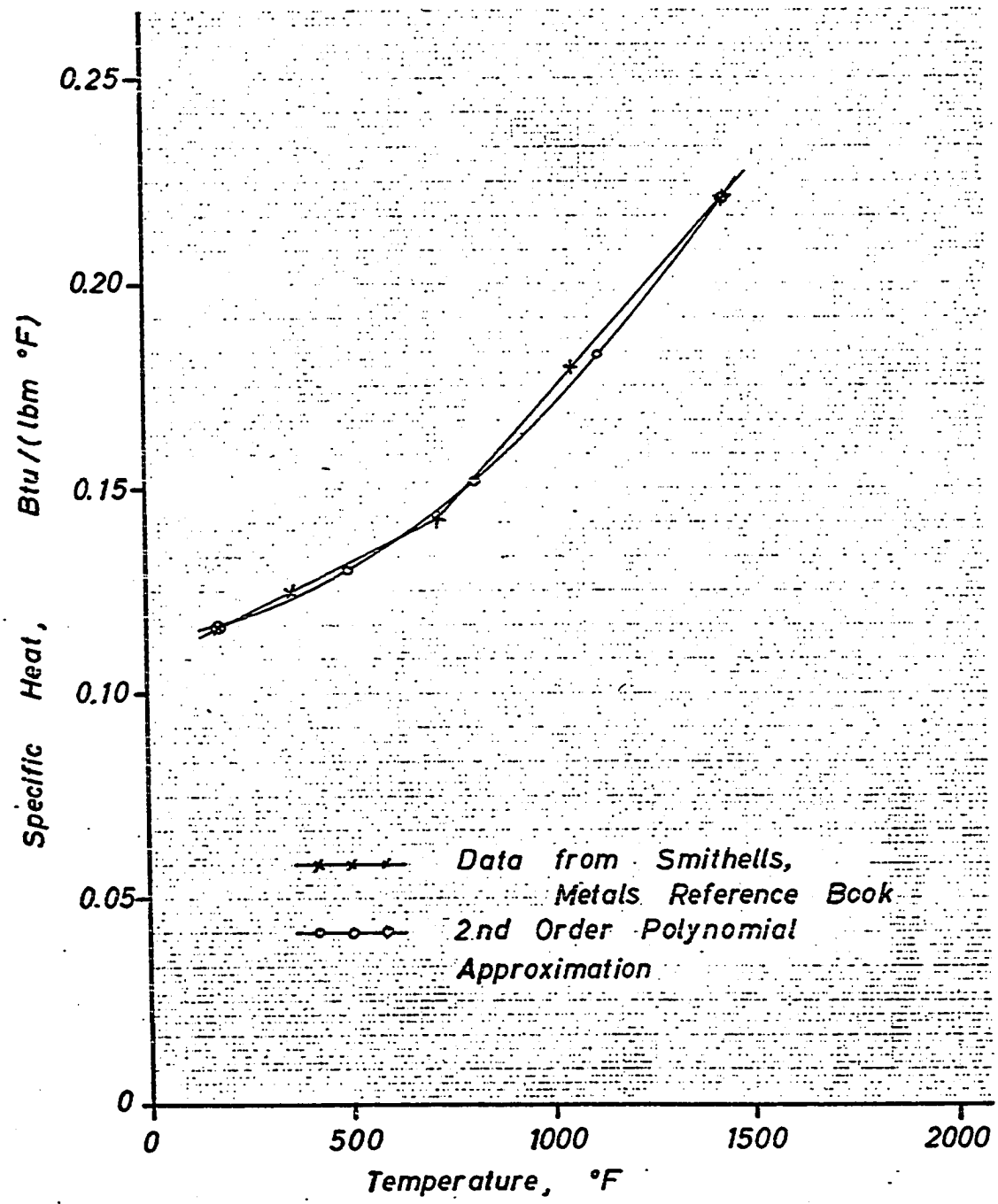

Figure 3.17 Specific Heat of Steel AISI 1018 as a Function of Temperature
(From Reference [31])

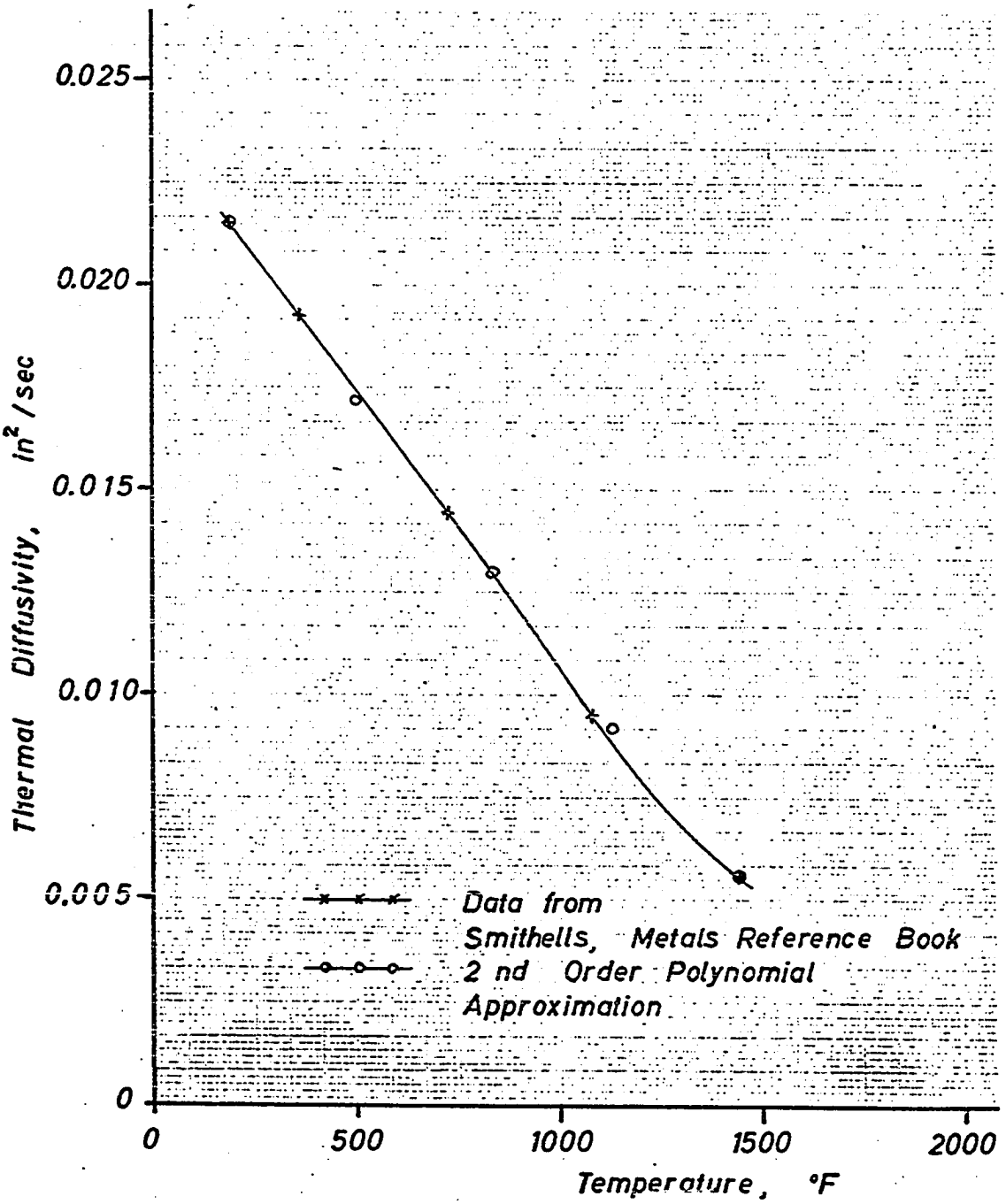

Figure 3.18 Thermal Diffusivity of Steel AISI 1018 as a Function of Temperature (From Reference [31])

The temperature field must satisfy the same boundary and initial conditions which were derived before (equations 3.36 and 3.37). For the solution of this nonlinear differential equation a finite difference method will be used. The following coordinate transformations are made in order to be able to handle a semi-infinite region on a computer:

$$\xi_\ell = e^{x/\ell} \quad \text{for } -\infty < x \leq 0$$

$$\xi_r = e^{-x/\ell} \quad \text{for } 0 \leq x < \infty \tag{3.65}$$

$$\gamma = e^{-z/\ell} \quad \text{for } 0 \leq z < \infty$$

The differential and boundary equations transform into:

$$0 = \pm V\rho\left(T\frac{dc}{dT} + c\right)\frac{\xi}{\ell}\frac{\partial T}{\partial \xi} + q_V + \frac{k}{\ell^2}\left\{\xi^2\frac{\partial^2 T}{\partial \xi^2} + \gamma^2\frac{\partial^2 T}{\partial \gamma^2} + \xi\frac{\partial T}{\partial \xi} + \gamma\frac{\partial T}{\partial \gamma}\right\} + \frac{1}{\ell^2}\left\{\left(\xi\frac{\partial T}{\partial \xi}\right)^2 + \left(\gamma\frac{\partial T}{\partial \gamma}\right)^2\right\}\frac{dk}{dT} \tag{3.66}$$

where the first term is added for $\xi = \xi_\ell$ and subtracted for $\xi = \xi_r$.

$$\frac{\partial T}{\partial \gamma}(\xi,1) = \ell(q_S - q_H)/k$$

$$T(\xi,0) = 0$$

$$T(0,\gamma) = 0$$

$$\frac{\partial T}{\partial \xi_\ell}(1,\gamma) = -\frac{\partial T}{\partial \xi_r}(1,\gamma) \tag{3.67}$$

$$T(\xi_\ell = 1,\gamma) = T(\xi_r = 1,\gamma)$$

where:

$$q_V = \begin{cases} 0 & \text{for } 0 \leq \xi < \frac{1}{e} \\ q_V(\xi,\gamma) & \text{for } \frac{1}{e} \leq \xi \leq 1 \end{cases}$$

$$q_S = \begin{cases} 0 & \text{for } 0 \leq \xi < \frac{1}{e} \\ q_S(\xi) & \text{for } \frac{1}{e} \leq \xi \leq 1 \end{cases}$$

$$q_H = h\, T(\xi,1)$$

The differential terms in these equations are then replaced by difference expressions which are obtained from Taylor Series approximations. Numerical values of the temperature dependent material properties are taken from Smithells [31]. Polynomials of the order indicated in Figures 3.16, 3.17, and 3.18 are fitted to the tabulated data so that the values of the thermodynamic properties can easily be calculated for any temperature in the range from 70°F to 1500°F. The expected maximum temperature rise of the bulk of the material lies well within these limits.

The difference equations and the polynomial approximations for thermal conductivity and specific heat are programmed for a digital computer. For any set of conditions two runs of the program are made. First using temperature dependent properties yields the exact numerical solution of the steady state temperature field. Second, the average properties are determined for the resulting temperature range and the computation is repeated assuming constant properties. In the third step the temperature field is determined using analytical models with the same set of parameters. For this comparison bulk temperatures are considered only. The numerical values of one set of parameters are given in Table 3.3. In Figure 3.19 the resulting three surface temperatures at $z = 0$ are plotted versus the horizontal position and in Figure 3.20 the temperatures at $x = 0$ are plotted versus depth.

A comparison of the finite difference solution for constant properties with the analytical solution reveals the inaccuracies of the finite difference method. They are caused by the finite number of grid points used which is not quite sufficient to represent the very large temperature gradients in the region $0 \leq x \leq \ell$. In separate computations it was established that the temperature field due to the volume heat source is calculated more accurately than the temperature field due to the surface heat source the computation of which involves a maximum error of about 5% of the local temperature when a grid of 36 by 71 points is used.

Table 3.3 Parameters for Comparison of Analytical Solution with Finite Difference Solution

Parameter	Numerical Values
halflength of heat source,	ℓ = 0.05 in
velocity of solid,	V = 10.0 ips
strength of heat source,	q_0 = 50.0 Btu/(in^2 sec)
energy fraction of surface heat source,	α_1 = 0.4
energy fraction of volume heat source,	α_2 = 0.6
decay coefficient of volume heat source,	β = 20.0 1/in
convection coefficient,	h = 0.0 Btu/(in^2 sec °F)
initial temperature,	T_1 = 70.0 °F
maximum temperature,	T_2 = 630.0 °F
average thermal conductivity,	k = 0.000674 Btu/(in sec °F)
average thermal diffusivity,	κ = 0.01931 in^2/sec
average specific heat,	c = 0.12326 Btu/(lbm °F)

Since the finite difference solutions for both constant and temperature dependent thermodynamic properties use the same number of grid points the same errors will be made. A comparison between those two solutions should yield similar results with respect to the effect of variable properties as a comparison between more accurate finite difference solutions using a far greater number of grid points.

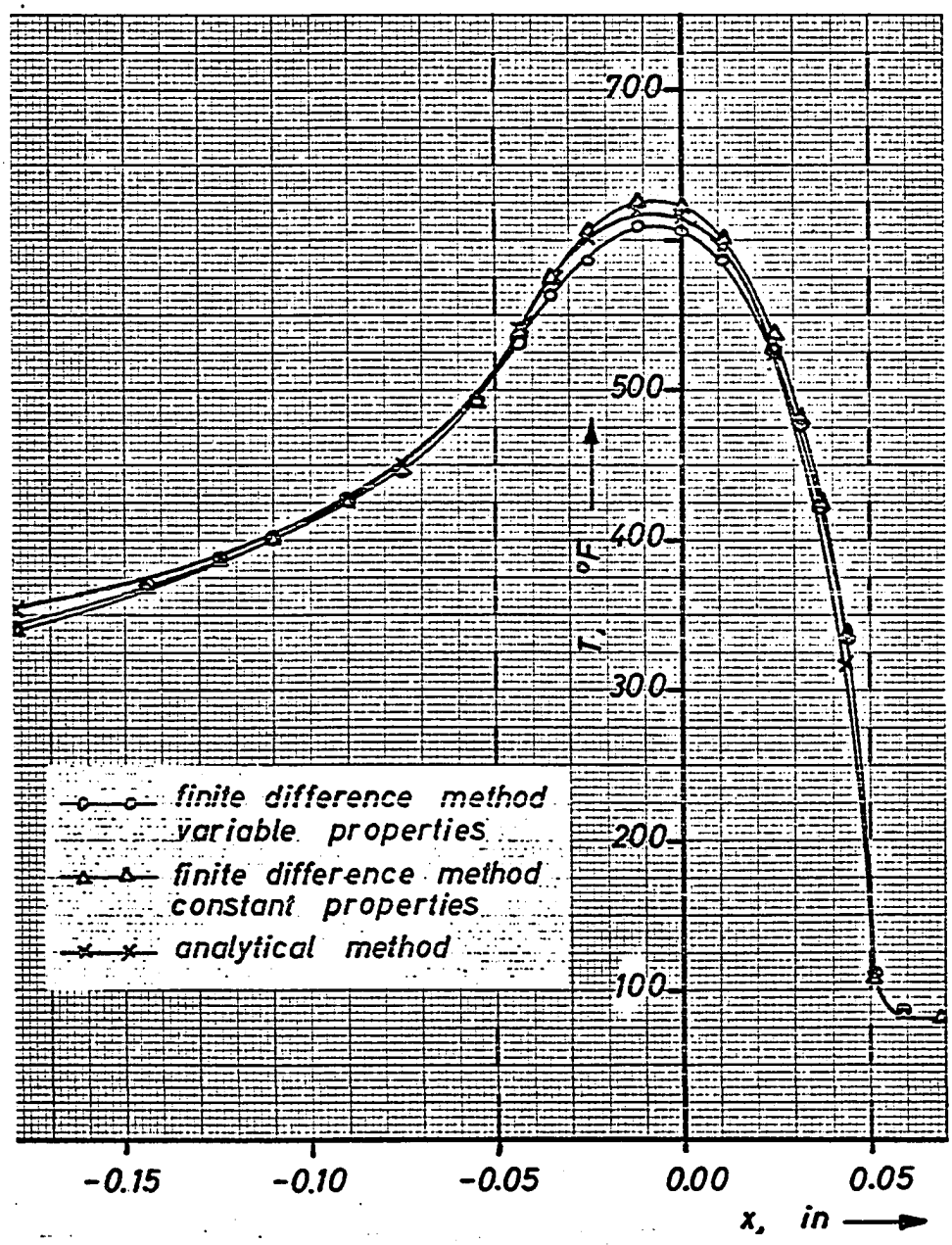

Figure 3.19 Surface Temperatures, Comparison of the Methods of Solution

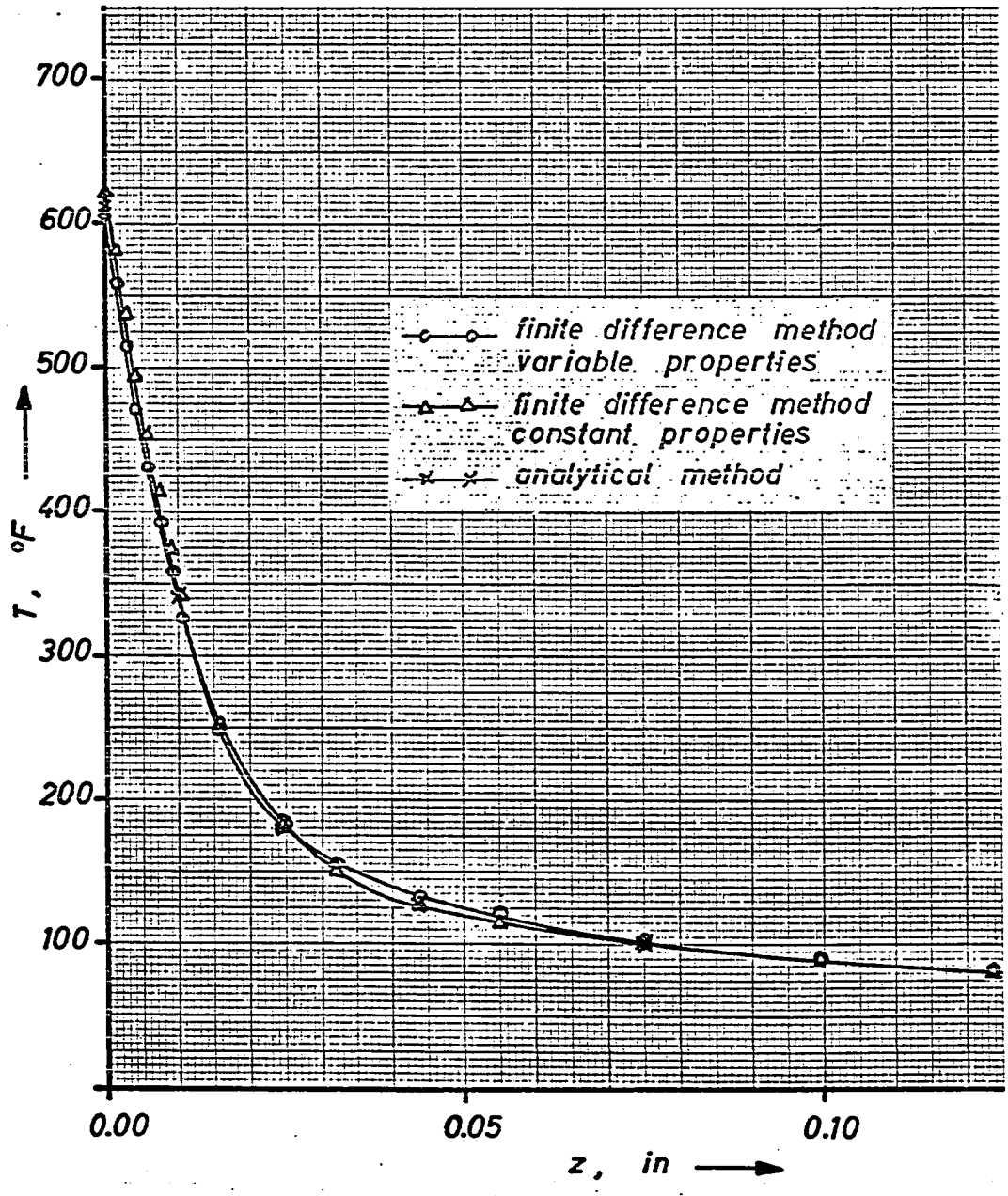

Figure 3.20 Temperature Under the Center of the Heat Source, Comparison of the Methods of Solution

When the two finite difference solutions are compared it is found that only under the center of the heat source the solution for constant properties gives slightly higher surface temperatures $\{(\Delta T_{max}) \doteq 12°F\}$. At some depth both temperatures are equal and for greater depth the solution for constant properties yields somewhat lower temperatures than are obtained with temperature dependent properties. Upon investigation of the complete region the maximum difference between the two solutions is found to be about 2% and occurs at the point $x = z = 0$. The maximum error caused by assuming constant thermodynamic properties is smaller than the typical error made in temperature measurements and can, therefore, be neglected.

3.3 Discussion of Parameters and Optimization Procedure

With the equations describing the analytical model of the grinding process the temperature rise at any point in the workpiece due to a single pass of the grinding wheel can be computed. In order to carry out these computations a large number of parameters which characterize the wheel, the workpiece, and the grinding process is required. They are collected in Table 3.4. While most of them can be determined either theoretically or by direct measurements during the grinding process others are difficult to measure and, therefore, their variations with the grinding conditions have not yet been studied.

Table 3.4 Parameters for Temperature Calculations

Group	Parameter	Symbol	Dimension
Machine	downfeed	d	in
	table speed	V_W	ips
	wheel speed	V_S	ips
Wheel	diameter	D	in
	number of cutting points	C	$1/in^2$
	ratio of chip width to chip thickness	r	
Workpiece	width	B	in
	thermal conductivity	k	Btu/(in sec °F)
	thermal diffusivity	κ	in^2/sec
	warm hardness	H_W	lbf/in^2
	decay coefficient of deformation	β	1/in
Dependent	horizontal component of grinding force	F_P	lbf
	cooling coefficient	h	Btu/(in^2 sec °F)
	energy fraction for frictional heat source	α_1	
	energy fraction for deformation heat source	α_2	

The machine parameters can directly be measured during or after grinding as well as the other geometric parameters, the wheel diameter and the workpiece width. The two remaining wheel parameters have been studied in their dependence on the grinding conditions and approximate formulae are available. In reference [20] the following expression was used to approximate measured values of the number of cutting points per unit area:

$$C = C_0(t - t_0) \tag{3.7}$$

The same set of data can be approximated by another, more convenient expression of the form

$$C = \left(\frac{t}{t_1}\right)^{n_C} \tag{3.68}$$

In Table 3.5 numerical values of the two constants t_1 and n_C for three wheel types are listed which were obtained by fitting curves of the type of equation (3.68) to the data in reference [20] and in Table 3.6 numerical values of the ratio of undeformed chip width to chip thickness are given which were obtained by Brückner [4].

Table 3.5 Fitted Constants of Equation (3.68) to Data from Reference [20]

Wheel	t_1	n_C
24 H	0.000007	2.0
60 H	0.0000147	3.0
80 H	0.000029	6.0

Table 3.6 Ratio of Undeformed Chip Width to Chip Thickness (from Reference [47]

Grain Size	Ratio r
36	18
46	15
60	12.5
80	10
120	7.6

Numerical values of the thermodynamic properties of different workpiece materials can be found in the literature. They depend on temperature but the discussion in the previous section shows that only small errors will result when the temperature field is calculated using average values.

Two parameters are introduced which describe the way in which the work material deforms under the influence of the grinding action. The hardness, H_W, and the decay coefficient, β, are both functions of the local workpiece temperature. At this time not enough test data are available to determine the numerical values of these two parameters accurately. An approximate value of the warm hardness can be obtained from measurements of the yield stress at elevated temperatures. Theories of hardness tests predict that the hardness value is about three times the value of the yield stress. In Figure 3.21 the yield stress, Y, of mild steel (0.21% C) is plotted

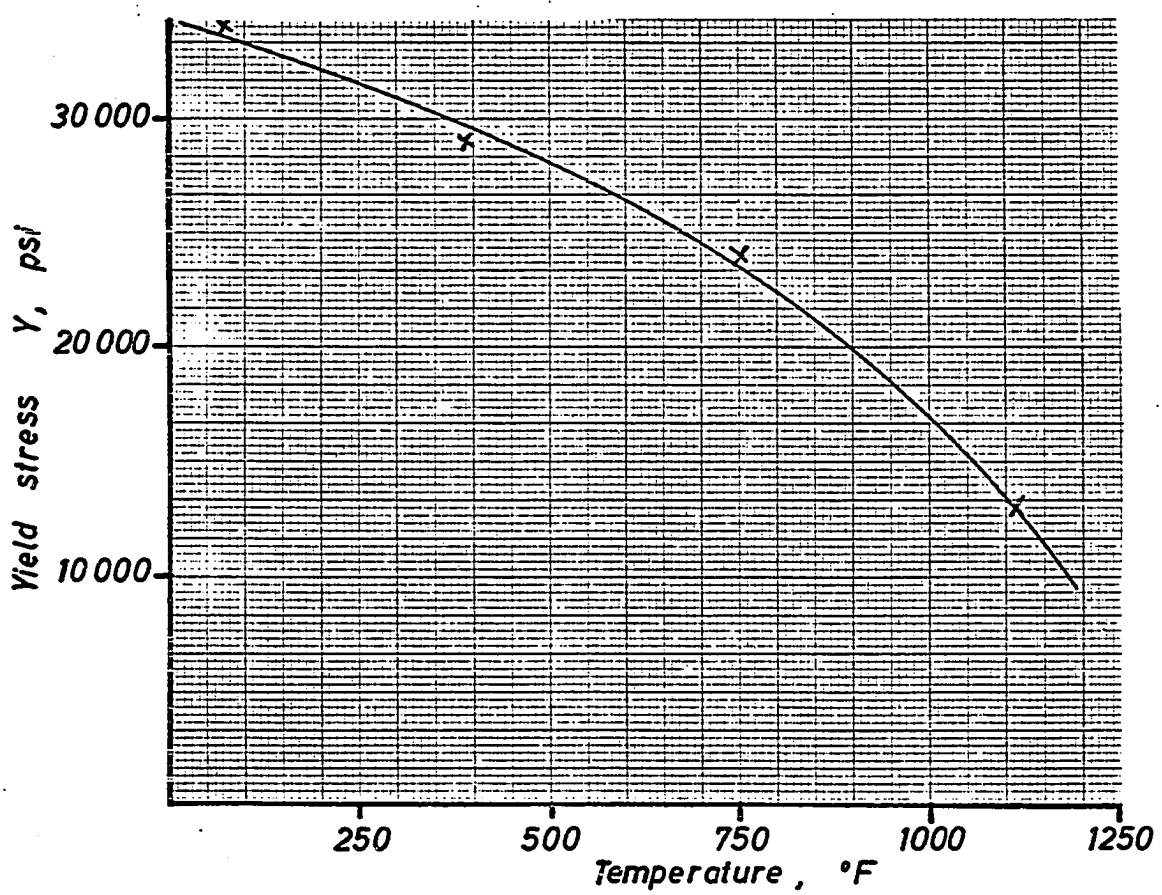

Figure 3.21 Yield Stress as a Function of Temperature for Steel (0.21% C) (From Reference [31])

versus temperature from data in reference [31]. The chip forming process in grinding is affected by the hardness of the workpiece beneath the contact zone. The average temperature of the bulk of the material in this zone will be used to find the yield stress and consequently an average hardness value of this material. In the grinding tests and the subsequent analysis in the following section this average temperature is determined to be about 550°F. The corresponding hardness value for mild steel is H_W = 80,000 psi.

The decay coefficient, β, which specifies the extent of the deformation into the depth of the workpiece has been defined for the first time in this thesis. In the appendix an experiment is described which allows this parameter to be evaluated. Its two limiting values are $\beta_{max} = \infty$ in the case that all deformation takes place at the surface and $\beta_{min} = 0$ if the deformation is constant throughout the depth.

The grinding force is one parameter of the grinding process which has been studied extensively. In tests with controlled downfeed or infeed as here the force is a dependent parameter while other investigators [10] control the pressure force component such that the rate of infeed depends on the grinding conditions. For the purpose of adaptive controlling the grinding machine it is often advantageous to control the power force component or, what is equivalent, the power consumed in the process. Both components of the grinding force can be measured with specially designed grinding dynamometers or their values can be calculated on the basis of previous results.

$$F_P = Bdu\ V_W/V_S \tag{3.69}$$

In reference [1] the specific energy of grinding, u, was shown to be a strong function of the maximum chip thickness which can be expressed as

$$u = \left(\frac{t}{t_2}\right)^{n_u} \tag{3.70}$$

where t_2 and n_u are constant over a limited range of t. By means of equations (3.3), (3.69), and (3.70) it is possible to predict the effect of changes in some grinding conditions on the power component of the grinding force which is related to the pressure component by the ratio μ which assumes values that vary slightly about an average value of $\mu = 0.5$.

$$\mu = F_P/F_Q \tag{3.71}$$

While the grinding force is the primary cause for the heat generation and, therefore, for the temperature rises in grinding it can be reduced by the lubricating properties of grinding fluids and under otherwise constant conditions can be used as a measure of those properties. The cooling capability of grinding fluids is measured by the convection coefficient, h. A large convection coefficient causes large temperature reductions which can be calculated analytically. Figures 3.9, 3.11, 3.13, and 3.15 show the maximum reductions which occur at the surface of the workpiece for a wide range of the nondimensional convection coefficient H which is related to h by:

$$H = \frac{2\kappa}{V}\frac{h}{k} \tag{3.40a}$$

From these figures it is clear that only coefficients H > 0.01 cause significant temperature reductions and if H > 10 they are as large as the temperature rise so that the resultant workpiece temperatures are effectively zero.

In the past several attempts have been made to determine the convection coefficients of fluids experimentally [11, 33, 14]. Except for the last study the test situation differed considerably from grinding so that there are doubts whether the results apply directly to grinding. The test situation in reference [14] simulates cylindrical grinding but the heat is generated by electrical heating elements and the wheel runs idle not touching the workpiece. A heavy stream of fluid is directed over the entire workpiece. This arrangement simulates grinding processes in which the wheel passes repeatedly over the workpiece and the fluid reduces the ambient temperature of the work. In the analysis and test program considered here only one pass is taken per test with sufficient time for cooling between tests. The cooling coefficients in the above equations are, therefore, different from those in reference [14] which can be considered only a first approximation. The maximum value for water-based coolants was found to be about h = 3000 Btu/(ft^2 hr °F) $\doteq$ 0.006 Btu (in^2 sec °F). The effectiveness of the coolant in reducing the temperatures due to single grain and interference zone heat sources becomes clear when the corresponding dimensionless convection coefficients are calculated as in the following example.

A workpiece from mild steel AISI 1018 is ground on a horizontal spindle surface grinder using a wheel speed of V_s = 800 ips and a table speed of V_w = 5 ips. The average thermal properties of the work material are k = 0.000664 Btu/(in sec °F) and κ = 0.01875 in^2/sec. for the single grain heat source:

$$H_G = 2 \frac{0.01875}{800} \frac{0.006}{0.000664} = 0.000424$$

for the interference zone heat source:

$$H_I = 2 \frac{0.01875}{5} \frac{0.006}{0.000664} = 0.0678$$

Under the assumed grinding conditions the fluid causes a reduction of the bulk temperature of about 15% but there will be no reduction of the temperature peaks under the grains.

This temperature reduction is not large, even though a very large convection coefficient is assumed. It follows that the cooling properties of the fluid are most important in reducing the ambient workpiece temperature due to many successive grinding passes. In order to reduce the peak temperature of a grinding pass the lubricating properties of the fluid must be improved which will reduce the grinding forces and, thereby, the total energy consumed in grinding. The temperatures depend primarily on the total amount of heat energy generated during one pass which is related to the consumed mechanical energy by the energy fractions α_1 and α_2.

Calorimeter studies [3] of dry surface grinding indicate that $\alpha = \alpha_1 + \alpha_2$ may take values between 0.5 and 0.85. This method is only applicable in dry grinding while all or most surface grinding is done wet which situation is complicated by the cooling effect of the fluids used.

This problem can be solved with a procedure which has been developed to extract the numerical values of the energy fractions α_1 and α_2 as well as the value of the cooling coefficient h from measured workpiece temperatures. If values of α_1 and α_2 and h are assumed the temperatures can be calculated with equation (3.61) at exactly the same locations at which the temperatures have been measured. Since only assumed and not the correct values were used there will be a difference between the experimental (T_e) and the calculated (T_c) temperatures. If the correct values were used the difference ($T_e - T_c$) would be zero at all points. Due to experimental errors and uncertainties in the analytical model the differences will not vanish for any set of these three parameters. But it is possible to find the set which minimizes the sum of squared differences. If the mean difference for this optimum set is small, say less than three times the experimental error, the matching of experimental and calculated temperatures can be called successful and the numerical values of the parameters are found.

With this in mind equation (3.61) can be considered a function of α_1, α_2 and h and rewritten as

$$T_c = \alpha_1 \{T_3' - T_7'(h) + \max(T_1')\} + \alpha_2 \{T_4' - T_8'(h) + \max(T_2')\} \tag{3.72}$$

For every value of h, T_c is a linear function of α_1 and α_2. The optimum set of α_1 and α_2 which minimizes

$$E = \sum_{i=1}^{M_P} (T_e - T_c)^2 \tag{3.73}$$

for a fixed h can be found by standard optimization techniques:

$$T_S = T_3' - T_4'(h) + \max(T_1')$$

$$T_V = T_4' - T_8'(h) + \max(T_2')$$

$$\det = (\Sigma T_S T_V)^2 - \Sigma T_S^2 \, \Sigma T_V^2$$

$$\alpha_1' = \frac{1}{\det} \{\Sigma T_S T_V \, \Sigma T_V T_e - \Sigma T_V^2 \, \Sigma T_S T_e\}$$

$$\alpha_2' = \frac{1}{\det} \{\Sigma T_S T_V \, \Sigma T_S T_e - \Sigma T_S^2 \, \Sigma T_V T_e\}$$

where the sums are taken over all M_P data points considered.

If these optimized values α_1 and α_2 are introduced into equation (3.72) T_c becomes a nonlinear function of h only. Standard subroutines are available on digital computers to find the value of h which minimizes equation (3.73).

This two level approach reduces the number of variables which must be optimized numerically from three to one and is far more accurate and efficient than multi-dimensional search techniques. It works well because the functions describing the temperature fields due to the different sources of heat are linearly independent. As a test of the algorithm used temperature fields are calculated for several sets of parameters and then used as "experimental" temperatures for the optimization routines. In Table 3.7 these sets are listed. The optimized parameters are accurate to within six digits in all cases and the standard deviation of the calculated temperatures

$$\Delta T = \sqrt{E/M_p} \tag{3.74}$$

is of order 10^{-5}.

Table 3.7 Parameter Set for Optimization Procedure

α_1	α_2	h	ΔT
0.001000	0.875000	0.000000	0.00002
0.750000	0.015000	0.000000	0.00001
0.500000	0.500000	0.000000	0.00000
0.500000	0.500000	0.000010	0.00001
0.500000	0.500000	0.000100	0.00001
0.500000	0.500000	0.001000	0.00001
0.500000	0.500000	0.010000	0.00001

If this procedure is to be used with experimentally measured temperatures it is necessary not only to accurately measure the temperatures but also the position where the temperature reading is taken. This requirement complicates the testing procedure considerably as is shown in the following section.

3.4 Plunge Grinding Tests

3.4.1 Test Description

In order to test the accuracy of temperature calculations with the equations for the analytical model and in order to gain some new insight into the fundamental energy dissipation during grinding several test series were designed. The grinding process for which the thermal analysis was carried out is the surface grinding process under plunge grinding conditions. Although the analysis can easily be adopted for regular surface grinding with cross feed all tests run are plunge grinding tests without cross feed and with linear table motion.

The test machine is a

Do-All surface grinder Model D 842 - 12

with an infinitely fine variable hydraulic table drive and infinitely fine variable wheel speed. The grinding wheel is the same for all tests reported in this chapter. Made by the Carborundum Company it carries the designation

60 - L8 - V (8 x 3/4 x 3)

The grain material is C34, white aluminum oxide.

All workpieces are made from the same material, carbon steel key stock, AISI 1018, in the as delivered state. Their size is selected with the theoretical model in mind. A length of 3 inch is chosen which is sufficiently long that the temperature distribution in the middle of the piece is not disturbed by end effects. Also, it is short enough to yield constant force readings when mounted on top of a grinding dynamometer. The width of the workpiece should be wide enough to satisfy the two-dimensional model even without insulating the sides of the piece and it should be small enough in order that the available spindle power is not exceeded during the plunge cuts. The height of the workpiece is determined from the condition that an undisturbed temperature field can develop in the region of interest for temperature measurements. A square cross section of 0.25 inch by 0.25 inch fulfills the requirements. Figure 3.22 shows the workpiece mounted in its holder. The assembly is placed either directly on the grinding table or on a grinding dynamometer which sits on the table.

Each test consists of one plunge grinding pass of the wheel over the workpiece in the up-grinding configuration. The height of the workpiece is measured to within 0.00005 inches before and after the cut at five positions along the length with a dial indicator mounted on the machine bed. During the cut the table speed, the wheel speed, the grinding force, and the workpiece temperature are measured and recorded continuously.

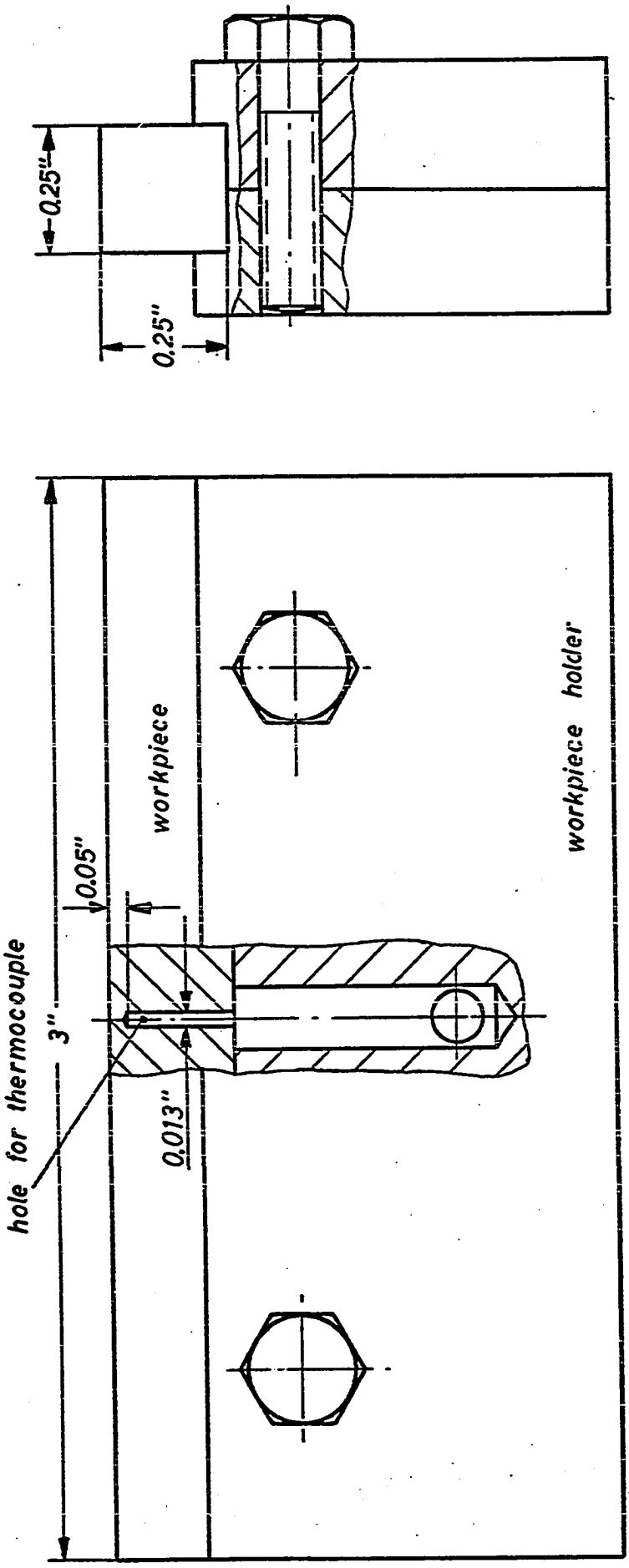

Figure 3:22 Workpiece for Plunge Grinding Tests

A test series consists of all tests performed under constant conditions using the same workpiece. In order to achieve repeatable settings of depth of cut and table speed it was found necessary to grind one workpiece under constant conditions only. The following cycle is maintained throughout this test program:

1) Dress the wheel with a single point cone shaped diamond under conditions as follows:

   Wheel speed = 1840 rpm

   Downfeed = 0.001 in/pass

   Crossfeed = 10 ipm

2) Make 5 or 6 grinding passes under the chosen grinding conditions without taking measurements. The passes are done in not too rapid sequence with sufficient time for cooling to maintain a constant initial temperature in the workpiece.

3) Make 2 measured grinding passes under constant conditions.

4) Repeat steps 2) and 3) until a layer of predetermined thickness (about 0.04 in) is removed from the workpiece. Measurements of the grinding forces indicate that the sharpness of the wheel remains essentially constant during one test series so that dressing is not required between tests.

5) Measure the horizontal position of the workpiece on the table.

6) Remove the workpiece from its holder and determine the depth of the thermocouple embedded in the workpiece.

At the end of such a test series about ten temperature traces and grinding force diagrams have been obtained under conditions as identical as possible. From pass to pass the depth of the thermocouple below the workpiece surface reduces so that in the course of the test series the two-dimensional temperature field in the workpiece is measured with one thermocouple. This data can then be compared with calculated values and it can be analyzed further to obtain information about the energy dissipation in the workpiece which knowledge will help in the understanding of the grinding process.

3.4.2 Measurement of Workpiece Temperatures

The temperatures in the workpiece are measured with a steel-constantan thermocouple at one location in the workpiece. In order to minimize the disturbance caused by the thermocouple its size must be kept as small as possible. For this reason the body of the workpiece is used as part of the couple. A thin constantan wire of 0.005 inch diameter insulated with a layer of Teflon of 0.0005 inch thickness is introduced from the bottom of the workpiece through a hole of 0.013 inch diameter to within about 0.05 inch of the top surface. It is spot welded at the tip of the hole thus forming a thermocouple with the workpiece material. The quality of every junction is

checked by measuring the resistance of the couple. The exact depth below the surface of the tip of the hole and the junction are measured by sectioning the testpiece after grinding. Figure 3.23 shows photographs taken of the cross section through the hole and the constantan wire. It was not possible in all cases to obtain sections through the thermocouple junction which then is assumed to lie at the tip of the hole.

This arrangement of the thermocouple is similar to the ones used by Littmann and Wulff [17] and Takazawa [32]. The sizes of the hole and the junction are considerably smaller in the present program than they were in the tests of those investigators. The length of contact between the wheel and the workpiece is about seven times larger than the diameter of the hole and fifteen to twenty times larger than the thermal junction. No temperature measurements will be considered if the depth is less than the diameter of the hole. It is, therefore, expected that the measured temperatures are only very slightly influenced by the equipment and closely reflect the true undisturbed temperature field in the workpiece.

The circuit for measuring the emf of the thermocouple is completed by attaching an iron wire to the workpiece which is connected to a reference iron-constantan thermocouple kept at room temperature in a dwell container and feeding the output into an electron beam oscilloscope. This oscilloscope, Hewlett-Packard Model 141A, has a persistent scope with a split beam. That feature allows a signal

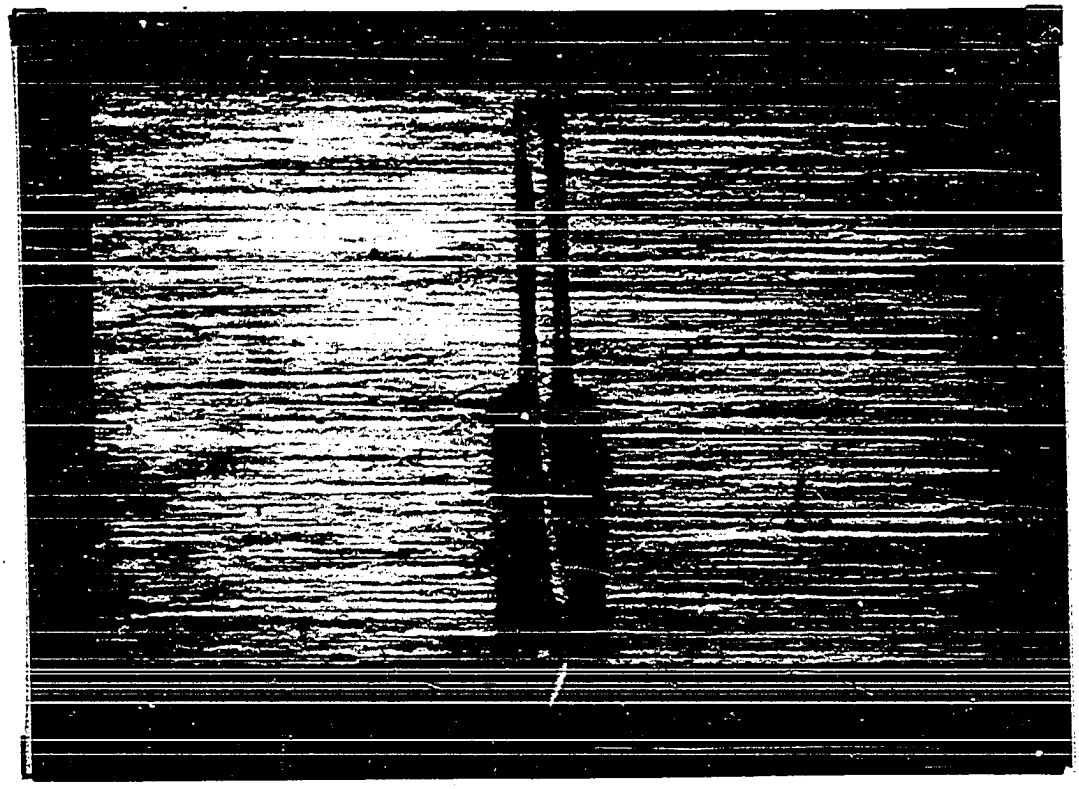

a) Magnification 17.5x

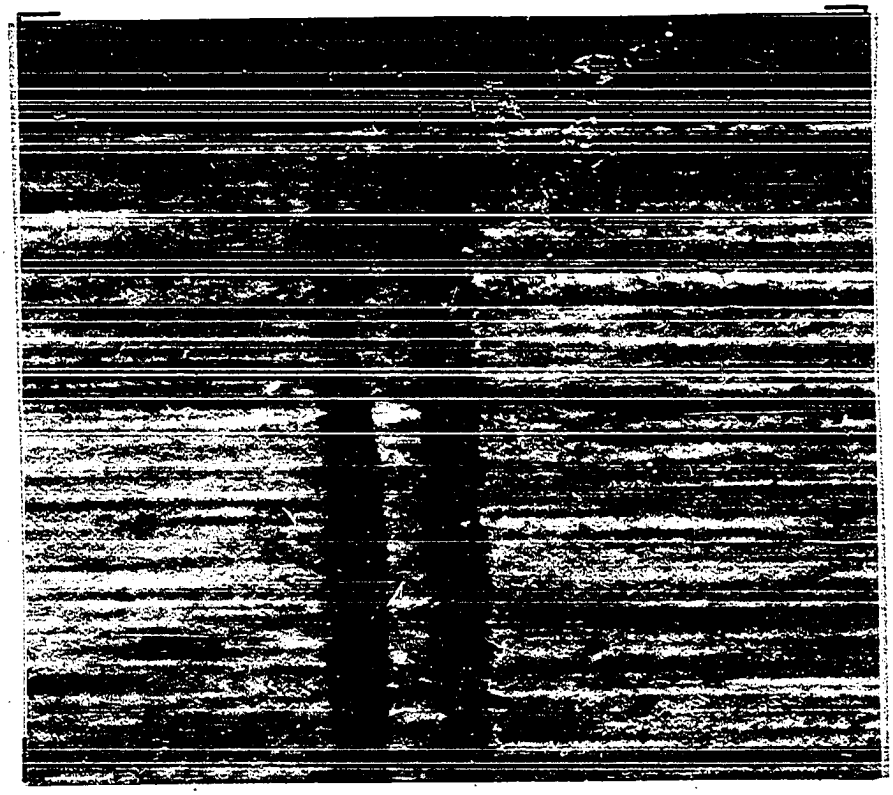

b) Magnification 61.3x

Figure 3.23 Sectioned Thermocouple Junction

to be stored and viewed on the scope a long time after it actually occurred. This is very handy in temperature measurements because an impulse of very short duration is generated by the thermocouple. The retained image is then photographed on Polaroid Slide Film No. 146. The traces on the slides are measured on a scanning machine which records the temperature in small increments along the trace on punched cards.

The accuracy of the temperature measurements is determined mainly by the available magnification and the width of the traces of the scope. The highest magnification is 0.5 mV/mm and the average width of the traces is 0.5 mm. It is estimated that on the scanning machine the center of the trace can be determined to within 0.1 mm so that the probable error in reading the traces is about 0.05 mV.

The steel-constantan thermocouple was calibrated using a metallurgical furnace and an actual workpiece thermocouple with a calibrated copper-constantan thermocouple as reference. In the temperature range from 70 °F to 1200 °F the workpiece thermocouple was found to be linear. It generated an emf of 0.0299 mV/°F. The probable error of reading the temperature traces is, therefore, about 1.7 °F.

For the subsequent analysis of the measurements all traces must have a reference point which relates their position to the position of the wheel. This point is provided by displaying a stepped signal together with the temperature trace on the scope. The instance at which the step in the reference signal occurs is determined by

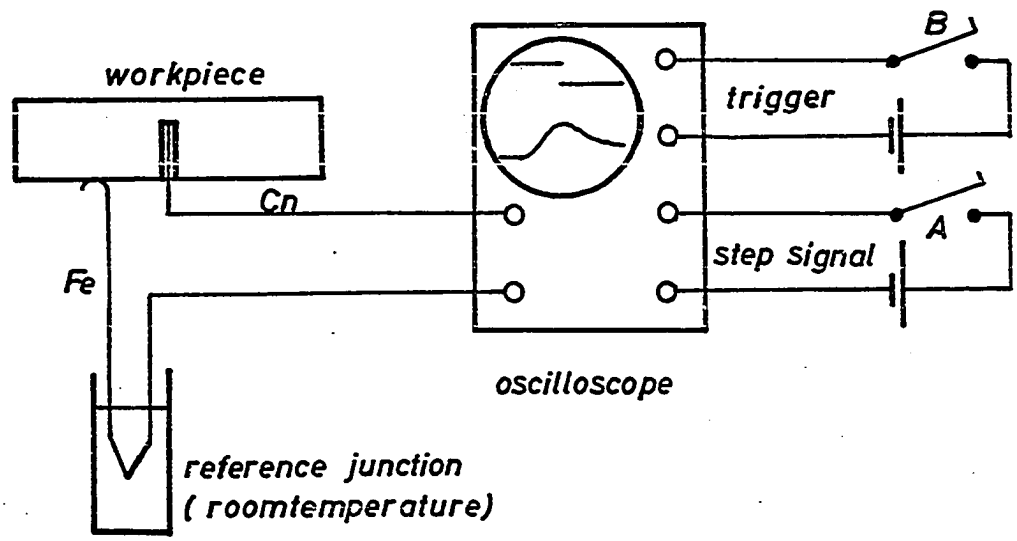

Figure 3.24 Circuit Diagrams

microswitch A which is actuated by a cam fixed to the table. A second microswitch, B, is used to trigger the scope just before the thermocouple reaches its position under the wheel so that the temperature impuise can be recorded using a fast time sweep. Figure 3.24 shows the circuit diagrams for thermocouple and reference circuits and Figure 3.25 illustrates a typical image on the scope. The relative positions of the moving thermocouple and the grinding wheel at the instance at which the reference mark is produced is determined from a photographic picture (Figure 3.26a) of the wheel and workpiece taken by a single flash of a stroboscope. It is triggered by microswitch A and in order to determine the exact time of the flash it is picked up by a photocell having a very high frequency response and recorded on the oscilloscope together with the reference step signal as shown in Figure 3.26b.

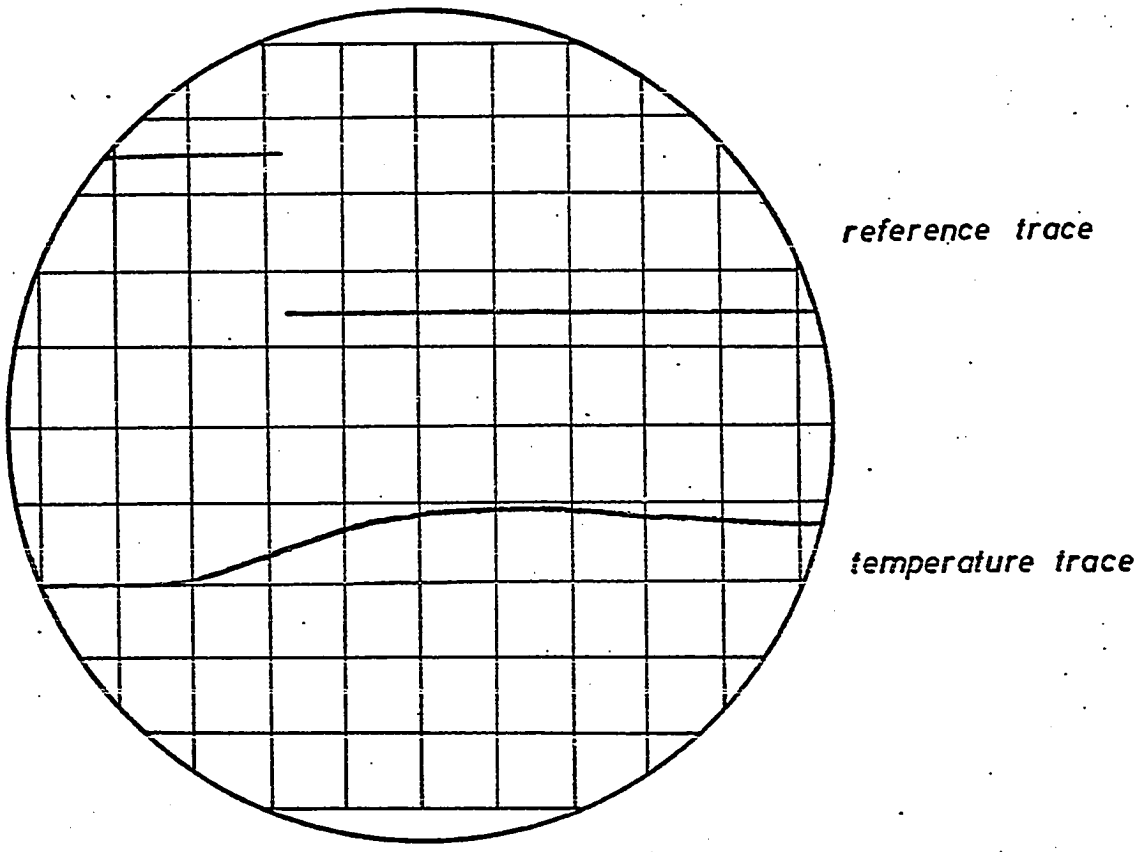

Figure 3.25 Temperature and Reference Traces on the Scope

This photograph is taken at some time before or after every test series with the table moving at the same speed as used in the grinding tests but with the wheel standing still and disengaged from the workpiece. The horizontal distance x_0 of the thermocouple from the center of the wheel at the instance at which the reference step signal occurs can then be found from equation (3.75).

$$x_0 = x_1 - V_w \Delta\tau \qquad (3.75)$$

where x_1 and $\Delta\tau$ are defined in Figures 3.26a and b, respectively.

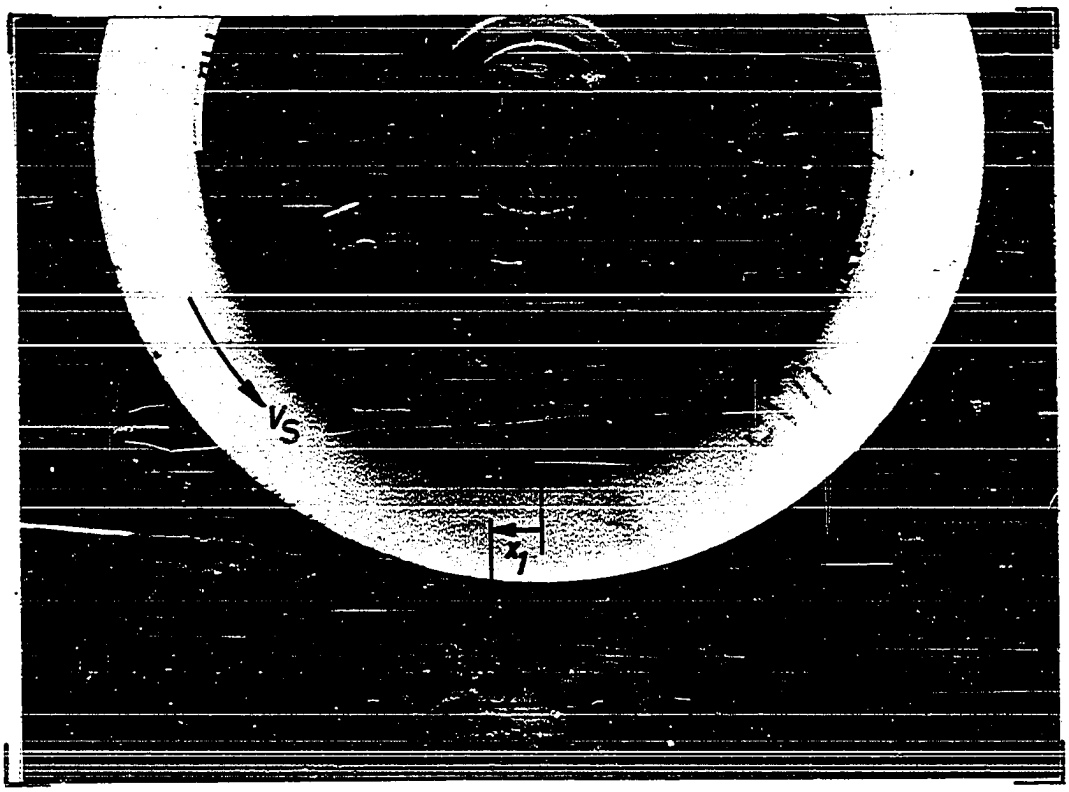

a) Photograph of Wheel and Workpiece

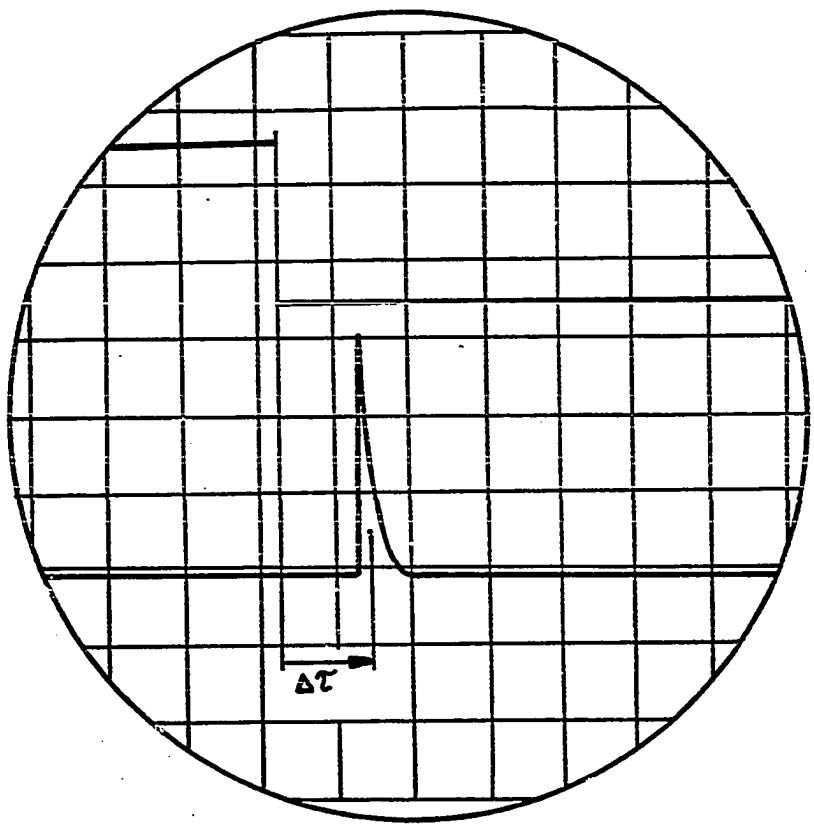

b) Traces of Reference Signal and Strob-Flash

Figure 3.26 Measurement of the Relative Distance Between the Wheel and the Thermocouple

3.4.3 Velocity and Force Measurements

The table speed is measured with a linear transducer of 36 inch length which generates a voltage proportional to the speed over the entire range of travel of the table. This signal is fed into a Sanborn Model 320 DC Duo-Channel Recorder and is recorded together with the change of the wheel speed during the cut. A tacho-generator driven by a belt and pulley system from the grinding wheel spindle produces a voltage proportional to the wheel speed. In order to obtain higher resolution to detect small changes in speed during the cut an electric circuit for suppressing the signal at idle speed was designed. The output signal of this circuit is proportional to the variation of the spindle speed and when fed into the recorder can be used to detect changes as small as 1 rpm.

Both the power and the pressure components of the grinding force can be measured with a two component strain ring grinding dynamometer, the principle of which is described by Shaw in reference [25]. This instrument is calibrated together with a Sanborn Model 321 AC Duo-Channel Recorder to give 5 mm stylus deflection per 1 lbf vertical load and 10 mm deflection per 1 lbf horizontal load.

Measurements of both the horizontal grinding force (power component) and the drop in wheel speed during the first few test series revealed a linear relationship between the force and the maximum drop in speed as shown in Figure 3.27. Traces of the change of wheel speed show an

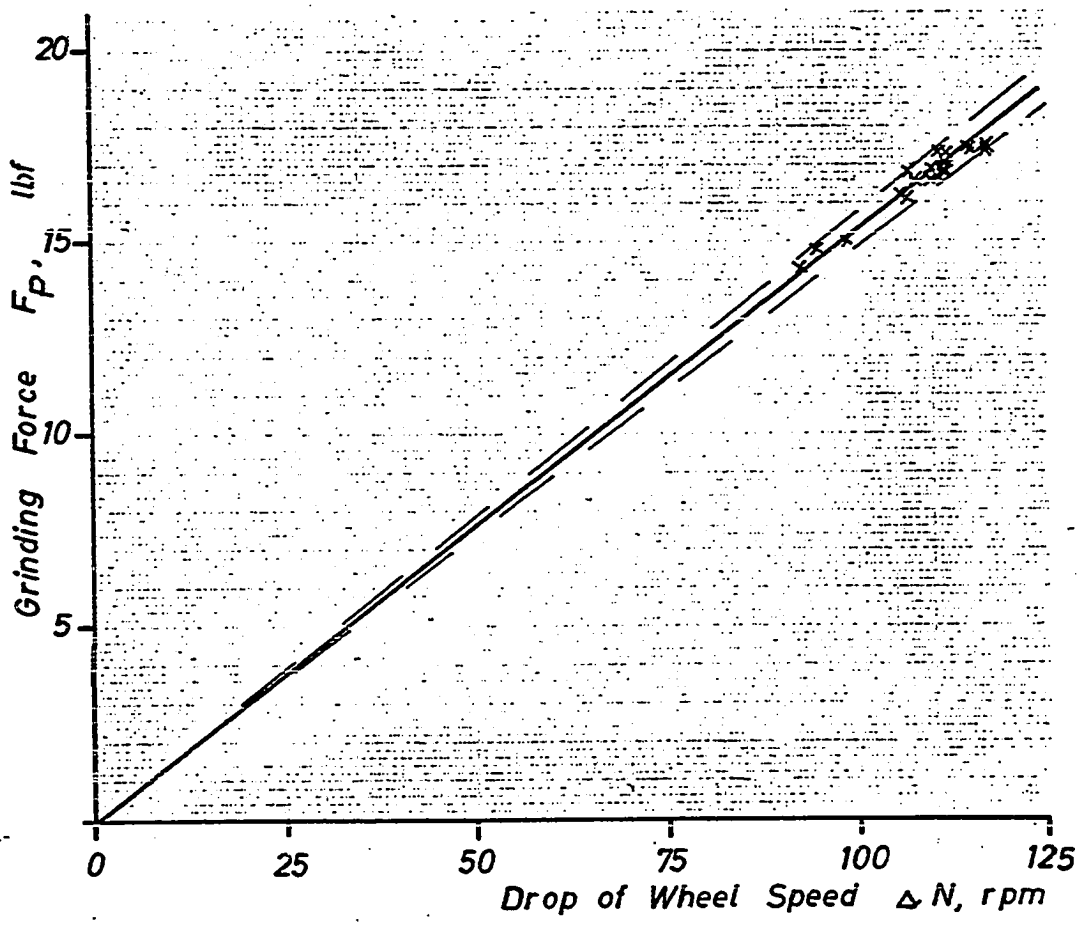

Figure 3.27 Experimental Relationship Between the Horizontal Grinding Force and the Drop of Wheel Speed

almost linear decrease with cutting time. This behavior suggests that all the grinding energy is supplied by the kinematic energy stored in the wheel and the drive system and that the electric drive motor reacts too slowly to the increased load to be able to put out more energy. The total time of grinding per pass is $\tau_0 <$ 0.5 sec for all tests of this program. The power component of the grinding force can be calculated from the measured drop of wheel speed according to the following analysis.

it is assumed that the motor supplies just enough energy during the short time of cut to account for all windage losses as it does when the wheel is running at constant idle speed, N_0, before every grinding pass. All of the grinding energy is supplied by the kinetic energy of the wheel-drive system. If the grinding force F_P is assumed to be constant during the cut the drop in speed can be calculated as:

$$\Delta N = N_0 - N = \frac{2\pi}{60} \frac{R \bar{F}_P}{I} \tau \qquad (3.76)$$

Equation (3.70) describes mathematically the observed linear relationship between ΔN and F_P. From the experiments for which ΔN, F_P and τ_0 are known the moment of inertia of the system can be determined:

$$I = \frac{\pi}{30} \frac{F_P}{\Delta N} R \tau_0 \qquad (3.77)$$

$$I = 0.02485 \text{ in lbf sec}^2$$

Knowing the moment of inertia of the system, the average value of the power component of the grinding force can be calculated.

$$F_P = 0.0592 \frac{\Delta N}{\tau_0} \text{ , lbf} \qquad (3.78)$$

This second method of measuring the grinding force has been adopted for the later part of the test program. Its advantages are that

the process is not disturbed by introducing an additional elastic member of low rigidity into the grinding system and that it works as well in dry as in wet grinding whereas great care must be taken to insulate the dynamometer against the grinding fluid without to effect its accuracy.

The disadvantages are that this method gives only an average value of one force component and it is applicable only if the grinding time per pass is small. For the purpose of this investigation the disadvantages do not pose any problem so that all necessary information can be obtained from this indirect method.

3.4.4 Test Conditions and Results

In this test program twelve test series were conducted, the conditions of which are summarized in Table 3.8. In the first five series no grinding fluid is used. The table speed varies from 6.0 ips to 10.9 ips and the nominal depth of cut is 0.001 inch in all but one series where it is reduced to 0.00056 inch. In this test series difficulties were encountered in repeating the same small depth setting with sufficient accuracy. Difficulties were also anticipated for depth setting greater than 0.0015 inch because of increased grinding forces. It was therefore decided to limit the test program to one depth setting only. Three more test series are run with a water soluble grinding oil, TRIM EP in a concentration of 4%. The table speed varies from 6.6 ips to 12.1 ips. Three test series are

Table 3.8 Test Conditions for Horizontal Spindle Surface Grinding Program

No.	V_S ips	V_W ips	d in	ℓ_c in	t 10^{-3} in	C in^{-2}	u 10^6 psi	F_P lbf	$\dot{Q}_F$ Btu/sec	Fluid
1	770	6.0	0.00105	0.0917	0.150	1058	6.551	13.4	1.108	dry
2	770	7.5	0.0011	0.0938	0.158	1226	6.123	16.4	1.352	dry
3	770	7.95	0.00056	0.0669	0.149	1037	7.057	10.2	0.842	dry
4	750	9.5	0.0011	0.0938	0.166	1437	6.279	21.9	1.761	dry
5	770	10.9	0.001	0.0894	0.168	1491	8.618	30.5	2.569	dry
6	750	6.6	0.0011	0.0938	0.154	1151	5.306	13.8	1.029	Trim EP 4%
7	750	9.5	0.00102	0.0903	0.165	1407	6.565	21.3	1.711	Trim EP 4%
8	750	12.1	0.00099	0.0890	0.173	1609	6.628	26.5	2.130	Trim EP 4%
9	750	9.2	0.00098	0.0885	0.163	1356	7.952	23.8	1.913	Trim EP 10%
10	750	9.2	0.00102	0.0903	0.164	1380	7.224	22.7	1.825	Trim EP 20%
11	750	9.6	0.00095	0.0872	0.164	1380	4.094	12.5	1.005	oil
12	1360	9.8	0.00096	0.0876	0.146	985	4.032	7.0	1.020	oil

conducted with approximately the same machine setting using different grinding fluids, TRIM EP (10%), TRIM EP (20%), and MOBIL VACMUL 0-15-L. In all these test series the same spindle speed of N_w = 1840 rpm is used which gives a wheel speed of V_s = 770 ips with a wheel of 8 inch diameter. At the end of the test program the wheel is worn to a diameter of 7.8 inch so that the wheel speed dropped to V_s = 750 ips. For the last test series the wheel speed is raised to the maximal possible speed of V_s = 1360 ips and as the grinding fluid an oil, MOBIL VACMUL 0-15-L, is used.

The values given for table speed, wheel depth of cut, and horizontal grinding force are average values over all test runs considered in the temperature analysis of the series. From these the values for chip length, chip thickness, number of active grains, and specific energy have been calculated.

For every test series about ten measured test runs were made and temperature profiles were produced for each of them. From these test runs about three or four are selected for further analysis. The selection is made such that the full range of depth is covered and the test conditions are as identical as possible especially with respect to the depth of cut. As an example of the complete record of a test series Table 3.9 gives the test data for test series No. 9. Figure 3.28 illustrates a typical recording of the table speed and the grinding force and was obtained in test No. 9.5. The temperature profile of the same test is shown in Figure 3.29a while Figure 3.29b

Table 3.9 Measurements of Test Series 9

Test Series 9 Date: September 28, 1970

Wheel: 60 - L8 - V (C34), V_s = 750 ips
Workpiece: AISI 1018 CR
Fluid: TRIM EP 10%

Test No.	Dial	Indicator		Readings	, in	d, 10^{-3} in	z, in	V_w, ips	F_p, lbf
1	0.1466	0.1444	0.1442	0.14415	0.14425	1.1	0.0371	8.9	25.4
2	0.1454	0.1436	0.1431	0.14315	0.14355	0.7	0.0360	9.0	25.2
	0.1445	0.1424	0.1424	0.1424	0.1427		0.0353		
3	0.1396	0.1377	0.1374	0.1374	0.1379	0.8	0.0303	9.2	22.7
4	0.1386	0.1368	0.1366	0.1366	0.1371	0.95	0.0295	9.2	23.3
	0.1377	0.1358	0.13565	0.13565	0.1361		0.02855		
5	0.1327	0.1310	0.1309	0.1308	0.1311	0.9	0.0238	9.2	21.8
6	0.1318	0.1301	0.1300	0.1299	0.13025	1.1	0.0229	9.2	22.0
	0.1308	0.1291	0.1289	0.1289	0.1293		0.0218		
7	0.1217	0.12045	0.1205	0.12045	0.1207	1.2	0.0134	9.2	23.5
8	0.1211	0.1195	0.1193	0.11925	0.1197	0.9	0.0122	9.3	20.9
	0.11995	0.1185	0.1184	0.1183	0.1187		0.0113		
9	0.1153	0.1138	0.1137	0.1137	0.1139	0.85	0.0066	9.4	20.1
10	0.1144	0.11305	0.11285	0.1128	0.1130	1.0	0.00575	9.3	20.9
	0.1134	0.1120	0.11185	0.11185	0.1121		0.00475		

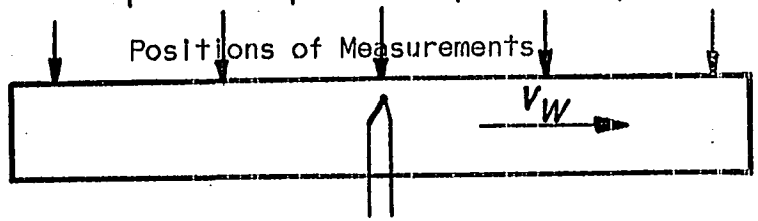

Depth of thermocouple after sectioning z_0 = 0.00475 in

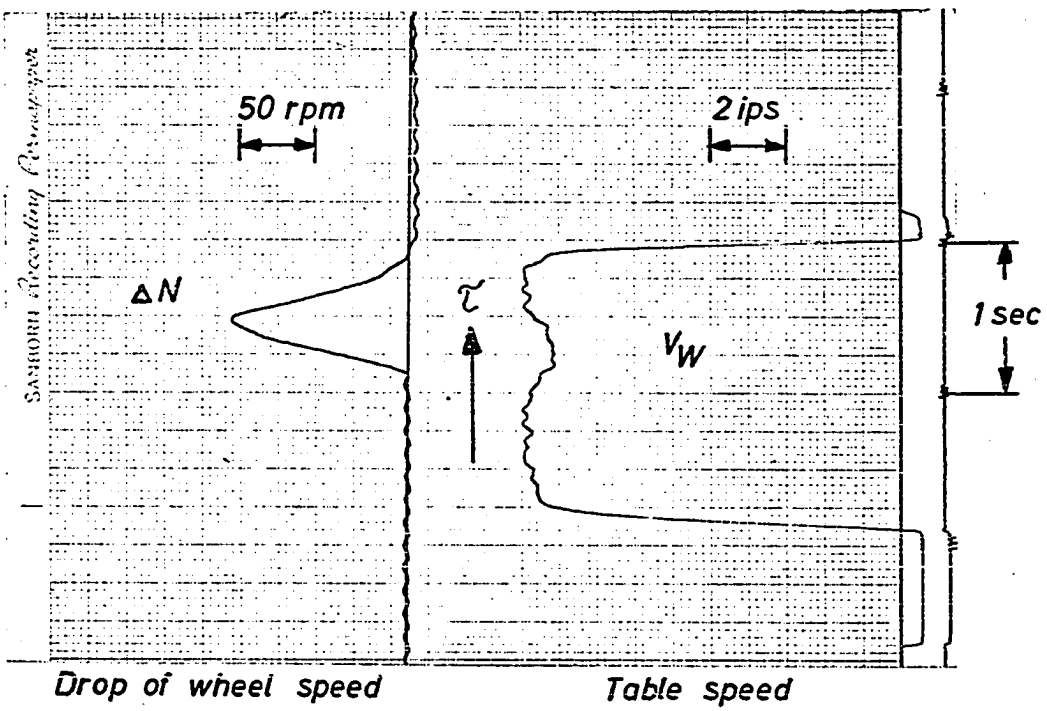

Table 3.28 Trace of Table Speed and Drop of Wheel Speed of Test 9/5

shows the temperature trace for test No. 9/10. The ragged profile of the trace represents the temperature peaks due to single grains. These peaks are picked up on all traces at the end of a test series whenever the depth of the thermocouple below the workpiece surface becomes small. These traces are not used in the subsequent analysis because large distortions in the data are anticipated due to the close proximity of the couple to the heat source.

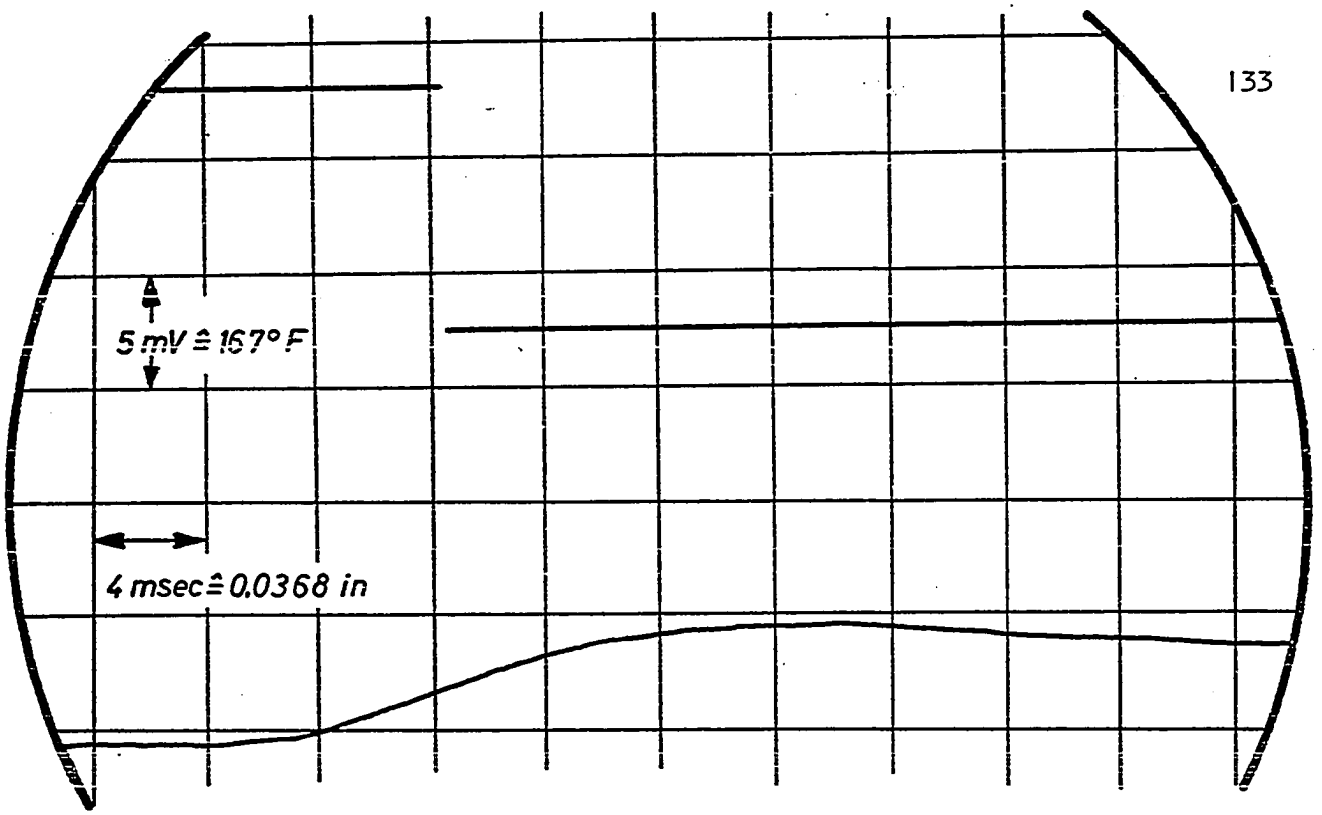

a) Test 9/5 (z = 0.0238 in)

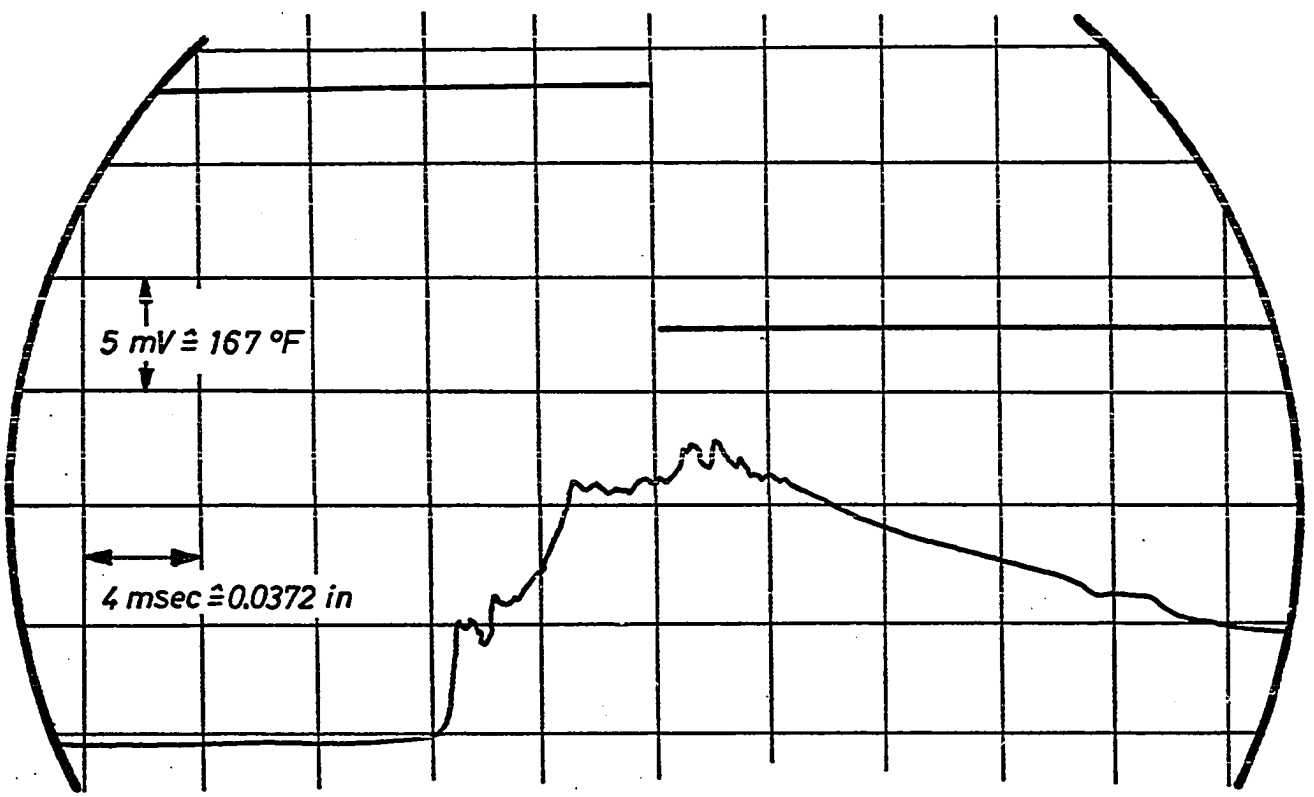

b) Test 9/10 (z = 0.0057 in)

Figure 3.29 Temperature Profiles for Test Series No. 9

Table 3.10 Results of Optimization Procedure

Test Series No.	α_1	α_2	α	h $\frac{Btu}{in^2 sec °F}$	ΔT °F	$\dot{Q}_H$ $\frac{Btu}{sec}$	$F_{C,max}$ °F	F_F °F
1	0.6912	0.0000	0.6912	0.0000	15.65	0.765	6450	877
2	0.4393	0.1186	0.5579	0.0000	18.26	0.755	4010	644
3	0.7298	0.0000	0.7298	0.0001	22.67	0.614	7130	717
4	0.5143	0.0086	0.5229	0.0000	5.41	0.921	4830	818
5	0.2172	0.0974	0.3146	0.0000	9.62	0.810	2680	516
6	0.1420	0.1366	0.2786	0.0000	5.56	0.286	1140	199
7	0.4270	0.0499	0.4769	0.0057	8.94	0.815	4140	688
8	0.3389	0.0374	0.3763	0.0017	11.34	0.802	3380	604
9	0.3387	0.0140	0.3527	0.0005	4.77	0.674	3770	619
10	0.4283	0.0000	0.4283	0.0007	13.66	0.781	4440	728
11	0.6589	0.0000	0.6589	0.0001	21.55	0.663	4420	614
12	0.6200	0.0000	0.6200	0.0001	8.00	0.632	5260	580

The following tests have been selected for the temperature analysis:

9/1, 9/4, 9/5, 9/8

From the temperature profiles of these four tests, 26 data points have been measured and punched on computer cards. By using the above described optimization procedure the energy fractions α_1 and α_2 and the convection coefficient, h, are determined from those temperature points. The results of this procedure for all test series are summarized in Table 3.10.

Together with the values of the three parameters the value of the root-mean-square error, ΔT, between the calculated and the experimental temperatures is given for each test series. The larger values of the error are such that the energy fractions α of the respective test series could only be determined with an accuracy of about 10% and the values of the convection coefficient, h, have no real meaning. In cases for which a better fit was obtained, the energy fractions are estimated to be accurate to within 1.0%. The uncertainties in the values of h are still large since the calculated temperatures vary only slightly for large variations of h and small variations in the experimental temperatures will cause large changes of the root-mean-square error. Therefore, only the average values of the convection coefficient h for each of the different cooling fluids used will have some realistic meaning. These values are given in Table 3.11.

Table 3.11 Average Values of the Convection Coefficients for Various Grinding Fluids

Grinding Fluid	Convection Coefficient Btu/(in^2 sec °F)
Air	0.0000
Trim EP, 4%	0.0032
Trim EP, 10%	0.0005
Trim EP, 20%	0.0007
Mobil, Vacmul 0 - 15 - L	0.0001

The further discussion of the results presented in Tables 3.8 and 3.10 is carried out in terms of the energies involved. First, a plot of the total cutting energy per unit time, $\dot{Q}_F$, versus the rate of metal removal, $\dot{M}$, (Figure 3.30) will be considered. It shows that the energy consumption increases progressively with the rate of metal removal. There is no significant effect of the soluble grinding oil on the required energy. Only when the straight grinding oil is used does the energy consumption drop. Similar conclusions could be drawn from a plot of the specific energy, u, versus the chip thickness, t, but the range of t is so narrow and the scatter of the values of u is so great that such a plot is not presented here.

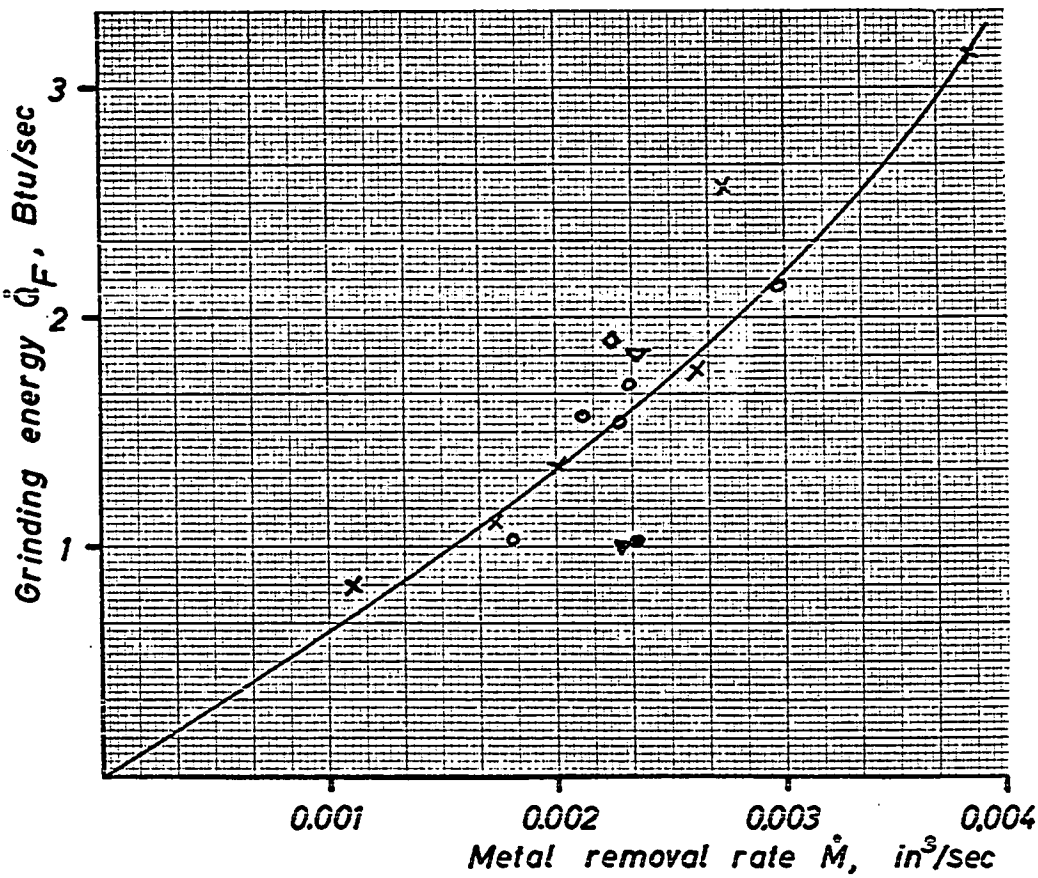

Figure 3.30 Energy Consumption as a Function of Metal Removal Rate

Symbol	Fluid
×	dry
○	Trim EP, 4%
◇	Trim EP, 10%
▽	Trim EP, 20%
▼	Oil, V_S 750 ips
●	Oil, V_S 1360 ips

The values of α_1 and α_2 which have been calculated tend to off-set this increase in consumption of mechanical energy with increasing removal rate. This can clearly be seen in Figures 3.31 and 3.32 in which the sum $\alpha = \alpha_1 + \alpha_2$ and the total heat energy generated in the workpiece, $\dot{Q}_H$, are plotted as functions of the removal rate.

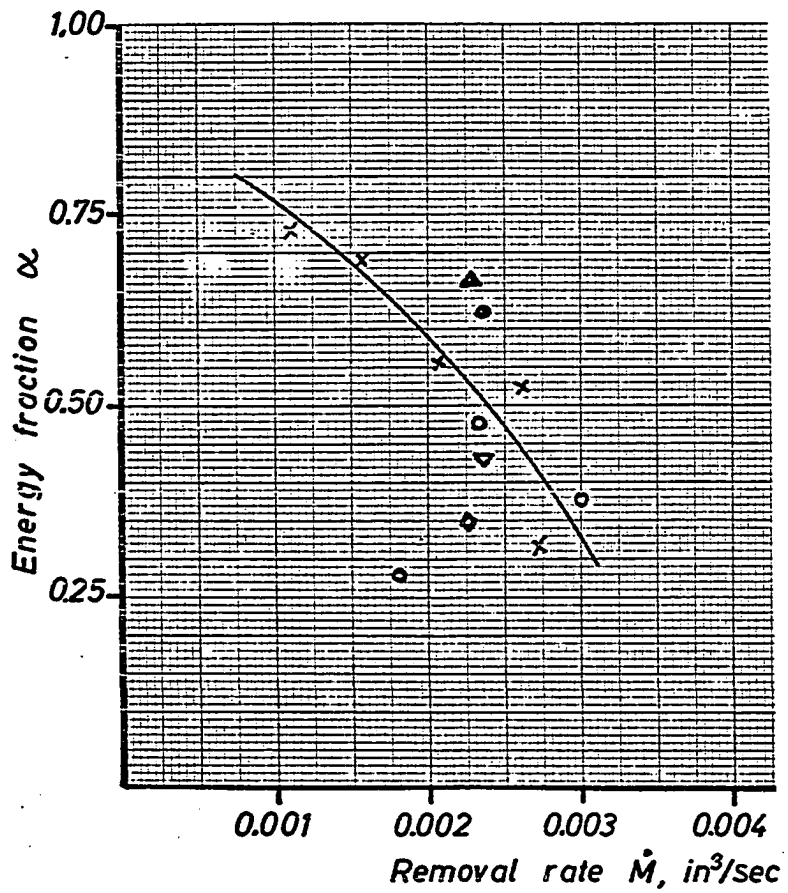

Figure 3.31 Energy Fraction as a Function of Metal Removal Rate
Index of Symbols Used is the Same as in Figure 3.30

The values of the total energy fraction α calculated for dry grinding are in good agreement with the values measured by R. Brown [3] with a calorimeter at low table speeds and, therefore, low removal rates. When the values of α_1 and α_2 are compared, it becomes apparent that for most test series the surface heat sources are much stronger than the volume heat sources. This is an important result with respect to the model of the chip formation process. The total amount of heat energy generated by the surface and the volume sources depends on the amount of strain and the volume of material envolved. Though the volume is small over which the surface heat source extends, the strain is very much larger than the strain of the material of the volume heat source. The combined effect is that the strength of the surface heat source is larger than the strength of the volume heat source.

Since the workpiece temperatures are directly proportional to the rate of heat generation, Figure 3.32 also shows that the temperatures will essentially be the same in dry grinding and with the soluble oil at a concentration of 4%. The temperatures will be about 20% lower if the straight grinding oil is applied or the soluble oil at a concentration of 10%.

This conclusion is confirmed by calculations of the temperature in the area of contact, T_C, and in the plane of the finished surface, T_F. These calculations are carried out with the values of the optimization parameters listed in Table 3.10 for each test series.

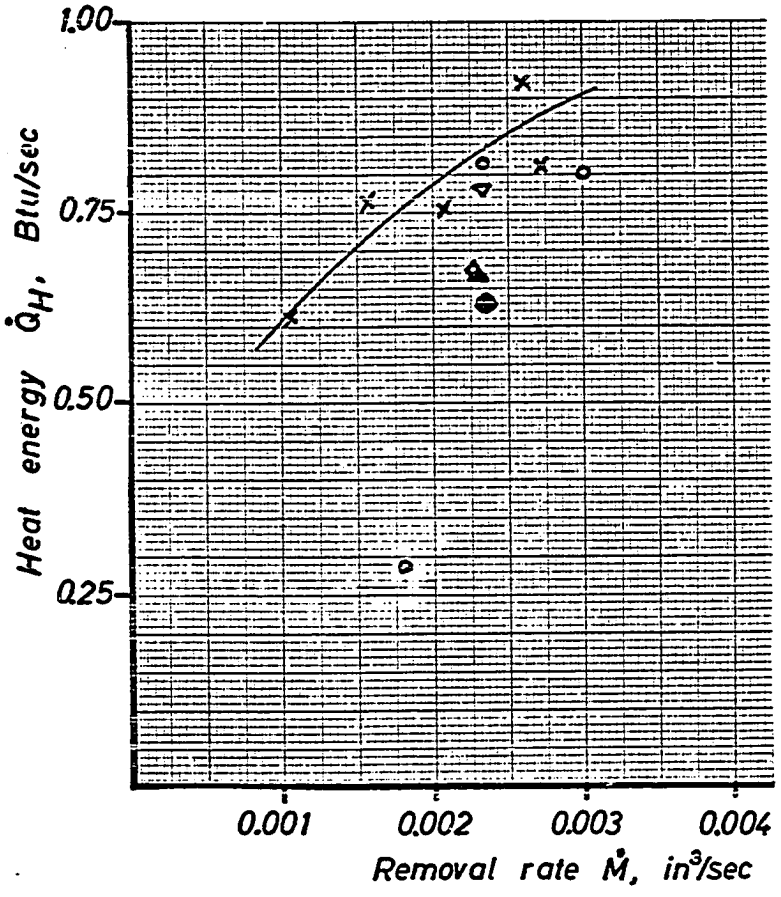

Figure 3.32 Heat Energy as a Function of Metal Removal Rate
Index of Symbols Used is the Same as in Figure 3.30

The maximum values of both profiles, $T_{C,max}$ and T_F, are also entered in that table. $T_{C,max}$ is the highest temperature at the interface between a grain and the workpiece and, therefore, controls the rate of chemical interaction between the two bodies. As shown in Figure 3.33, it is composed of a bulk temperature rise under the wheel and very large peak temperatures directly under the grain. These peak temperatures of several thousand degrees Fahrenheit can exist only at the surface of the grain and the workpiece for a very short time

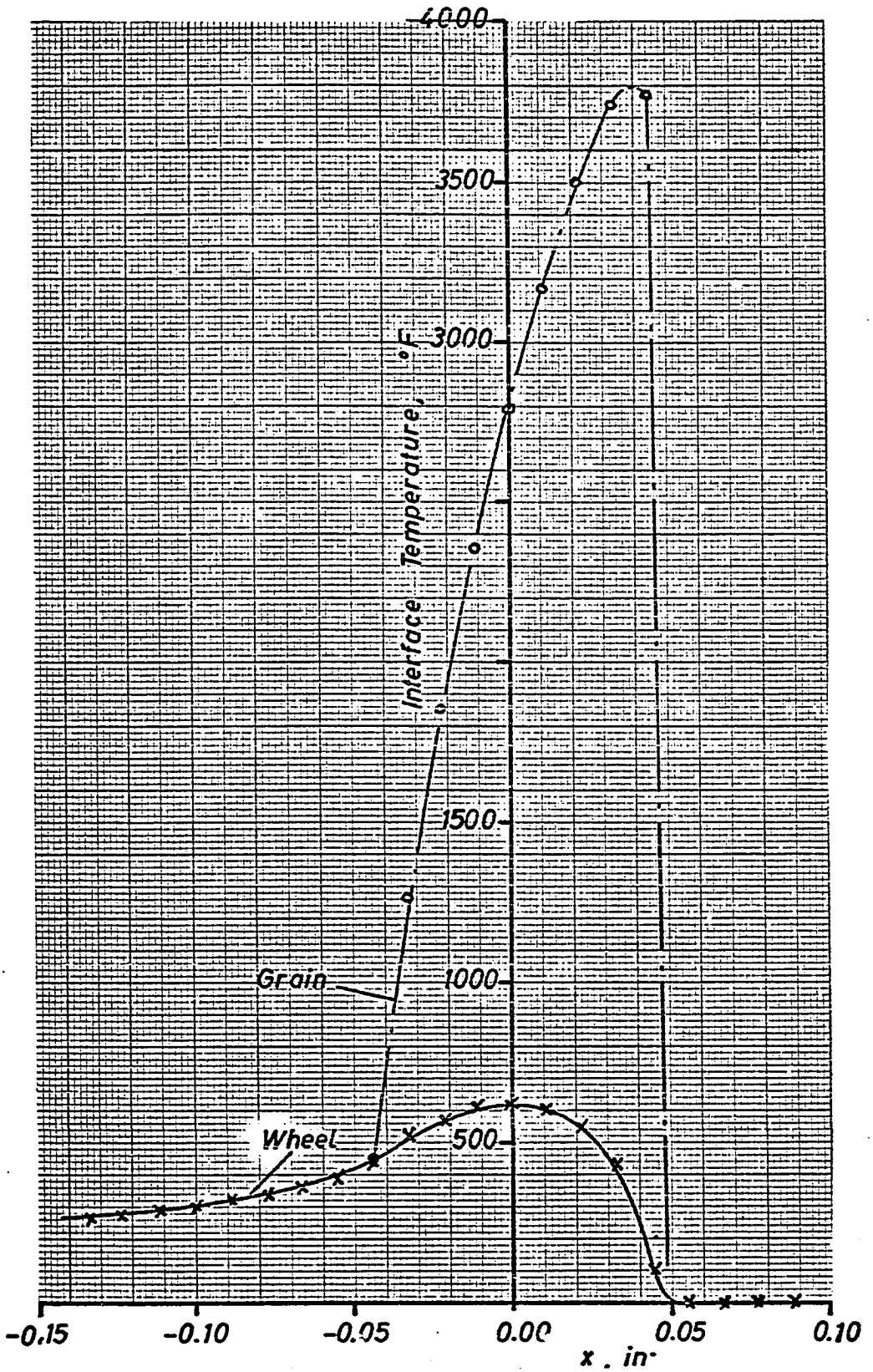

Figure 3.33 Maximum Temperatures at the Interface Between a Grain and the Workpiece (Data from Test Series 9)

without melting the two materials. The time during which a point of the workpiece surface is subjected to the peak temperature is of the order $\ell_G/V_S = \frac{0.005}{800} = 6.25$ µsec and the time it takes a grain to move through the wheel-workpiece contact zone is $\ell_c/V_S = \frac{0.1}{800} = 125$ µsec. Feuerstein and Smith discuss in reference [9] the effect of the heating rate on the transition temperatures Ac_1 (beginning of allotropic transformation and carbon solution). They show that the critical temperature increases as the heating rate increases. If their data is extrapolated beyond the maximum of the measured rate of heating to the much higher heating rates encountered by the workpiece under a grain, the beginning of the allotropic transformation is found to occur at the temperature $Ac_{1,Grain} = 28,500°F$. Such a high temperature is not reached in grinding and it can, therefore, be concluded that the temperature peaks under a grain do not contribute to possible thermal damage in the workpiece. The rate of heating due to the interference zone heat sources, on the other hand, is much smaller and so is the transformation temperature. Using the data from reference [9] again, the beginning of the transformation is estimated to occur at a temperature $Ac_{1,Wheel} = 2400°F$. The highest surface temperatures due to the interference zone heat sources are less than 1000°F in all tests conducted and no transformation has taken place.

Generally, it can be said that the highest contact temperatures result in dry grinding but they decrease rapidly as the removal rate is increased. The reason for this surprising result is the

fact that the chip thickness increases with increasing removal rate and that the number of active grains per unit area increases rapidly with increasing chip thickness. Due to the larger number of active grains in the area of contact between the wheel and the workpiece, the strength of the single grain heat sources is reduced even though the total heat energy input is increased.

This behavior is influenced only slightly by the equation used to describe the dependence of the number of active grains on the chip thickness. If equation (3.7) were used instead of equation (3.68) to approximate the same set of data, the same trend would have been observed in peak contact temperatures.

The temperatures due to the interference zone heat sources are not affected by variations of the number of grains that take part in the grinding process but only by the total rate of heat generation. Of practical importance is the maximum temperature in the plane of the final surface, T_F, which is determined at some small depth below the contact surface. All the material above the plane of the finished surface will be removed by the grinding wheel and it may be heated above a temperature at which thermal damage will first occur. The temperature in the upper layer of material which is not removed by the wheel is the critical temperature with respect to the damage of the workpiece. Figure 3.34 shows the temperature distribution in the plane of the final surface. Since the depth below the plane of contact is small, temperature peaks due to

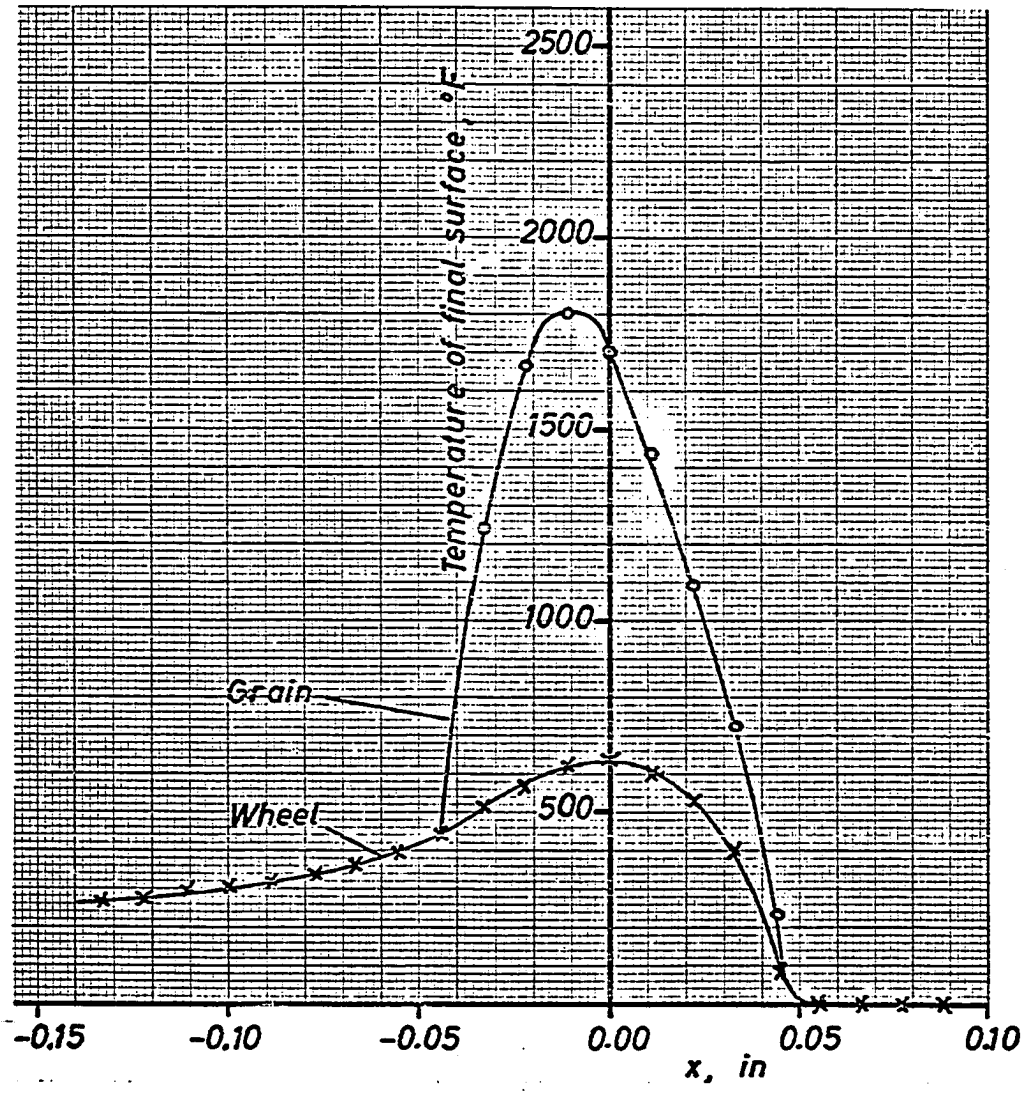

Figure 3.34 Temperatures in the Plane of the Final Surface of the Workpiece (Data from Test Series 9)

individual grains are noticeable but much smaller than directly in the area of contact. Because of the very short time involved, the effect of the temperature peaks on structural changes will be negligible.

The maximum temperature in the plane of the final surface remains approximately constant as the table speed is increased. The rate of heat energy generation increases and so does the nondimensional length of the interference zone heat source, but simultaneously the effective strength of the source decreases with increasing table speed. The application of grinding fluids can reduce the temperatures slightly. The best results are obtained with the Soluble oil at a concentration of 4% and with the straight grinding oil.

4. APPLICATION OF THE THERMAL MODEL

The thermal model of the workpiece which was developed in the previous chapter cannot only be used to determine dependent grinding parameters and to calculate the temperature field at workpiece locations where measurements are not possible, but it is also a useful tool for studying the effect which controllable parameters have on the workpiece temperatures due to a single pass of the grinding wheel. In most grinding situations, the wheel passes over the same workpiece surface several times in rapid succession. DesRuisseaux [7] has considered this problem in cylindrical grinding without crossfeed and shown that the temperature peaks die out between passes, causing only a rise of the ambient workpiece temperature. This ambient temperature can easily be reduced by simple improvements of the cooling system as is shown experimentally in reference [14].

The peak temperature, on the other hand, cannot be reduced greatly by a good cooling system. Under normal surface grinding conditions it would take a convection coefficient as large as h = 50,000 Btu/(hr ft^2 ^oF) to halve the peak temperature. Convection coefficients as large as this are not readily achieved in a grinding shop. The discussion in Sections 3.2.2 and 3.3 shows that the temperatures due to a single grinding pass depend on a dimensionless coefficient defined by equation (3.40a):

$$H = \frac{2\kappa}{V}\frac{h}{k} \qquad (3.40a)$$

For a given workpiece material, H can be increased by increasing h or reducing the speed of the heat source which here is the table speed. In this chapter some consequences of reducing the table speed are discussed and the results of tests under these conditions are presented.

4.1 Theory of Creep Table Speed Grinding

It is a generally accepted fact that in grinding the thermal damage in a workpiece can be reduced by increasing the table speed and reducing the downfeed per pass in the same proportion. This was found to be true in many applications and experiments. Part of this phenomenon is caused by a reduction of the specific energy due to increased chip thickness. Another reason could be that due to the increased table speed, the workpiece remains a shorter time at high temperature. Since the metallurgical changes of the work material are not only a function of temperature but also of time, increasing the table speed would reduce structural changes and, therefore, thermal damage of the workpiece. However, the main reason for this phenomenon lies in the physics of this thermodynamic problem and can be deduced from the above analysis which is best understood in terms of the dimensionless quantities defined by equations (3.40). Two of these quantities are most

impor.ant in this connection, the dimensionless length of the heat source:

$$L = \frac{V}{2\kappa} \ell_c/2 \tag{3.40b}$$

and dimensionless temperature:

$$\phi = \frac{\pi k V}{q_0 2\kappa} T \tag{3.40c}$$

As shown in Figure 4.1, the dimensionless temperature ϕ increases as the dimensionless length L increases. This figure is plotted for the temperatures ϕ_3 under a surface heat source whose strength varies linearly in the direction of motion but the temperature distributions under all heat sources considered in the analysis follow the same trend. Under the conservative assumption that the specific energy remains constant the effect of increasing the table speed while maintaining a constant removal rate by reducing the depth of cut can be traced. With equation (3.3) for the chip length and equations for the average strength of the heat sources, q_0, given in Table 3.2, the dependence of L and T on V_W can be expressed as:

$$L = \frac{K_1\sqrt{DV_W}}{2\kappa} \tag{4.1}$$

$$T = \frac{K_2 u\ 2\kappa}{k\sqrt{DV_W}} \phi \tag{4.2}$$

where K_1 and K_2 are constants.

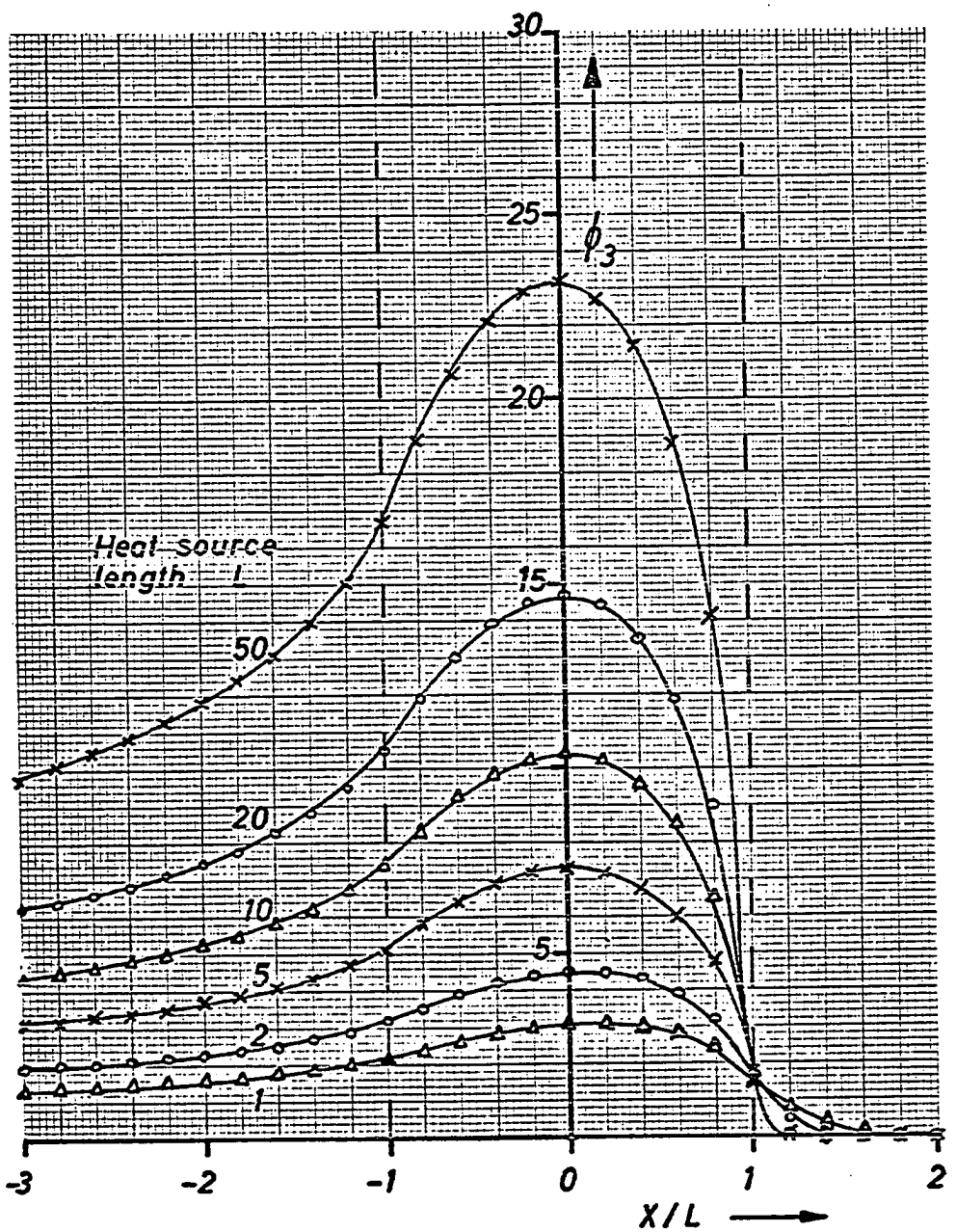

Figure 4.1 Dimensionless Temperature ϕ_3 as a Function of Heat Source Length L

For a constant dimensionless temperature ϕ, the actual temperature varies as $1/\sqrt{V_W}$. The length L varies as $\sqrt{V_W}$ thereby raising ϕ as V_W increases. From Figure 4.2 where the maximum dimensionless temperatures ϕ_{max} of all four heat source models are plotted versus the dimensionless L, it is found that ϕ_{max} does not increase proportional to L, but that

$$\phi_{max} = K_3 L^{n_T} \tag{4.3}$$

where the values of the constants K_3 and n_T are given in Table 4.1.

Source	K_3	n_T
ϕ_1	3.10	0.514
ϕ_2	0.287	0.932
ϕ_3	3.10	0.514
ϕ_4	0.287	0.910

Table 4.1 Constants of Equation (4.3) for Four Heat Source Models

Combining equations (4.1, 4.2, 4.3) yields an expression for the maximum surface temperature in the workpiece as a function of the table speed.

$$T_{max} = K_3 \frac{u}{k} \left(\frac{2\kappa}{\sqrt{DV_W}}\right)^{1-n_T} \tag{4.4}$$

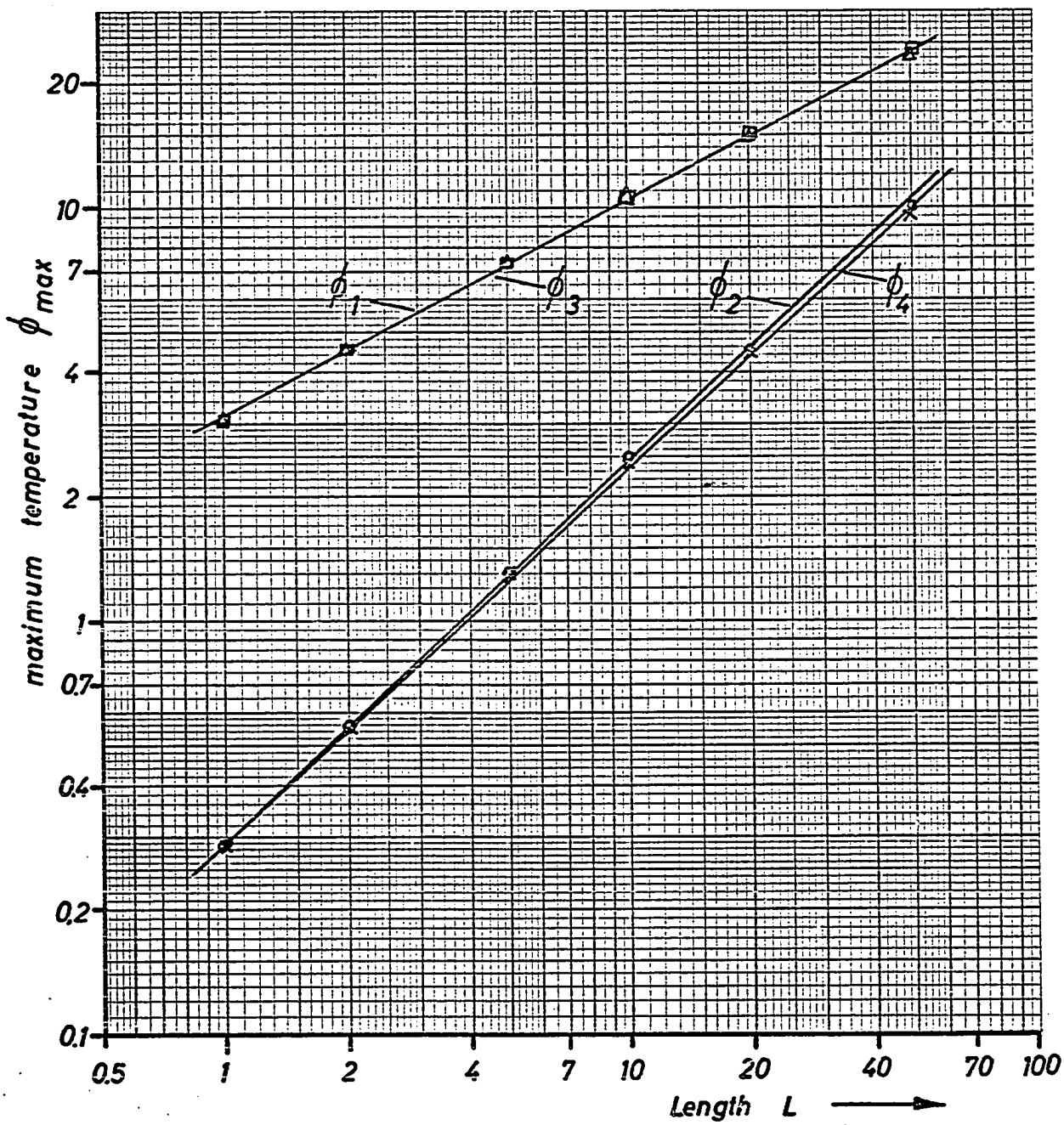

Figure 4.2 Maximum Dimensionless Temperature as a Function of Heat Source Length for Four Heat Source Models

Since the values of the constant n_T are less than unity for all heat source models T_{max} will decrease as V_w increases. A heat source of the same total strength is thus less effective at higher table speed.

Despite this general experience and analytical reasoning, some grinding shops are using very slow table speeds and large depth of cut to grind profiled surfaces in one pass on a horizontal spindle surface grinder. It is claimed that a longer wheel life and less thermal damage of the workpiece results from this procedure. While the claim of a longer wheel life cannot be investigated with this thermal model, the model has the capability to explain the fact that less thermal damage can result when very slow table speeds and large depth of cut are used.

So far in this discussion, convection cooling from the workpiece surface has not been considered. From equation (3.40a) it is clear that the dimensionless cooling coefficient H decreases as the table speed increases. On the other hand, if the table speed is reduced, H can reach a value large enough to completely compensate for any temperature increase due to more effective heat sources. This compensating effect of surface cooling is shown in Figure 4.3 in which the temperature at the point $x = 0$, $z = d/4$ is plotted versus table speed for different values of the convection coefficient h. In the calculations for this graph, the increases in specific energy due to reduced chip thickness at

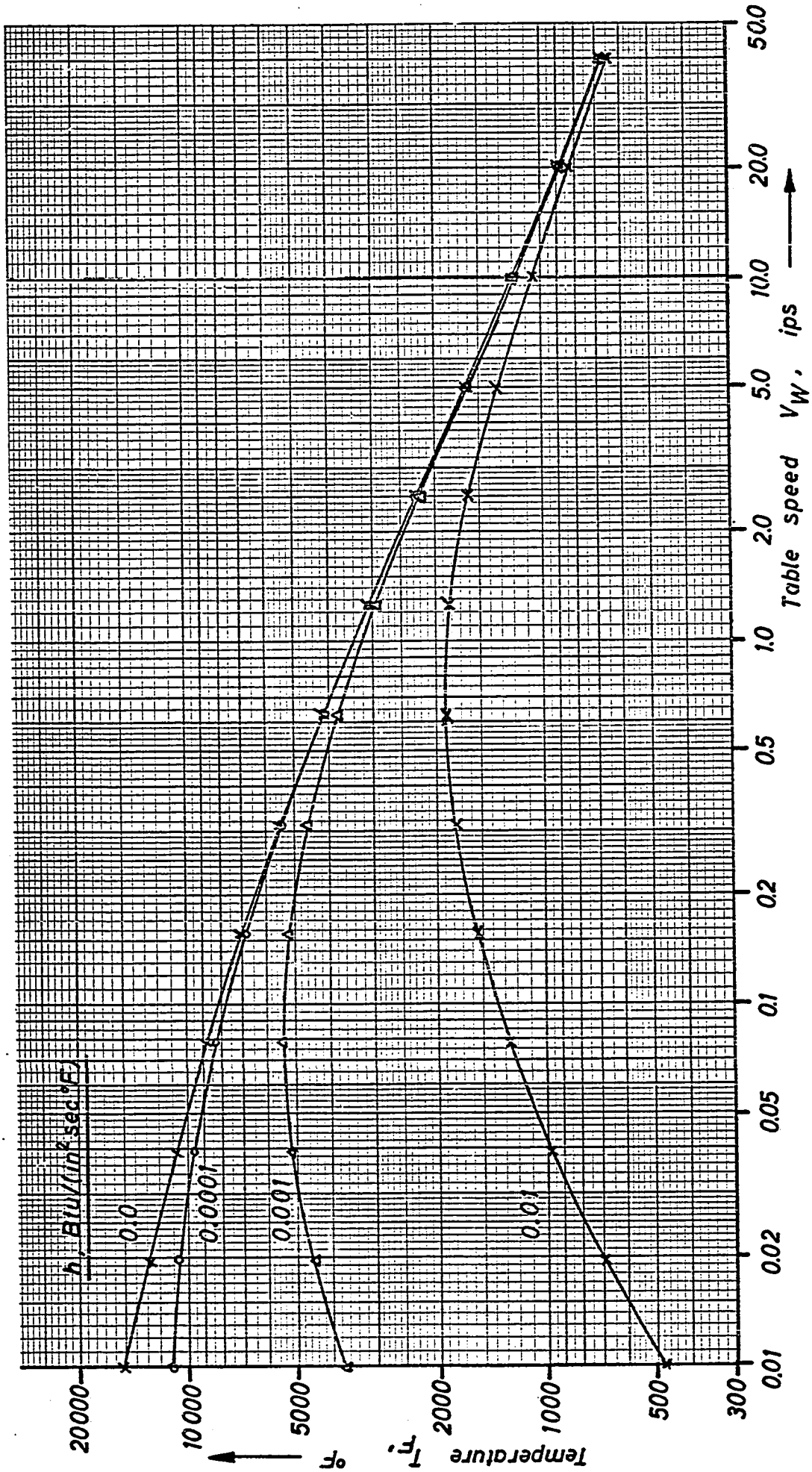

Figure 4.3 Temperature In the Final Surface as a Function of Table Speed and Convection Coefficient

lower table speeds are included. At speeds greater than V_w = 10 ips almost no temperature reduction can be detected for increased values of h. At low speeds large reductions are possible and it is clear that a reversal of the trend occurs at some slow table speed which depends on the convection coefficient. Further reduction of speed will reduce the workpiece temperatures.

These remarks are valid only for the temperature due to the interference zone heat sources. The temperature peaks under single grains are not effected by variations in the convection coefficients. The peaks are, however, influenced by changes of the table speed as they vary with the area of contact and the total strength of the single grain heat sources. Calculations show that the maximum temperature at the interface between a grain and the workpiece increases only by about 5% as the table speed is reduced from 40 ips to 0.01 ips.

Based on these thermal considerations, it appears feasible to grind with very slow table speed and large depth of cut. In order to give satisfactory results this process depends on an efficient cooling system. For a chosen table speed the resulting temperatures are a strong function of the cooling coefficient and care must be taken to maintain it at a constant value.

4.2 Grinding Tests Using Creep Table Speeds

The calculations leading to Figure 4.3 were done with the assumption that the energy fractions α_1 and α_2 remain constant as the table speed is decreased. Because of changing chip geometry, this assumption may not be valid. The undeformed chip length increases with the square root of the depth of cut and the chip thickness varies approximately as the fourth root of the table speed. Increased chip length and reduced chip thickness will cause more rubbing to take place as the grain moves through the workpiece. For this reason, a test program was designed in order to determine the energy fractions using the same procedure and analytical models developed in Chapter 3.

The same grinding machine as in the former test series is used. Because of the slower table speed, the heat energy will penetrate deeper into the workpiece of steel AISI 1018 whose size had to be increased to a length of 8 inches and a height of 1 inch. This height is not sufficient to allow the development of a temperature distribution equivalent to the temperature field in a semi-infinite solid. It is, therefore, necessary to reduce the thermal resistance of the interface between workpiece bottom and holder as much as possible. This is done by inserting a soft aluminum foil between the members and squeezing them together on a press. It is hoped that this procedure removes the air pockets at the interface, thereby minimizing the thermal resistance. The

width of the workpiece is maintained at 0.25 inch so that it becomes necessary to insulate the sides of the workpiece against cooling by the grinding fluid. This is done by clamping thin (0.125 in) plexiglass strips onto both sides. These strips extend to the top surface and are ground together with the workpiece. In preliminary tests it was established that the force to grind both strips is negligible compared to the force caused by grinding the workpiece. A constantan wire of 0.010 inch in diameter is inserted through a hole of 0.029 inch in diameter which extends from the bottom to within 0.4 inch of the top surface. The wire is spotwelded to the workpiece at the tip of the hole and forms a thermocouple with the workpiece, the output of which is fed through an amplifier into a Sanborn Model 320 Duo-Channel Recorder together with a reference signal which determines the horizontal alignments of different temperature traces and their position relative to the wheel.

The experimental set-up is very similar to the one described in the previous chapter. The main differences are that a pen recorder is used instead of an electron beam oscilloscope and that the grinding force cannot be measured by the inertia method used before. Because of the very long grinding time which is greater than 130 sec in all test of this program, the wheel speed reaches a constant value which can be related to the grinding force. Over the range of F_p from 0 to 20 lbf a linear relationship was

found to exist between the horizontal component of the grinding force and the drop of wheel speed.

In initial tests it was found that a wheel of coarse grain size and low hardness value should be used in order to obtain a wheel life sufficiently long to complete one pass over the workpiece. A wheel, AA24-F8-V, was found to give best results and is, therefore, used in this test program. All passes must be done with a heavy stream of good grinding fluid flowing over the surface of the workpiece before and after it passes under the wheel. The fluid with the best cooling properties of the former test program was selected, Trim EP in a concentration of 4%.

This test program consists of four test series of two tests each. All tests are carried out using the same workpiece by cyclic varying the test conditions which are summarized in Table 4.2. Because of the large volume of metal removed during one pass and the large wheel wear encountered the wheel is dressed after every pass. Since the wheel tends to become loaded, a layer about one grain diameter thick must be dressed off from the wheel face in order to ensure repeatable grinding conditions. Figure 4.4 shows the recordings of the workpiece temperatures and of the grinding force as a function of grinding time for the second test of test series 15.

Test Series No.	V_S ips	V_W ips	d in	ℓ_c in	t μ in	C in^{-2}	u 10^6 psi	F_P lbf	$\dot{Q}_F$ Btu/sec	Fluid
13	750	0.0270	0.0305	0.494	70	101	21.46	5.9	3.83	Trim EP 4%
14	750	0.0275	0.0155	0.352	65	86	18.20	2.59	2.36	Trim EP 4%
15	750	0.0570	0.0310	0.498	85	147	10.60	6.25	4.03	Trim EP 4%
16	750	0.0570	0.0155	0.352	78	123	12.72	3.75	3.42	Trim EP 4%

Table 4.2 Grinding Conditions for Slow Table Speed Grinding

Test Series No.	α_1	α_2	α	h $\frac{Btu}{in^2\ sec\ ^oF}$	ΔT ^oF	$\dot{Q}_H$ Btu/sec	$T_{C,max}$ ^oF	T_F ^oF
13	0.1350	0.0395	0.1745	0.0053	2.94	0.668	1997	63.4
14	0.0073	0.0878	0.0951	0.0028	0.99	0.224	121	34.6
15	0.0642	0.0427	0.1069	0.0025	2.35	0.431	662	96.9
16	0.0000	0.1178	0.1178	0.0042	1.43	0.403	59	60.5

Table 4.3 Result of Optimization Procedure

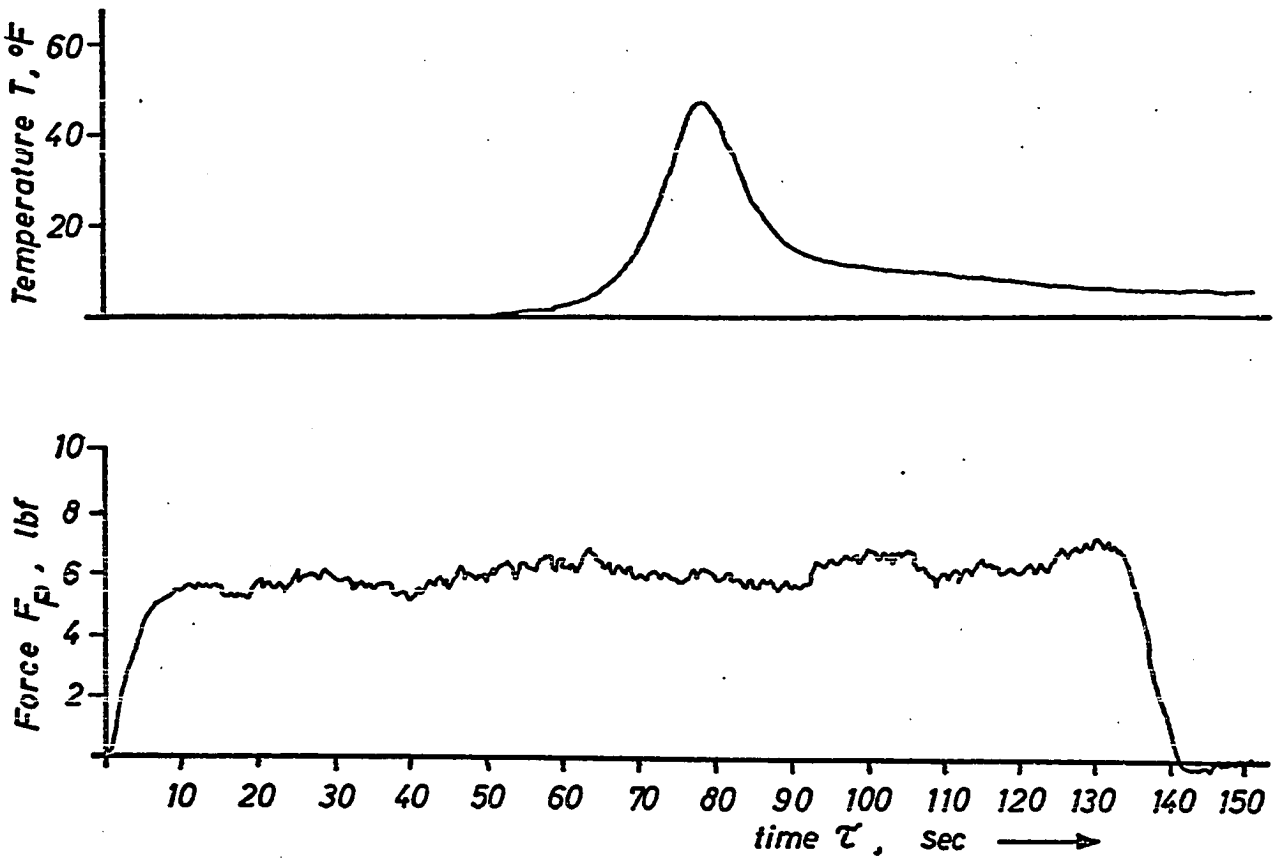

Figure 4.4 Workpiece Temperature and Grinding Force for Test Series 15 (V_W = 0.057 ips, d = 0.031 in)

The temperature data is further analyzed to obtain the values of the energy fractions and of the convection coefficient. The procedure is the same as described above. The numerical values are given in Table 4.3. The average value of the fraction of total heat energy input into the workpiece is found to be only

$$\bar{\alpha} = 0.1$$

which compares with an average value of about 0.4 for the tests at normal table speeds for the same grinding fluid. When the relative magnitudes of α_1 and α_2 are compared, it can be seen that in these tests both have roughly the same value, while in the tests at normal table speeds α_1 is always much larger than α_2. Both of these results are caused by a large reduction of the magnitude of the energy fraction for surface heat sources, α_1, while the magnitude of the energy fraction for volume heat sources, α_2, is unchanged. These observations can be explained by the fact that a layer of greater thickness is removed from the surface of the workpiece so that a larger amount of heat energy is carried away with the chips. The ratio of the volume removed to the volume deformed under the final surface is very much larger for the slow table speeds and large depth of cut that it is for fast table speeds and small depth of cut.

When the average values of the convection coefficient for the same grinding fluid are compared between the two test programs, they are found to agree very well. The convection coefficient of Trim EP, 4% concentration, has the average value

$$h = 0.0035 \text{ Btu/(in}^2 \text{ sec } ^\circ\text{F)} = 1815 \text{ Btu/(ft}^2 \text{ hr } ^\circ\text{F)}$$

under the conditions described in this thesis.

The maximum calculated temperatures at the interface between the grain and the workpiece and in the plane of the final surface are much smaller than they were in the former tests. One of the reasons for this result is that smaller metal removal rates are achieved in the later tests. The removal rates are on the average reduced by a factor of 0.096. All temperatures with the exemption of the contact temperature of test series 13 are reduced by about the same factor from the values calculated for the former test series. Therefore, it appears feasible to achieve the same metal removal rates when grinding with low table speeds as are achieved in regular surface grinding without overheating the workpiece.

The reason that higher removal rates are not obtained in these tests lies in the fact that the wheel wears out before the pass is finished when the removal rates are higher. This is illustrated quite clearly in Figure 4.5 which shows a recording of the grinding

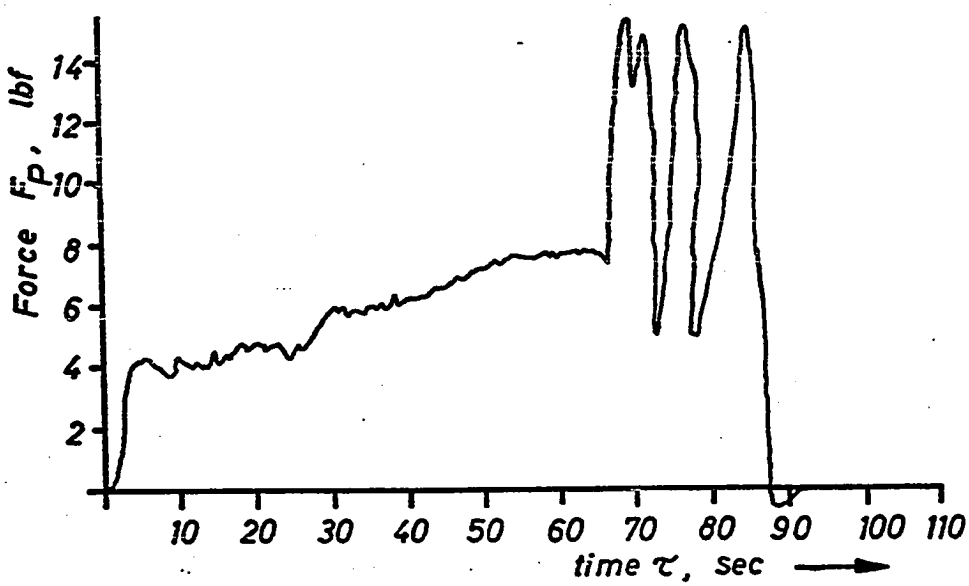

Figure 4.5 Grinding Force During a Severe Grinding Pass

force during a severe path. Starting from an initial low value, the force increases slowly until it suddenly jumps to about four times the last value and starts to oscillate. Observation of the grinding action at this moment reveals that a zone of bright red glowing material has formed under the contact area which appears and disappears with the same frequency as the force diagram shows. The cause of the sudden increase of the grinding force is believed to be the softening of the work material as soon as the workpiece temperature reaches some critical value. The work material will flow plastically under the load of the grains thereby increasing the area of contact which causes the force to increase. This in turn raises the workpiece temperature to such a high value that the material becomes red hot and softens completely. The force drops which again reduces the temperature and increases the hardness of the material. The cycle starts again with the force increasing which raises the temperature in the workpiece and so on.

There are a number of variables which control this cyclic process. The main variable is the workpiece temperature which must be so low as to avoid thermal softening of the work material. The temperature itself is a function of the grinding conditions. It can be kept low by an effective grinding fluid whose main property must be to provide good cooling. Also, the wheel must be dressed

in such a way as to maintain sharp, long-lasting cutting points. The selection of grain size and hardness must also be carefully considered.

The selection of the wheel, the fluid, and the work material used in these tests cannot be considered optimal since no prior experience with this process was given and only a limited number of tests could be carried out. Nevertheless, the tests serve to indicate the feasibility of the process and confirm the analytical conclusions.

5. CONCLUSIONS AND RECOMMENDATIONS

In this thesis a procedure is described which allows the determination of important grinding parameters such as the fraction of the total grinding energy which remains in the workpiece in the form of heat energy and the coefficient of convection of grinding fluids under surface grinding conditions. With the appropriate thermal model, this procedure can be applied to any grinding operation and the principle is also valuable in areas other than grinding.

A simple model of the workpiece of the abrasive cut-off operation has been developed in Chapter 2 and the energy fraction was determined for various grinding conditions. The values are in good agreement with values determined by a different method. The model does not allow the temperatures in the cutting zone to be predicted. In Chapter 3, a thermal model of the workpiece for horizontal spindle surface grinding has been developed. It is sufficiently detailed to allow the calculation of the temperatures directly in the zone of contact between the wheel and the workpiece.

The energy fraction α assumes values from 0.1 to 0.3 in the abrasive cut-off operation and in surface grinding the values of α vary from 0.3 to 0.75. The energy ratio was also determined under extreme surface grinding conditions, for table speeds as slow as 0.027 ips and depth of cut as large as 0.031 in. Under

these conditions α has a value of about 0.1. This low value is explained in terms of the changed geometry of the chips and of the contact zone. It appears that a larger percentage of heat energy which was originally generated in the top layer of the workpiece is removed with the chips.

The temperatures which could cause thermal damage of the workpiece were found to be less than 900°F for all tests conducted and the peak temperatures under a grain which reach several thousand degrees Fahrenheit were shown to be present only for such a short time that no melting can take place. The thermal model is used to provide a rational explanation for the observation that thermal damage of the workpiece is reduced if the table speed is increased while keeping the removal rate constant. It is shown that a heat source is less effective when its length is large and the strength per unit length is low then when the length is small and its strength per unit length is large.

The workpiece temperatures can be reduced by grinding with good grinding fluids. At normal table speeds it was found that the fluid should have good lubricating properties while large variations of the cooling properties have only a very small effect on the resulting temperatures. When grinding with extremely small table speeds the cooling property of the fluid becomes more and more important. The cooling can become so

effective that it overcomes the effect of reduced table speeds and the workpiece temperatures are as low or lower than when grinding with normal table speeds.

There are other areas of surface grinding not yet mentioned in which the techniques and analytical models may be used with advantage. It is of interest, for example, to study the effects which a segmented wheel has on the grinding temperatures. Segmented wheels are all wheels which have an interrupted grinding surface such that periods of grinding are followed by periods during which the workpiece can cool. The main effect which such a wheel would have is that the temperatures in the workpiece may not reach their steady state value before the grinding action is over and cooling begins. Under the assumption that the cooling is complete, i.e., the workpiece temperatures reach their initial low value before grinding starts again, the temperatures in Figure 5.1 were calculated. It is also assumed that segments are as long as the spaces between them. Since only half as many grains have to remove the same amount of material as a complete wheel the steady state temperature will be twice as large as before. When a table speed of 10 ips is used, eight segments are enough to give the same temperature as the complete wheel. If the number of segments were increased to fifty, the temperature would be one-third the temperature for the complete wheel. At lower table speeds the segmentation is even more effective. This

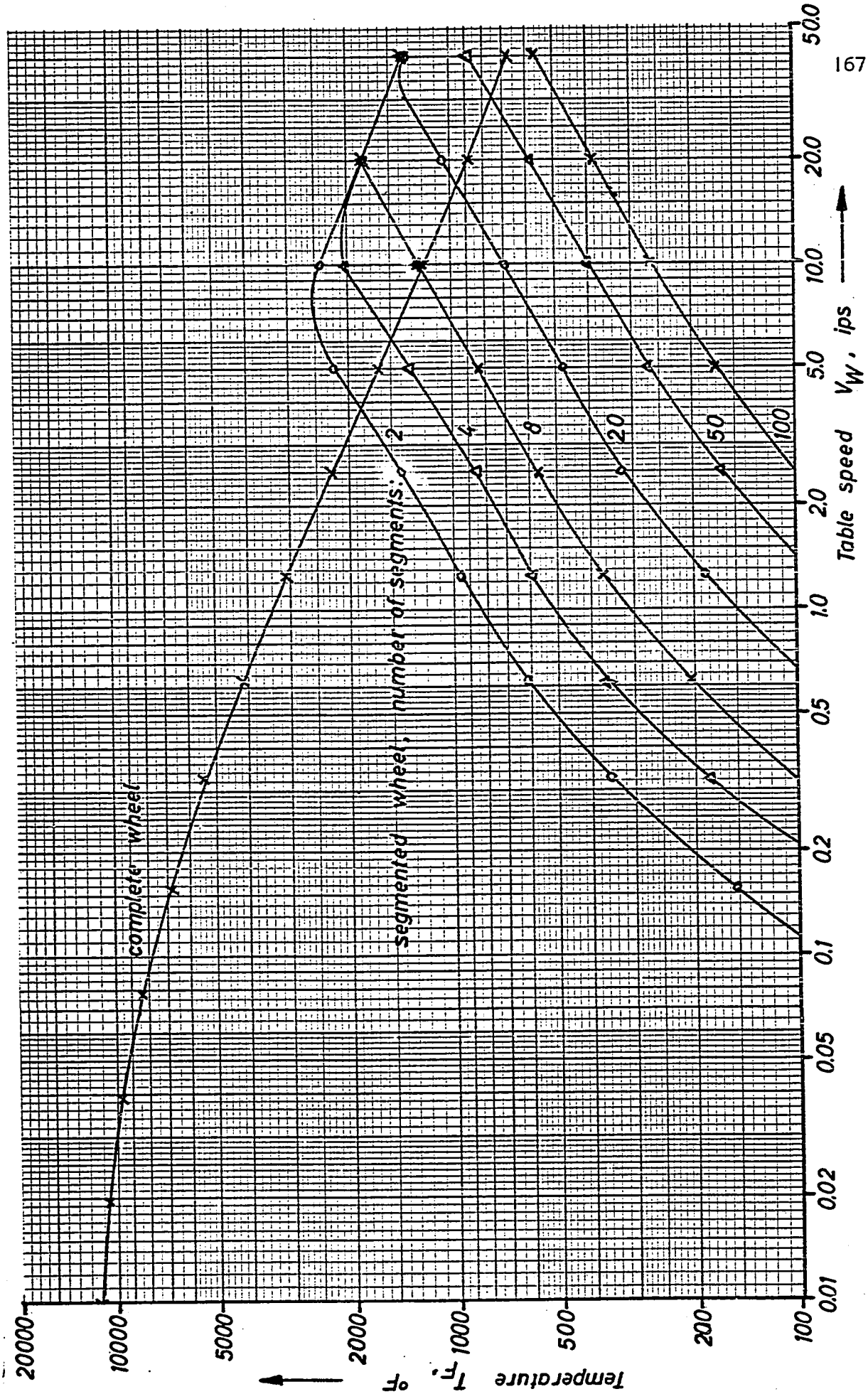

Figure 5.1 Temperature In the Final Surface for a Segmented Wheel with a Convection Coefficient h = 0.0001 Btu/(in^2 sec ^oF)

analysis is not complete, though. The cooling between segments is not complete, so that the initial temperature will increase. Further analysis and tests are needed to explore all the advantages and disadvantages of segmented wheels.

REFERENCES

1. Backer, W. R., et al., "The Size Effect in Metal Cutting," Trans. ASME, January 1952.

2. Backer, W. R. and Merchant, M. E., "On the Basic Mechanics of the Grinding Process," ASME Paper No. 56-A-43, 1956.

3. Brown, R., "Calorimeter Measurements of Grinding Energy," App. I, AGA Report No. 4, Carnegie-Mellon University, Pittsburgh, 1969.

4. Brueckner, K., "Der Schleifvorgang und seine Bewertung durch die auftretenden Schnittkraefte," Dissertation, TH Aachen, 1962.

5. Carslaw, H. S. and Jaeger, J. C., Conduction of Heat in Solids, Oxford University Press, London, 1947.

6. Crisp, J. N., "Transient Thermal Effect in Surface Grinding," Ph.D. Thesis, Carnegie-Mellon University, Pittsburgh, 1968.

7. DesRuisseaux, Neal, "Thermal Aspects of the Grinding Process," Ph.D. Thesis, University of Cincinnati, 1968.

8. Eshghy, S., "Thermal Aspects of the Abrasive Cut-Off Operation," Part 1: ASME Paper No. 66-WA/PROD-21; Part 2: ASME Paper No. 67-WA/PROD-10.

9. Feuerstein, W. J. and Smith, W. K., "Elevation of Critical Temperatures in Steel by High Heating Rates," Trans. American Society for Metals, Vol. 46, p. 1270.

10. Hahn, R. S., "On the Nature of the Grinding Process," Proc. Third International Conference on Machine Tool Design and Research, Birmingham, September, 1962.

11. Hain, G. M., "Measuring the Cooling Properties of Cutting Fluids," Trans. ASME, August 1952.

12. Hastings, C., Jr., Approximations for Digital Computers, Princeton University Press, Princeton, New Jersey, 1955.

13. Jaeger, J. C., "Moving Sources of Heat and the Temperature at Sliding Contacts," Proc. Royal Soc. of New South Wales, October 1942.

14. Jeffries, N., et al., "Grinding Process Optimization," Air Force Materials Laboratory, Contract F33615-C-1792, Wright-Patterson Air Force Base, Ohio, 1970.

15. Kassen, G., "Beschreibung der elementaren Kinimatik des Schleifvorganges," Dissertation TH Aachen, June 1969.

16. Lindsay, R. P., "Stock Removal Rates in Internal Grinding - A Model of the Process," M.Sc. Thesis, M.I.T., 1966.

17. Littmann, W. E. and Wulff, J., "The Influence of the Grinding Process on the Structure of Hardened Steel," Trans. ASM, Vol. 47, 1955.

18. Malkin, S., "The Attritious and Fracture Wear of Grinding Wheels," Ph.D. Thesis, M.I.T., February 1968.

19. Marshall, E. R. and Shaw, M. C., "Forces in Dry Surface Grinding," Trans. ASME, January 1952.

20. Nakayama, K. and Shaw, M. C., "An Analytical Study of the Finish Produced in Surface Grinding," Proc. Instn. Mech. Engrs. 1967-68, Vol. 182, Pt. 3K.

21. Outwater, J. O. and Shaw, M. C., "Surface Temperatures in Grinding," Trans. ASME, January 1952.

22. Reichenbach, G. S., et al., "The Role of Chip Thickness in Grinding," Trans. ASME, May 1956.

23. Rowe, G. W. and Wetton, A. G., "Theoretical Considerations in the Grinding of Metals," Journal of the Institute of Metals, Vol. 97, 1969.

24. Sato, K., "Grinding Temperature," Bul. Japan Soc. Grinding Engrs., No. 1, 1961.

25. Shaw, M. C., Metal Cutting Principles, Third ed., M.I.T. Press, Cambridge, Massachusetts, 1968.

26. Shaw, M. C. and DeSalvo, G. J., "On the Plastic Flow Beneath a Blunt Axisymmetric Indenter," ASME Paper No. 68-WA/PROD-12, 1969.

27. Shaw, M. C., et al., "A New Theory of Grinding," Fourth Annual Report of the Abrasive Grain Association Investigation, Carnegie-Mellon University, Pittsburgh, November 1969.

28. Shaw, M. C., et al., "Overcut Fly Milling," Fifth Annual Report of the Abrasive Grain Association Investigation, Carnegie-Mellon University, Pittsburgh, November 1970.

29. Shaw, M. C., et al., Third Annual Report of the Grinding Wheel Institute Investigation, Carnegie-Mellon University, Pittsburgh, October 1966.

30. Shaw, M. C., et al., Fourth Annual Report of the Grinding Wheel Institute Investigation, Carnegie-Mellon University, Pittsburgh, October 1967.

31. Smithells, C. J., Metals Reference Book, Vol. II, Third edition.

32. Takasawa, K., "Effects of Grinding Variables on the Surface Structure of Hardened Steel," Bul. Japan Soc. of Precision Engineering, Vol. 2, No. 1, Tokyo, April 1966.

33. Ueno, T., et al., "Experiments on the Cooling Ability of Cutting Fluids," Bul. JSME, Vol. 13, No. 59, May 1970.

Appendix: DETERMINATION OF THE DECAY COEFFICIENT β

In an effort to develop a suitable model of the grinding process, it was noted that a grain in contact with the workpiece resembles a hardness indenter [27]. The theory describing the elastic and plastic deformation of the testpiece under the indenter was then applied to the workpiece loaded by the grain of a grinding wheel. As in the hardness test, the workpiece is deformed to a depth far greater than the depth of the indentation which in grinding is the instantaneous chip thickness.

If this model of the chip formation process is true it should be possible to evaluate the extent of flow below the surface from model tests. In these tests, a steel ball is pressed in the surface of a workpiece which is then moved perpendicular to the direction of loading so that a groove is formed on the surface of the piece. In order to study the deformation below the surface, the specimen was split in half before the test and a regular grid printed on the split surface. The specimen is then clamped together tightly and the indentation is made such that the center of the groove is directly over the interface between the halves of the split workpiece. The specimen is then dissembled and the grid examined for evidence of the extent of plastic flow. Figure A.1 shows part of the deformed grid and in Figure A.2, the horizontal displacement of the grid points in a region far away from the ends of the groove is plotted as a function of depth. The data points

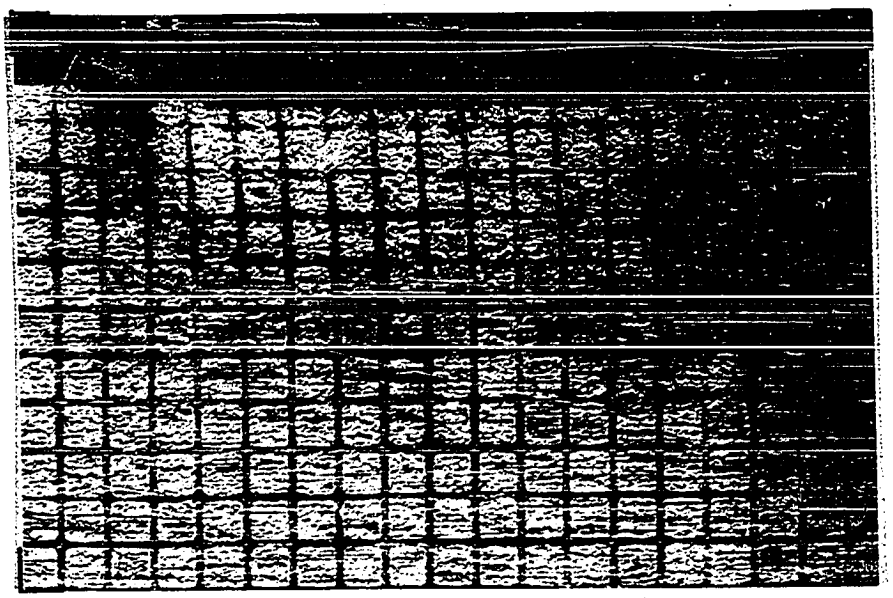

Figure A.1 Deformed Grid in Simulated Grinding Test

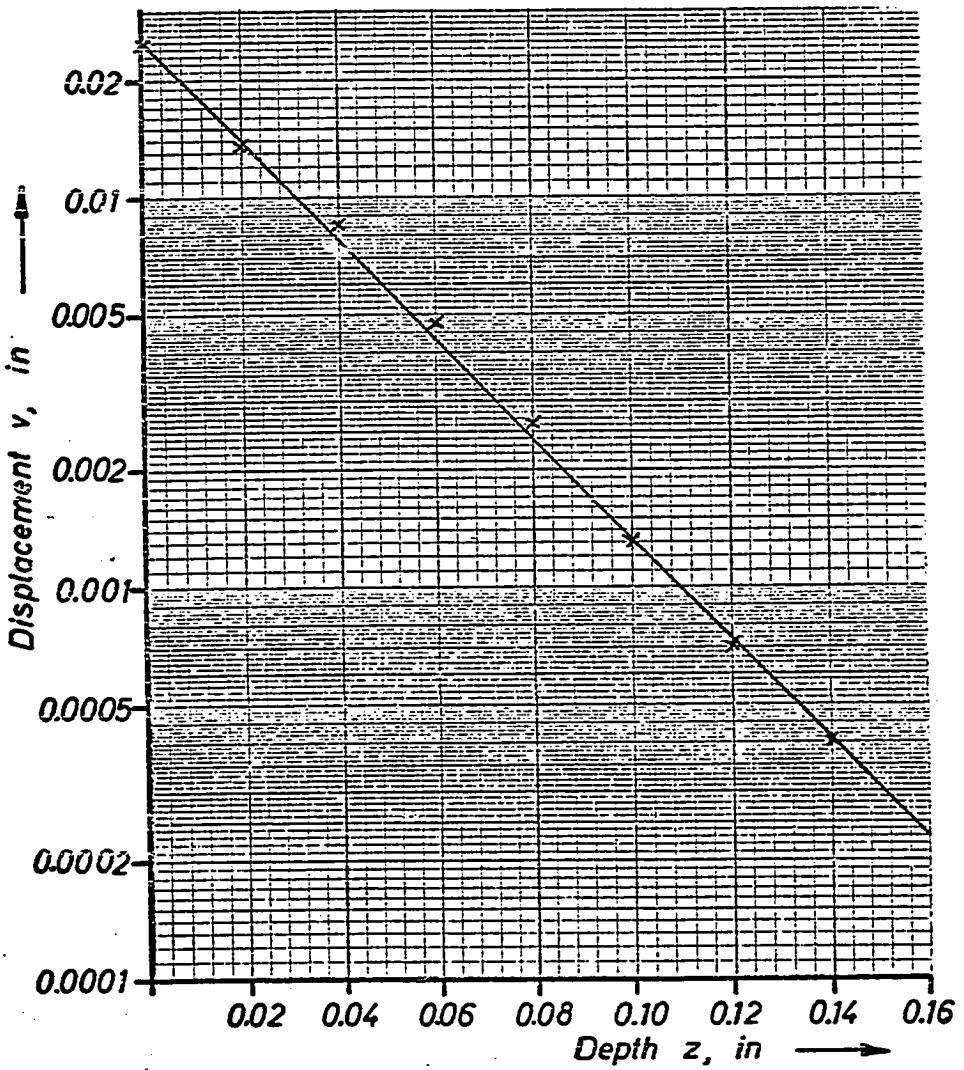

Figure A.2 Horizontal Displacement of Grid Points as a Function of Depth

lie on a straight line when plotted on a semi-logarithmic scale. The relationship between displacement v and the depth z can, therefore, be expressed as

$$v = v_0 e^{-\beta z} \tag{A.1}$$

The values of the two constants can be evaluated from Figure A.2:

$$v_0 = 0.025 \text{ in}$$
$$\beta = 27.73 \text{ 1/in}$$

To a first approximation the energy expended in deforming the grid is proportional to displacement and the yield stress of the material. If the yield stress is assumed to be constant throughout the body, the energy will vary as $e^{-\beta z}$ with the depth below the surface.